Density Functional Theory (DFT) Studies of the Homogeneous Activation of Small Molecules Using Transition Metal and Main Group Based Compounds

Thesis Submitted to AcSIR for the Award of the Degree of

DOCTOR OF PHILOSOPHY

in Chemical Sciences

By

Ms. Nishamol Kuriakose

Registration Number: 10CC11J26037

Under the guidance of

Dr. Kumar Vanka

Physical Chemistry Division

CSIR- National Chemical Laboratory,

Pune - 411008, India

May 2015

राष्ट्रीय रासायनिक प्रयोगशाला
(वैज्ञानिक तथा औद्योगिक अनुसंधान परिषद)
डॉ. होमी भाभा रोड, पुणे - 411 008. भारत
NATIONAL CHEMICAL LABORATORY
(Council of Scientific & Industrial Research)
Dr. Homi Bhabha Road, Pune - 411008. India

Certificate

This is to certify that the work incorporated in this Ph.D. thesis entitled ***Density functional theory (DFT) studies of the homogeneous activation of small molecules using transition metal and main group based compounds*** submitted by Ms. ***Nishamol Kuriakose*** to Academy of Scientific and Innovative Research (AcSIR) in fulfillment of the requirements for the award of the Degree of ***Doctor of Philosophy in Chemical Sciences***, embodies original research work under my supervision. I further certify that this work has not been submitted to any other University or Institution in part or full for the award of any degree or diploma. Research material obtained from other sources has been duly acknowledged in the thesis. Any text, illustration, table etc., used in the thesis from other sources, have been duly cited and acknowledged.

Nishamol Kuriakose

(Student)

Dr. Kumar Vanka

(Supervisor)

Date: 08/05/2015

Place: Pune

Communications Channels ☎ +91 20 25902000 +91 20 25893300 +91 20 25893400 Fax +91 20 25902601 (Director) +91 20 25902660 (Admin.) +91 20 25902639 (Business Development) URL : www.ncl-india.org

Dedicated to

My Parents…

Acknowledgements

It is my great pleasure to thank all the people who have helped and supported me throughout my Ph.D life.

I would like to express my gratitude to my research guide ***Dr. Kumar Vanka*** *for his constant support, encouragement and guidance to overcome all the difficulties during my research. I feel extremely fortunate to have worked under his supervision. I believe that his advises as well as constructive suggestions have helped me to improve all quarters of my life. He encouraged me not only to grow as a student but also as an independent researcher. He also motivated me to enjoy books and movies along with research. Thank you Sir, for making my research life smooth and enjoyable.*

I take the opportunity to thank my DAC members; Dr. Amol Kulkarni, Dr. Sudip Roy, Dr. Sarika Bhattacharyya, my internal expert Dr. Neelanjana Sengupta and my external expert Dr. Arun Venkatnathan for their valuable comments and suggestions during the tenure of my research. I am grateful to Dr. Saurav Pal for his wonderful theory classes as well as Dr. Nayana Vaval, Dr. Durba Sengupta, Dr. Kavita Joshi and Dr. D. Sreenivas for the course work classes. All other scientists and staffs of CSIR-National Chemical Laboratory and whole ESTG group are also duly acknowledged for their timely help.

I would also like to thank ***Dr. Sourav Pal****, Director, CSIR-NCL and* ***Dr. Anil Kumar****, Head and Chairman of physical and materials chemistry division for providing me all infrastructural facilities. I am grateful to UGC, New Delhi, for the research fellowship and to Academy of Scientific & Innovative Research (AcSIR) for giving me an opportunity for the perusal of doctoral degree. I would like to thank Dr. C. G. Suresh, SAO chairman, all SAO staff and all administrative staff for their helpful services.*

My sincere thanks to Dr. Abraham Jose, Mar Ivanios College, for opening my way to computational chemistry and Dr. Anup Thomas and Dr. Bhanuprakash at IICT, Hyderabad for teaching me the initial lessons of computational chemistry. I thank Dr. Laxmi Gayatri for her suggestions and help to complete my CSIR-800 course. I also thank Dr. Ashutosh Kelkar and Dr. Vinay Bhandari for their guidance.

I am grateful to all my friends Bessy D' Cruz, Prajitha K. P, Manoj Mane, Amrita Pal, Jaya C. Jose, Leena George, Sneha Menon, Prathith Chatterjee, Roshna Nair, Nupur Bansal, Baljinder Grewal, Ruby Singh and Sruti Vandana for providing all emotional support. I also acknowledge Shantanu Kadam, Jugal Kumawat, Yuvraj Dangat, Mrityunjay Tiwari, Tamal Das, Subrashish Banerjee, Kamalika Ghatak, Debarati Bhattacharyya, Deepthi Mishra, Achintya, Susanto, Chandan, Himadri, Sayali, Anagha, Manzoor, Dr. Mazood, Turbasu, Deepak, Sudip, Chandan, Prithvi Raj, Swagata, Anil, Souvik, Atreyee, Asis, Aryya, Saba, Vidhika, Madhulita, Anju, Xavier, Praveen, Vaibhav, Samik, Rahul, Collins, Mukunda, Mudit, Sumantra, Lalita, Subrado, Viji, Vishwajeet, Vaishali, Pushpanjali, Anshu, Preeti Padhye, Preeti Jain, Suman, Jaya, Soumya, Sreekuttan, Arun, Bindhu, Rajesh, Jijil, Anish, and all my malayalee friends and scientists in NCL and IISER, Pune.

Finally, I extend my gratitude to all my family members and relatives for their support and encouragement throughout my life. I specially thank ***my father*** *without whom I would not have reached at this level. Thank you very much for considering my ambition as yours and teaching me to be persistent in what I pursue. Thanks* ***mummy*** *for supporting me always. I thank my dearest sisters,* ***Mable chechi*** *and* ***Noble chechi****, for being there for me always. I acknowledge Ajishachachan and Tonichachan and my dearest buddies Ammu, Akku and Annu.*

Thank you ***Jesus*** *and* ***Mother Mary*** *for everything….*

Nishamol Kuriakose

Contents

Abstract				v
Abbreviations				ix
List of publications				xi
1.	**Introduction to Small Molecule Activation**			
	1.1		Introduction	3
	1.2		The homogeneous reactions considered in the thesis	
		1.2.1	The water gas shift reaction	3
	1.3	1.2.2	Olefin metathesis	6
		1.2.3	Ammonia borane dehydrogenation	8
		1.2.4	Dihydrogen generation from water and alcohols	10
		1.2.5	Small molecule activation using silylene compounds	11
	1.3		Conclusions	13
	1.4		References	13
2.	**Theoretical Methods and Computational Aspects**			
			Abstract	23
	2.1		The Schrödinger equation	25
		2.1.1	The Born-Oppenheimer approximation	25
	2.2		Density functional theory	26
		2.2.1	Thomas Fermi model	26
		2.2.2	Hohenberg-Kohn theorem	27
		2.2.3	Kohn-Sham equations	28
		2.2.4	Exchange-correlation functional	30

2.3		Energetic span model	31
2.4		Free volume correction for translational entropy	32
2.5		Spin component scaled MP2	34
2.6		RI-J and MARI-J approximations	34
2.7		Solvent correction	35
2.8		References	36
3	**Small Molecule Activation Using Homogeneous Transition Metal Complexes**		
3A	**The Role of Metal-Metal Cooperativity in the Homogeneous Water Gas Shift Reaction**		
		Abstract	41
3A.1		Introduction	43
3A.2		Computational details	46
3A.3		Results and discussion	51
	3A.3.1	Proposed bi-nuclear mechanism	51
	3A.3.2	Comparison of the efficiency of the different mechanisms using the energetic span model	55
	3A.3.3.	Designing improved catalysts for the WGSR	61
3A.4		Conclusions	64
3A.5		References	65
3B	**Substituted Allenes as Highly Efficient Leaving Groups in Catalytic Processes**		
		Abstract	69
3B.1		Introduction	71
3B.2		Computational details	74
3B.3		Results and discussion	74
	3B.3.1	Allene as a leaving group in the Grubbs' catalyst system	74
	3B.3.2	Supramolecular interaction between the	80

		substituents on the ligand	
	3B.3.3.	The possibility of hidden carbone character affecting the binding energy	82
	3B.3.4	Competitive metathesis reaction of the allene ligand	86
3B.4		Conclusions	89
3B.5		References	89
4	**Homogeneous Catalytic Processes Using Main Group Compounds**		
4A	**Ga-N Cage Compounds for Effective Small Molecule Activation**		
		Abstract	95
4A.1		Introduction	97
4A.2		Computational details	99
4A.3		Results and discussion	100
	4A.3.1	Reactivity of a dimeric aluminium-phosphorus Lewis pair towards CO_2 activation	100
	4A.3.2	Catalysis of ammonia borane (AB) dehydrogenation by the Ga-N Cage	102
4A.4		Conclusions	110
4A.5		References	110
4B	**Catalytic Dihydrogen Generation Reaction Using Ge(II) Hydride Compound**		
		Abstract	113
4B.1		Introduction	115
4B.2		Computational details	117
4B.3		Results and discussion	119
	4B.3.1	Dihydrogen production with a reported germanium (II) hydride	119
	4B.3.2	On demand hydrogen generation by the new Ge (II) hydride, GeH-2, from water, methanol	121

		and ethanol	
	4B.3.3.	Protolysis in ROH (R=H, CH_3, C_2H_5) molecules: a comparative study of GeH-2 with an experimentally reported system	126
	4B.3.4.	The full catalytic cycle for the formation of H_2 from ROH (R=H, CH_3, C_2H_5) by the GeH-2 catalyst	128
4B.4		Conclusions	133
4B.5		References	133
5	**Small Molecule Activation by Acyclic Silylene Complexes**		
		Abstract	139
5.1		Introduction	141
5.2		Computational details	144
5.3		Results and discussion	144
	5.3.1	Competitive pathways for dihydrogen activation	144
	5.3.2	Further reactions of the “Si-H” silylene	148
	5.3.3	Intramolecular ring formation for the silylenes	150
	5.3.4	Solution to the problem of side reactions	153
5.4		Conclusions	156
5.5		References	156
6.	**Summary**		
6.1		Introduction	163
6.2		Focus of the thesis	163
6.3		Methodology used	164
6.4		Summary of the results	164
6.5		References	165

Abstract

Activation or cleavage of chemical bonds is essential in most chemical reactions such as biological processes, industrially important chemical reactions, as well as in the conversion of toxic molecules to less toxic or useful feed stocks. The development of catalysts for such reactions is an intriguing research area. These catalysts can be divided into two major families: heterogeneous and homogeneous catalysts. Many of the industrially important reactions are carried out with the aid of heterogeneous catalysts. However, in most cases such catalysts require severe reaction conditions such as higher temperature and pressure. The developments in the field of homogeneous catalysis allow the reactions to be completed in mild conditions with high efficiency. In homogeneous systems, both transition metal and main group based compounds have proved to play an indispensible role in activation processes, either stoichiometric or catalytic. In order to explore the catalysts and catalytic processes, a better understanding of the nature of catalysts in a reaction medium is essential, which can be attained from mechanistic investigations.

Advances in the field of computational techniques have made the modeling of chemical reactions easy and accurate. In this regard, density functional theory (DFT) is the state-of-the-art method for the study of kinetics and thermodynamics of chemical reactions. In this thesis, our interest is to model some of the important homogeneous chemical reactions using DFT and use various strategies to modify the existing catalysts or to predict new catalyst systems for these reactions processes.

The thesis entitled “Density functional theory (DFT) studies of the homogeneous activation of small molecules using transition metal and main group based compounds” is organized into five chapters.

Chapter 1

Chapter 1 begins with a brief introduction on the activation or cleavage of a chemical bond in small molecules and the importance of homogeneous reactions based on transition metal or main group compounds performing stoichiometric or catalytic activation of the specific bonds. This

chapter also recounts the catalytic small molecule activation process in important chemical reactions such as the water gas shift reaction (WGSR), olefin metathesis, ammonia borane dehydrogenation (AB), dihydrogen generation from water and alcohol and the stoichiometric activation of H_2 using silylenes, along with the associated problems. A detailed survey on these reactions and our motivation behind the research carried out has also been discussed.

Chapter 2

Chapter 2 describes the theoretical background for the methods used in the calculations. It begins with the introduction to the basics of DFT, which includes the Hohenberg-Kohn theorems and the Kohn-Sham formulation. Then we discuss about the Energetic Span Model (ESM) proposed by Shaik and co-workers, a method to calculate Turn Over Frequency (TOF) from a theoretically obtained energy profile. Following this, the free volume correction introduced by Mammen *et. al*. for the calculated translational entropy on the basis of the ideal gas law in Turbomole and other softwares has been described. Chapter 2 also narrates the spin-component scaled MP2 approach, solvent correction and the approximations incorporated in Turbomole, such as the resolution of identity (RI), along with the multipole accelerated resolution of identity (MARIJ) approximations.

Chapter 3

In this chapter, the small molecule activation using transition metal based catalysts have been investigated using DFT. Our focus has been to modify the experimentally known compounds for important reactions. Here, we have considered two reactions i) the homogeneous $Fe(CO)_5$ catalyzed water gas shift reaction ii) homogeneous olefin metathesis using the second generation Grubbs' catalyst. The chapter is divided into two parts, Chapter 3A and Chapter 3B, where the reactions (i) and (ii) and our approach to modifying the corresponding catalysts have been discussed respectively.

Chapter 3A

Cooperative interaction of metal centres in binuclear catalysts has proved to have advantages in catalysis over mononuclear catalysts. This has led us to rethink the possibility of binuclear

interaction in mononuclear systems during reaction processes. Full quantum mechanical calculations on the newly proposed binuclear mechanism for the $Fe(CO)_5$ catalyzed water gas shift reaction (WGSR) show the significance of metal−metal cooperativity in WGSR, an important reaction which enhances the H_2 production from CO and H_2O.The calculations indicate that the binuclear mechanism leads to lower barriers in comparison to the previously proposed mononuclear mechanisms. The comparison of the free energy profiles and the turn over frequency (TOF) obtained from the Energetic Span Model (ESM) indicate that bimetallic catalysts would be likely to be more highly active than mononuclear metal-based catalysts for the WGSR.

Chapter 3B

In catalytic processes, dissociation of an ancillary ligand, namely the leaving group, is required to generate an active catalytic centre with a vacant coordination site. One such catalyst is the ruthenium based second Generation Grubbs' catalyst for olefin metathesis where the well studied leaving group is PCy_3. However, the initiation step is slow in this system due to the presence of a strong Ru-P bond. Better leaving groups accelerate the initiation step through the facile dissociation and can be scavenged easily from the reaction medium. The modification of the Grubbs' catalysts with allenes and their derivatives as leaving groups show that they would perform significantly better than the existing PCy_3 ligand. The calculations also suggest that the most effective leaving groups are those having electron withdrawing groups, especially those that have the potential for supramolecular interactions between the substituent groups in the dissociated state.

Chapter 4

This chapter depicts the theoretical investigation on small molecule activation using main group based catalysts. Here, we have predicted new catalysts for reactions such as i) ammonia borane (AB) dehydrogenation and ii) dihydrogen generation from water and alcohols. This chapter is divided into two parts, Chapter 4A and Chapter 4B, where the reactions (i) and (ii) with the new catalysts have been discussed respectively.

Chapter 4A

The development of catalysts based on main group compounds is an interesting topic of research since recent studies show that these compounds can imitate transition metal compounds in activation processes. In this regard, new main group compounds that can mediate important reactions such as the catalytic dehydrogenation of ammonia borane have been predicted by employing DFT/SCS-MP2 methods. Computational investigations on recently synthesized Ga−N molecular cage compounds shows that they can catalyze the ammonia borane dehydrogenation reaction through the opening and closing of labile bonds present in the Ga-N molecular compound. The calculations also suggest that the cage contains multiple favorable sites for the activation of small molecules.

Chapter 4B

Hydrogen is considered as the fuel of the future. Main group compounds that can assist the catalytic dihydrogen production can provide a greener or cheaper solution to the problems associated with it. Our studies show that a modified germanium (II) hydride with boron atoms, such as $HC\{CMeArB\}_2GeH$ (Ar = 2,6-$^{i}Pr_2C_6H_3$), with the assistance of silicon based compounds such as SiF_3H, can perform significantly better than the existing state-of-the-art post-transition metal based systems for catalyzing the dihydrogen generation from water and alcohols through the protolysis reaction.

Chapter 5

Recently synthesized acyclic silylene compounds show that main group compounds can imitate transition metal compounds in small molecule activation processes. This chapter discusses the stoichiometric activation of H_2 molecule using acyclic silylenes. A full quantum chemical investigation with density functional theory demonstrates that undesired side reactions would be competitive in these systems during small molecule activation. Our studies show that for silylenes that cannot display single site small molecule activation due to the preference for competing side reactions, the desired final product can still be obtained by employing other reagents, such as hydrogenating agents in the place of dihydrogen.

Abbreviations

DFT	density functional theory
WGSR	water gas shift reaction
AB	ammonia borane
ESM	energetic Span Model
TOF	turn over frequency
MP2	second-order Møller–Plesset perturbation theory
SCS-MP2	spin-component scaled - MP2
RI	resolution of identity
MARIJ	multipole accelerated resolution of identity
ROMP	ring opening metathesis polymerization
NHC	N-heterocyclic carbene
DADB	diammonate of diborane
CDB	Cyclodiborazane
BCDB	B-(cyclodiborazanyl)aminoborohydride
CTB	Cyclotriborazane
0D	zero dimensional
Dipp	2,6-i$Pr_2C_6H_3$
CI	configuration interaction
CC	coupled cluster
KS	Kohn-Sham
LDA	local density approximation
GGA	generalized gradient approximation
PW	Perdew and Wang
LYP	Lee, Yang and Parr
PBE	Perdew, Burke and Ernzerhof
TST	transition state theory
TS	transition state
IRC	intrinsic reaction coordinate

TDTS	TOF determining transition state
TDI	TOF determining intermediate
COSMO	conductor-like screening model
SAS	solvent accessible surface
QM	quantum mechanical
PCM	polarizable continuum model
SMD	Solvation Model Based on Solute Electron Density
NBO	natural bond orbital
ECP	effective core potential
HOMO	highest occupied molecular orbitals
LUMO	lowest unoccupied molecular orbitals
PA	proton affinity
MO	molecular orbital
FLP	frustrated Lewis pair
Tptm	Tris(2-pyridylthio)methyl

List of Publications

1. **Nishamol Kuriakose**, Shantanu Kadam, and Kumar Vanka, A Theoretical Study of Metal−Metal Cooperativity in the Homogeneous Water Gas Shift Reaction, *Inorg*. *Chem*., **2012**, 51, 1, 377−385.

2. **Nishamol Kuriakose** and Kumar Vanka, Can Molecular Cages Be Effective at Small Molecule Activation? A Computational Investigation, *Inorg*. *Chem*., **2013**, 52, 8, 4238–4243.

3. **Nishamol Kuriakose** and Kumar Vanka, New insights into Small Molecule Activation by Acyclic Silylenes: A Computational Investigation, *Dalton Trans*., **2014**, 43, 2194-2201.

4. Vaishali S. Shende, Savita K. Shingote, Sudhindra H. Deshpande, **Nishamol Kuriakose**, Kumar Vanka and Ashutosh A. Kelkar, Asymmetric Transfer Hydrogenation of Imines in Water/Methanol Co-solvent System and Mechanistic Investigation by DFT study, *RSC Adv*., **2014**, 4, 46351-46356.

5. **Nishamol Kuriakose** and Kumar Vanka, Can Substituted Allenes be Highly Efficient Leaving Groups in Catalytic Processes? A Computational Investigation, *J*. *Comput*. *Chem*., **2015**, 36, 795-804 (*Invited inside cover page*).

6. **Nishamol Kuriakose** and Kumar Vanka, Can Main Group Systems Act as Superior Catalysts for Dihydrogen Generation Reactions? A Computational Investigation, *manuscript communicated*.

Chapter 1

Introduction to Small Molecule Activation

1.1 Introduction

The present thesis discusses small molecule activation and the use of transition metal and main group compounds to assist the activation processes. Generally, small molecules such as H_2O, CO, CO_2 and N_2 possess strong chemical bonds. In order to activate or break such bonds and to make the activation processes more efficient, we need the help of transition metal or main group based compounds. Such chemistry is important in many biological processes,[1-3] for example, in nitrogen fixation where nitrogenase enzymes assist the reaction. Water splitting and the subsequent generation of O_2 and H_2 requires very high energy and the development of catalytic systems for such reactions is an important area of research.[4-6] Another important process is the conversion of toxic molecules such as CO and CO_2 to less toxic or useful feed stocks such as methanol, HCOOH etc.[7,8] Activation processes and catalyst development are also important in other areas of research such as hydrogen production and storage.[9-11]

Many of the homogeneous catalysts provide improved yield in mild reaction conditions. Therefore, current research focuses on the development of homogeneous catalysts which offer high efficiency at mild reaction conditions. Our focus is to model some of the homogeneous chemical reactions which involve cleavage or activation of the chemical bond, using DFT. The reactions we have considered in the thesis include the water gas shift reaction (WGSR), olefin metathesis, ammonia borane dehydrogenation (AB), dihydrogen generation from water and alcohols and dihydrogen activation by silylene compounds. Our aim is to use various approaches to develop new compounds that can perform efficient catalytic or stoichiometric activation of these reactions. A detailed survey of each of these reactions and our research focus is discussed below.

1.2 The homogeneous reactions considered in the thesis

1.2.1 The water gas shift reaction (WGSR)

The WGSR is a key process in hydrogen production because it improves the hydrogen content of water gas, thereby enhancing the steam reforming process, as shown in equations 1.1 and 1.2.

$$CH_4 + H_2O \rightarrow CO + H_2 + CO_2 \qquad (1.1)$$

$$CO + H_2O \rightarrow CO_2 + H_2 \quad (1.2)$$

This reaction is also important as a side reaction in hydroformylation and the Fischer-Thorpe processes. Another important area where WGSR has implications is in the catalytic conversion of biomass to liquid fuels,[12-

can be the case in the WGSR where a monometallic pathway is conventionally considered. It is also important to note that the presence of a bimetallic species, $Fe_2(CO)_8OH^-$ has been reported during gas-phase experimental studies on the $Fe(CO)_5$-catalyzed WGSR, at increased flow rates of $Fe(CO)_5$.[23] Therefore, further investigation on a bimetallic pathway can bring out new insights and possible methods for the development of a catalyst for WGSR.

1.2.2 Olefin Metathesis

Olefin metathesis is an organic reaction in which the double bond is regenerated through the redistribution of the alkene fragments produced by the scission process. The development of catalysts for this reaction has been well studied. The initial catalytic systems used for the redistribution of the carbon-carbon double bond involve many homogeneous and heterogeneous catalysts. The first reports on olefin metathesis reaction include the use of the MoO_3/Al_2O_3 catalyst by Eleuterio and co-workers[34,35] in the ring opening polymerization of cycloolefin as well as the disproportionation of olefin at higher temperatures by Banks and Bailey[36] using heterogeneous catalysts. Some of the other reported heterogeneous catalysts for metathesis process are WCl_6/Bu_4Sn, $WOCl_4/EtAlCl_2$, MoO_3/SiO_2, and Re_2O_7/Al_2O_3[37]. The main limitation of these heterogeneous catalytic combinations is the requirement of severe experimental conditions to carry out the reaction and their incompatibility for most of the olefinic substrates bearing functional groups. Later, the homogeneous catalytic systems were developed for ring-opening polymerization of cycloolefin by Zeigler and co-workers[38,39] in 1963 and in the subsequent years, they were derived mainly from $MoCl_5$, WCl_6 and organoaluminum derivatives. However, the similar chemistry involved in ring-opening polymerization of cycloolefin as well as the olefin disproportionation has been recognized only in the late 1960s by Calderon and co-workers[40,41] and they coined the term “olefin metathesis” in 1967. Further attempts to understand the mechanism resulted in the proposal of a pair-wise exchange of alkylidene through a quasicyclobutane mechanism[41] and a metallacyclopentane rearrangement.[42] In 1971, Chauvin proposed a widely accepted metal-alkylidene based mechanism[43] for the metathesis process and the subsequent research led to the development of many catalytic systems including tungsten[44-46] and molybdenum based catalysts.[47,48]

Progressing research to improve the catalytic systems has focused on the development of functional group tolerant catalyst based on transition metals such as ruthenium. Initially, $RuCl_3$(hydrate)[49,50] and $Ru(H_2O)_6(tos)_2$[51] complexes were found to be good for ring opening metathesis polymerisation (ROMP) in the presence of water as solvent. However, the first well-defined ruthenium catalyst reported for the metathesis process is **1**[52] (see Figure 1.2), which was able to polymerize norbornene effectively, both in the presence and the absence of water or methanol as solvents. In the meantime, Grubbs and co-workers discovered an increased activity of the ruthenium catalyst with larger and more basic phosphines like PCy_3. The first ruthenium-PCy_3 complex reported to activate the acyclic olefin is **2**,[53] which has shown very good functional group tolerance. In this category, **3**[54,55] is the most active catalyst with a strong electron donating PCy_3 ligand and a benzylidene moiety and it is regarded as the first generation Grubbs' catalyst. Mechanistic studies revealed the presence of a monophosphine coordinated metal intermediate in the reaction process,[56,57] which suggested the development of catalysts with one of the ancillary ligands labile for improved catalytic activation.

The development in the field of carbene chemistry[58] and the strong σ donating ability of N-heterocyclic carbene (NHC) has made it a versatile ligand for olefin metathesis. Hermann and co-workers synthesized a Ru-metal complex **4**[59] by replacing both PCy_3 groups in the first generation catalyst **3**, by NHC ligands, which did not show any enhanced activity compared to **3** due to the presence of the less labile NHC ligand. An analogous compound **5** based on the NHC ligand has been synthesized independently by the groups of Nolan[60], Grubbs[61] and Fürstner,[62] by replacing one of the ancillary PCy_3 ligands with an unsaturated NHC ligand that was found to be very effective. However, an unsaturated analogue **6**[63] was even more active than **5**. Hence, this was recognized as the second generation olefin metathesis catalyst (see Figure 1.2). "For the development of the metathesis method in organic synthesis," Robert H. Grubbs[64] shared the Nobel Prize in 2005 along with Yves Chauvin[65] and Richard R. Schrock[66].

Further developments in the field of metathesis in order to improve the activity, stability, selectivity and other catalytic parameters led to the origin of various catalysts including a third generation Hoveyda-Grubb's catalyst **7**[67] (Figure 1.2), second generation pyridine derivatives[68], various ruthenium-alkylidine catalysts with

different alkylidine species[69], and so on. Water soluble analogues of the Grubbs' catalyst also have been reported.[70,71] This allows an easy removal of the dissociated ligand either by chemical trapping[72] or by phase transfer into an orthogonal solvent[73]. All these developments show that an easily removable ancillary labile ligand is necessary for the generation of the active centre. Also, it is important that the dissociated ligand should not participate in competitive side reactions. It is therefore important to consider the aspect of leaving group modification in the catalyst in all catalytic processes where dissociation of the leaving group is necessary to generate the active catalytic centre. Recent advances in the field of allene {$R_2C=C=CR_2$ (R = H)} chemistry show interesting aspects in this family of compounds.[74-79] Our aim has been to investige the potential of allene and their derivatives to act as efficient leaving groups in catalytic processes by considering Grubbs' second generation catalyst.

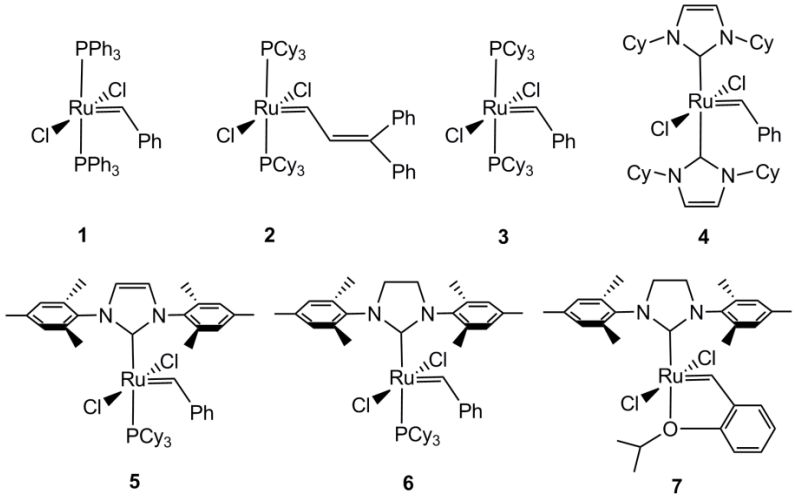

Figure 1.2 Reported ruthenium catalysts for olefin metathesis reaction.

1.2.3 Ammonia Borane Dehydrogenation

Ammonia Borane (AB) is an inorganic analogue of hydrocarbons. It is an important material for the hydrogen economy because of its low molecular weight and the highest weight percentage of hydrogen (19.6%).[9] AB was first prepared by Shore and Parry in 1955.[80] Generally, the synthesis of AB can be categorized into three types of reactions: salt-metathesis followed by H_2 release, Lewis acid-Lewis base exchange, or isomerisation of the diammonate of diborane (DADB).[9] AB exists as a molecular solid at room temperature.[81] Its experimental and material properties have been

explored by various spectroscopic and crystallographic techniques.[9] The thermal decomposition of AB in the solid state has been reported to take place in three steps. The first two temperature dependent pyrolysis steps occur at 110 ^{0}C-125 ^{0}C and 130 ^{0}C-155 ^{0}C, releasing one mol equivalent of dihydrogen per mole of ammonia borane (AB) at each of these steps.[82-86] The NH_2BH_2 moiety formed after the first dehydrogenation step is very unstable and it forms poly-amino borane which, in turn, gives the second equivalent of dihydrogen at 130 ^{0}C-155 ^{0}C. Here, the side product formed is borazine, an insoluble molecule. The third step begins only above 1170 ^{0}C leading to the semi-crystalline hexagonal boron nitride as a side product.[81] The three step dehydrogenation can be summarized as

$$NH_3\text{-}BH_3 \rightarrow 1/x\,(NH_2\text{-}BH_2)_x + H_2 \quad (1.3)$$

$$(NH_2\text{-}BH_2)_x \rightarrow (NH\text{-}BH)_x + H_2 \quad (1.4)$$

$$(NH\text{-}BH)_x \rightarrow BN + H_2 \quad (1.5)$$

The thermal decomposition study of AB in solution suggests second order kinetics in AB and the reaction includes various intermediates or side products such as the diammoniate of diborane (DADB), cyclo diborazane (CDB), B-(cyclo diborazanyl) amino borohydride (BCDB) and cyclo triborazane (CTB) along with dihydrogen.[87,88] Various computational investigations also shed light into various mechanistic and thermodynamic aspects of AB and its use as a hydrogen storage material.[89-93] In order to exploit NH_3BH_3 for hydrogen storage, it requires the release of more than one equivalent of H_2. For this purpose, well defined catalysts are necessary. In the past years, various catalytic strategies such as the use of nanoscaffolds,[94] acids,[95] bases[96] and metal catalysts has been explored for AB dehydrogenation. Metal catalyst based catalytic processes were found to be superior over the other methods. Some of the metal based catalysts include Ru based complexes,[97] Ir-pincer complexes,[98] nickel N-heterocyclic carbene (NHC) catalysts,[99] zirconocene based frustrated lewis pair complexes[100] etc. However, the metal based catalysts affect the AB regeneration processes significantly. Hence, the recent developments in catalytic AB dehydrogenation try to move away from transition-metal based systems.[101] Some of the recent studies also suggest that the main group based compounds can imitate transition-metal compounds in activation processes. A remarkable material in this regard is graphitic carbon nitride.[102] Another main group

system is that of the zero dimensional (0D) porous organic cages, which can act as catalysts due to the presence of latent Lewis acidity and basicity in the atoms of the 0D cages.[103] The potential of the main group based molecular cages containing labile bonds can be explored for catalytic small molecule activation since cages have never been used as catalysts for important chemical reactions. In this regard, our focus has been to consider a recently synthesized Ga-N cage compound by Uhl and co-workers as a potential main group compound for the catalytic AB dehydrogenation.[104]

1.2.4 Dihydrogen generation from water and alcohols

The replacement of existing fossil fuels with an efficient alternative energy resource is essential to meet the growing energy demands. A promising candidate for this purpose is dihydrogen, a fuel which is known to have the highest energy density per unit of mass compared to other known fuels. Furthermore, dihydrogen is also non-toxic and green. Therefore, many attempts have been made through important chemical reactions such as the steam reforming processes,[105] the water gas shift reaction[16,17,106] (WGSR), as well as through the biomass conversion of hydrocarbons[14,107] and alcohols[108-112] to improve dihydrogen production. However, the handling of hydrogen fuel for practical applications is still difficult, since it requires better storage and transport facilities. Therefore, there is considerable interest in the possibility of the chemical storage of hydrogen. One of the important and suitable methods is protolysis of organosilanes[113-119] with water or alcohols. Organosilanes can generate dihydrogen by the protolytic cleavage of the Si-H bond with water or alcohols and the side products are also reported to have commercial value. However, the reaction is kinetically slow and therefore better catalysts are required for efficient transformation. Some of the heterogeneous catalysts for this reaction are $[RuCl_2(p\text{-cymene})]_2$ on carbon,[120] Pt-nanoparticle,[121] and a gold–nanotube hybrid.[122] Efficient homogeneous transition metal based catalyst systems also reported, which includes a cationic oxorhenium (V) catalyst,[123,124] arene $Cr(CO)_2(\eta^2\text{-}HSiHPh_2)$,[114] $(Ph_3PCuH)_6$,[115] iridium (III) bis-N-heterocyclic carbene complexes[125] and $Ru_2(CO)_4L_2X_4$ (L = CO or PPh_3; X = Cl or Br).[126] Recently, Parkin and coworkers reported a Zn metal based catalyst that could do efficient dihydrogen generation through hydrolysis or alcoholysis of organosilanes. All these catalysts are based on precious metals. As discussed previously, we can have better alternatives

from main group compounds that can imitate the transition metal complexes in activation processes. Recent developments in low-valent Group 14 hydrides have shown that these compounds can have significant contributions in small molecule activation.[127-132] In the conversion of carbonyl compounds to their hydroborated analogues, HBpin has been employed[132] along with germanium (II) and tin (II) hydride compounds, with efficiencies rivalling the most active catalysts presently available for such reactions. The monomeric terminal hydrides LMH [M = Ge or Sn, L = $CH\{N(Ar)(CMe)\}_2$, Ar = 2, 6-$^{i}Pr_2C_6H_3$] activate small molecules such as CO_2, ketones, alkenes, as well as azo and diazo compounds and lead to the corresponding formate, alkoxide, vinyl and hydrazone derivative of the Ge (II) hydride.[133-137] Due to the presence of a strong Ge-O bond, these derivatives are not able to regenerate the Ge (II) hydride. However Sakaki and coworkers have shown that a catalytic cycle can be obtained through the use of silanes.[131] If such a catalytic cycle can be generated for a Ge (II) hydride compound in dihydrogen generation through the protolysis or alcoholysis of silanes, then it can be utilized for the on-demand hydrogen storage processes. Since water and alcohols are important feedstock that can provide dihydrogen through protolysis, our focus has been to investigate the potential Ge (II) hydride compounds in the generation of dihydrogen through the protolytic cleavage of O-H bond in these molecules.

1.2.5 Small molecule activation using silylene compounds

The silicon analogue of carbene, namely silylene, is considered as the monomer of polysilanes. These are divalent compounds with +2 oxidation state and the reported systems include dicoordinated[172,173] or tricoordinated[138-143] silylenes. The first stable silylene has been reported in 1994 by West and co-workers,[144] and is analogous to the stable N-heterocyclic carbene isolated by Arduengo *et al*. in 1991.[58] Subsequently, Kira and co-workers have successfully isolated the first cyclic dialkyl silylene by the reduction of the corresponding dibromo silane with potassium graphite.[145] In the past two decades, an extensive number of stable silylenes and other higher metallylenes have been reported.[146,147] These include major contributions from the research groups of West,[144,148-152] Lappert,[153-157] Roesky,[138,139,158,159] Power,[157,160] and Driess.[161-163] The chemical properties of silylenes and other metallylene are important because of their similarities, as well as their differences when compared to

carbenes. The metallylenes synthesized to date have a singlet ground state, with the presence of a lone pair having predominantly s-character[147] and a vacant p-orbital.

Even though the reported systems of isolable cyclic silylenes,[58,144,145,161,164,165] and functionalized silylenes with increased coordination number at the silicon atom,[138-143] are extensive in literature, reports on acyclic dicoordinate silylenes have been rare, as the isolation of such compounds as stable monomeric species is difficult. The bis (diisopropy1 amino) carbene synthesized by Alder *et al*.[166] is regarded as the first successfully isolated acyclic carbene. Stable acyclic metallylenes having the molecular formula $E\{N(SiMe_3)_2\}_2$ (where E= Ge, Sn, and Pb) have been isolated as thermally stable compounds by Power and co-workers in 1977.[157] Its silicon analogue was found to be stable in solution at low temperature, with rapid decomposition above 0 ^{0}C.[150] Jutzi and co-workers have reported two acyclic silicon compounds made through the salt metathesis reaction.[167-169] An acyclic imino-substituted silylene was found to react with $B(C_6F_5)_3$ and form a stable silylene–borane adduct.[170] Other reported acyclic silylenes include the acyclic, monomeric tetrylene dichalcogenolates of the formula $M(ChAr)_2$ (M = Si, Ge, Sn, Pb; Ch = O, S, or Se; Ar = bulky *m*-terphenyl ligand), synthesized by Power and co-workers.[171] Rekken *et al*.[160] have reported the synthesis of a stable silylene coordinated to two thiolate sulphur groups, $Si\{S(C_6H_3\text{-}2,6(C_6H_2\text{-}2,4,6\text{-}Me_3)_2)\}_2$.

Several experimental[172-176] and theoretical studies[172,177-179] have explored the potential of silylenes and other metallylenes in activation processes. In addition to the activation of small molecules like O_2,[173,180] NO,[173] CO,[174] H_2O,[172,178,181,182] and CO_2,[179,183] the O-H bond activation in alcohols[151,155] by various silylenes and germylenes,[178,179,182] and the O-H bond activation in the water molecule by silylenes[172,177,181] have also been investigated. The reactivity of N-heterocyclic analogues of silylene, having a ring size varying from four to six, with various molecules has been well studied.[184-187] However, the cyclic silylenes are less reactive towards H_2 and NH_3 substrates and a computational study by Wang *et. al*. predicted that the acyclic derivatives featuring a more obtuse angle at silicon can offer enhanced reactivity towards such systems. Subsequent study by Aldridge and co-workers reported the synthesis of two stable acyclic silylenes, a stable mixed (amido) boryl silylene, $Si\{B(NDippCH)_2\}\{N(SiMe_3)Dipp\}$, (Dipp = 2,6-^{i}Pr$_2C_6H_3$),[188] and the silyl coordinated silylene, $Si\{Si(SiMe_3)_3\}\{N(SiMe_3)Dipp\}$.[189] These silylenes are

interesting because of their facile single site activation of the H_2 molecule at 0 ^{0}C, thereby imitating transition metal complexes in reactivity. In order to explore the potential of acyclic silylenes in bond activation, it is essential to understand why the other acyclic silylenes, such as the two thiolate sulphur groups coordinated silylene, such as $Si\{S(C_6H_3\text{-}2,6(C_6H_2\text{-}2,4,6\text{-}Me_3)_2)\}_2$ have not been reported to activate dihydrogen, [160] or show evidence of other types of small molecule activation. It is also required to investigate the possibility of competitive side reactions occurring during small molecule activation by the silylene, which can provide further assistance to the development of acyclic silylenes in the future.

1.3 Conclusions

As mentioned earlier, an efficient activation of small molecule can be attained by better catalysts. In this regard, transition metal and main group based compounds play an important role in the catalysis processes. The development of these compounds for homogeneous reaction conditions will be more significant since this will help the reaction process proceed in a mild reaction environment. Our aim has been to employ density functional theory (DFT) to model important homogeneous chemical processes and to use various strategies to develop new catalysts for such reactions. We have considered mainly five reactions: the water gas shift reaction (WGSR), olefin metathesis, ammonia borane dehydrogenation (AB), dihydrogen generation from water and alcohols and dihydrogen activation by silylene compounds. The detailed investigation and the results of each reaction are provided in the subsequent chapters.

1.4 References

(1) Shaver, M. P.; Fryzuk, M. D. *Adv*. *Synth*. *Catal*. **2003**, *345*, 1061-1076.

(2) Fryzuk, M. D.; Johnson, S. A. *Coord*. *Chem*. *Rev*. **2000**, *200*, 379-409.

(3) MacKay, B. A.; Fryzuk, M. D. *Chem*. *Rev*. **2004**, *104*, 385-402.

(4) Fillol, J. L.; Codolà, Z.; Garcia-Bosch, I.; Gómez, L.; Pla, J. J.; Costas, M. *Nat*. *Chem*. **2011**, *3*, 807-813.

(5) Wasylenko, D. J.; Palmer, R. D.; Berlinguette, C. P. *Chem*. *Comm*. **2013**, *49*, 218-227.

(6) Kohl, S. W.; Weiner, L.; Schwartsburd, L.; Konstantinovski, L.; Shimon, L. J. W.; Ben-David, Y.; Iron, M. A.; Milstein, D. *Science* **2009**, *324*, 74-77.

(7) Jessop, P. G.; Ikariya, T.; Noyori, R. *Chem*. *Rev*. **1995**, *95*, 259-272.

(8) Wang, W.; Wang, S.; Ma, X.; Gong, J. *Chem*. *Soc*. *Rev*. **2011**, *40*, 3703-3727.

(9) Staubitz, A.; Robertson, A. P. M.; Manners, I. *Chem*. *Rev*. **2010**, *110*, 4079.

(10) Staubitz, A.; Robertson, A. P. M.; Sloan, M. E.; Manners, I. *Chem*. *Rev*. **2010**, *110*, 4023-4078.

(11) Power, P. P. *Chem*. *Rec*. **2012**, *12*, 238-255.

(12) Kunkes, E. L.; Simonetti, D. A.; West, R. M.; Serrano-Ruiz, J. C.; Gärtner, C. A.; Dumesic, J. A. *Science* **2008**, *322*, 417-421.

(13) Kim, W. B.; Voitl, T.; Rodriguez-Rivera, G. J.; Dumesic, J. A. *Science* **2004**, *305*, 1280-1283.

(14) Huber, G. W.; Shabaker, J. W.; Dumesic, J. A. *Science* **2003**, *300*, 2075-2077.

(15) Luengnaruemitchai, A.; Osuwan, S.; Gulari, E. *Catal*. *Comm*. **2003**, *4*, 215-221.

(16) Ford, P. C. *Acc*. *Chem*. *Res*. **1981**, *14*, 31-37.

(17) Laine, R. M.; Rinker, R. G.; Ford, P. C. *J*. *Am*. *Chem*. *Soc*. **1977**, *99*, 252-253.

(18) King, R. B.; Frazier, C. C.; Hanes, R. M.; King, A. D. *J*. *Am*. *Chem*. *Soc*. **1978**, *100*, 2925-2927.

(19) Ungermann, C.; Landis, V.; Moya, S. A.; Cohen, H.; Walker, H.; Pearson, R. G.; Rinker, R. G.; Ford, P. C. *J*. *Am*. *Chem*. *Soc*. **1979**, *101*, 5922-5929.

(20) Kang, H. C.; Mauldin, C. H.; Cole, T.; Slegeir, W.; Cann, K.; Pettit, R. *J*. *Am*. *Chem*. *Soc*. **1977**, *99*, 8323-8325.

(21) Grice, N.; Kao, S. C.; Pettit, R. *J*. *Am*. *Chem*. *Soc*. **1979**, *101*, 1627-1628.

(22) Sunderlin, L. S.; Squires, R. R. *J*. *Am*. *Chem*. *Soc*. **1993**, *115*, 337-343.

(23) Lane, K. R.; Lee, R. E.; Sallans, L.; Squires, R. R. *J*. *Am*. *Chem*. *Soc*. **1984**, *106*, 5767-5772.

(24) Torrent, M.; Sola , M.; Frenking, G. *Organometallics* **1999**, *18*, 2801-2812.

(25) Barrows, S. E. *Inorg*. *Chem*. **2004**, *43*, 8236-8238.

(26) Rozanska, X.; Vuilleumier, R. *Inorg*. *Chem*. **2008**, *47*, 8635-8640.

(27) Zhang, F.; Zhao, L.; Xu, C.; Chen, Y. *Inorg*. *Chem*., *49*, 3278-3281.

(28) Xia, F.; Cao, Z. *J*. *Phys*. *Chem*. *A* **2006**, *110*, 10078-10083.

(29) Esswein, A. J.; Veige, A. S.; Piccoli, P. M. B.; Schultz, A. J.; Nocera, D. G. *Organometallics* **2008**, *27*, 1073-1083.

(30) Torkelson, J. R.; Antwi-Nsiah, F. H.; McDonald, R.; Cowie, M.; Pruis, J. G.; Jalkanen, K. J.; DeKock, R. L. *J*. *Am*. *Chem*. *Soc*. **1999**, *121*, 3666-3683.

(31) Burress, C. N.; Bodine, M. I.; Elbjeirami, O.; Reibenspies, J. H.; Omary, M. A.; Gabbaï, F. P. *Inorg*. *Chem*. **2007**, *46*, 1388-1395.

(32) Motta, A.; Fragala`, I. L.; Marks, T. J. *J*. *Am*. *Chem*. *Soc*. **2009**, *131*, 3974-3984.

(33) Luo, Y.; Hou, Z. *Organometallics* **2006**, *25*, 6162-6165.

(34) Eleuterio, H. S. *U*. *S*. *Patent* **1963**, *3, 074, 918*.

(35) Eleuterio, H. S. *J*. *Mol*. *Catal*. **1991**, *65*, 55-61.

(36) Banks, R. L.; Bailey, G. C. *Ind*. *Eng*. *Chem*. *Prod*. *Res*. *Dev*. **1964**, *3*, 170-173.

(37) Trnka, T. M.; Grubbs, R. H. *Acc*. *Chem*. *Res*. **2000**, *34*, 18-29.

(38) Natta, G.; Dall'Asta, G.; Mazzanti, G.; Motroni, G. *Makromol*. *Chem*. **1963**, *69*, 163-179.

(39) Natta, G.; Dall'Asta, G.; Bassi, I. W.; Carella, G. *Makromol*. *Chem*. **1966**, *91*, 87-106.

(40) Calderon, N. *Acc*. *Chem*. *Res*. **1972**, *5*, 127-132.

(41) Calderon, N.; Chen, H. Y.; Scott, K. W. *Tetrahedron Lett*. **1967**, *8*, 3327-3329.

(42) Grubbs, R. H.; Miyashita, A.; Liu, M.-I. M.; Burk, P. L. *J*. *Am*. *Chem*. *Soc*. **1977**, *99*, 3863-3864.

(43) Jean-Louis Hérisson, P.; Chauvin, Y. *Makromol*. *Chem*. **1971**, *141*, 161-176.

(44) Katz, T. J.; Sivavec, T. M. *J*. *Am*. *Chem*. *Soc*. **1985**, *107*, 737-738.

(45) Katz, T. J.; Lee, S. J.; Acton, N. *Tetrahedron Lett*. **1976**, *17*, 4247-4250.

(46) Kress, J.; Osborn, J. A.; Greene, R. M. E.; Ivin, K. J.; Rooney, J. J. *J*. *Am*. *Chem*. *Soc*. **1987**, *109*, 899-901.

(47) Schrock, R. R. *Tetrahedron* **1999**, *55*, 8141-8153.

(48) Schrock, R. R. *Acc*. *Chem*. *Res*. **1990**, *23*, 158-165.

(49) Hillmyer, M. A.; Lepetit, C.; McGrath, D. V.; Novak, B. M.; Grubbs, R. H. *Macromolecules* **1992**, *25*, 3345-3350.

(50) Novak, B. M.; Grubbs, R. H. *J*. *Am*. *Chem*. *Soc*. **1988**, *110*, 7542-7543.

(51) McGrath, D. V.; Grubbs, R. H.; Ziller, J. W. *J*. *Am*. *Chem*. *Soc*. **1991**, *113*, 3611-3613.

(52) Nguyen, S. T.; Johnson, L. K.; Grubbs, R. H.; Ziller, J. W. *J*. *Am*. *Chem*. *Soc*. **1992**, *114*, 3974-3975.

(53) Nguyen, S. T.; Grubbs, R. H.; Ziller, J. W. *J*. *Am*. *Chem*. *Soc*. **1993**, *115*, 9858-9859.

(54) Schwab, P.; France, M. B.; Ziller, J. W.; Grubbs, R. H. *Angew*. *Chem*. *Int*. *Ed*. *Eng*. **1995**, *34*, 2039-2041.

(55) Schwab, P.; Grubbs, R. H.; Ziller, J. W. *J*. *Am*. *Chem*. *Soc*. **1996**, *118*, 100-110.

(56) Adlhart, C.; Hinderling, C.; Baumann, H.; Chen, P. *J*. *Am*. *Chem*. *Soc*. **2000**, *122*, 8204-8214.

(57) Hinderling, C.; Adlhart, C.; Chen, P. *Angew*. *Chem*. *Int*. *Ed*. **1998**, *37*, 2685-2689.

(58) Arduengo, A. J.; Harlow, R. L.; Kline, M. *J*. *Am*. *Chem*. *Soc*. **1991**, *113*, 361-363.

(59) Weskamp, T.; Schattenmann, W. C.; Spiegler, M.; Herrmann, W. A. *Angew*. *Chem*. *Int*. *Ed*. **1998**, *37*, 2490-2493.

(60) Huang, J.; Stevens, E. D.; Nolan, S. P.; Petersen, J. L. *J*. *Am*. *Chem*. *Soc*. **1999**, *121*, 2674-2678.

(61) Scholl, M.; Trnka, T. M.; Morgan, J. P.; Grubbs, R. H. *Tetrahedron Lett*. **1999**, *40*, 2247-2250.

(62) Ackermann, L.; Fürstner, A.; Weskamp, T.; Kohl, F. J.; Herrmann, W. A. *Tetrahedron Lett*. **1999**, *40*, 4787-4790.

(63) Scholl, M.; Ding, S.; Lee, C. W.; Grubbs, R. H. *Org*. *Lett*. **1999**, *1*, 953-956.

(64) Grubbs, R. H. *Adv*. *Synth*. *Catal*. **2007**, *349*, 34-40.

(65) Chauvin, Y. *Angew*. *Chem*. *Int*. *Ed*. **2006**, *45*, 3740-3747.

(66) Schrock, R. R. *Angew*. *Chem*. *Int*. *Ed*. **2006**, *45*, 3748-3759.

(67) Kingsbury, J. S.; Harrity, J. P. A.; Bonitatebus, P. J.; Hoveyda, A. H. *J*. *Am*. *Chem*. *Soc*. **1999**, *121*, 791-799.

(68) Love, J. A.; Morgan, J. P.; Trnka, T. M.; Grubbs, R. H. *Angew*. *Chem*. *Int*. *Ed*. **2002**, *41*, 4035-4037.

(69) Romero, P. E.; Piers, W. E.; McDonald, R. *Angew*. *Chem*. *Int*. *Ed*. **2004**, *43*, 6161-6165.

(70) Lynn, D. M.; Mohr, B.; Grubbs, R. H.; Henling, L. M.; Day, M. W. *J*. *Am*. *Chem*. *Soc*. **2000**, *122*, 6601-6609.

(71) Hong, S. H.; Grubbs, R. H. *J*. *Am*. *Chem*. *Soc*. **2006**, *128*, 3508-3509.

(72) Thompson, L. A. *Curr*. *Opin*. *Chem*. *Biol*. **2000**, *4*, 324-337.

(73) Xi, Z.; Bazzi, H. S.; Gladysz, J. A. *Org*. *Lett*. **2011**, *13*, 6188-6191.

(74) Alcarazo, M.; Lehmann, C. W.; Anoop, A.; Thiel, W.; Fürstner, A. *Nat*. *Chem*. **2009**, *1*, 295-301.

(75) Fürstner, A.; Alcarazo, M.; Goddard, R.; Lehmann, C. W. *Angew*. *Chem*. *Int*. *Ed*. **2008**, *47*, 3210-3214.

(76) Hänninen, M. M.; Peuronen, A.; Tuononen, H. M. *Chem*. - *Eur*. *J*. **2009**, *15*, 7287-7291.

(77) Esterhuysen, C.; Frenking, G. *Chem*. - *Eur*. *J*. **2011**, *17*, 9944-9956.

(78) Dyker, C. A.; Lavallo, V.; Donnadieu, B.; Bertrand, G. *Angew*. *Chem*. *Int*. *Ed*. **2008**, *47*, 3206-3209.

(79) Weber, E.; Seichter, W.; Hess, B.; Will, G.; Dasting, H.-J. *J*. *Phys*. *Org*. *Chem*. **1995**, *8*, 94-96.

(80) Shore, S. G.; Parry, R. W. *J*. *Am*. *Chem*. *Soc*. **1955**, *77*, 6084-6085.

(81) Frueh, S.; Kellett, R.; Mallery, C.; Molter, T.; Willis, W. S.; King'ondu, C.; Suib, S. L. *Inorg*. *Chem*. **2011**, *50*, 783-792.

(82) Hu, M. G.; Geanangel, R. A.; Wendlandt, W. W. *Thermochim*. *Acta* **1978**, *23*, 249-255.

(83) Sit, V.; Geanangel, R. A.; Wendlandt, W. W. *Thermochim*. *Acta* **1987**, *113*, 379-382.

(84) Wolf, G.; Baumann, J.; Baitalow, F.; Hoffmann, F. P. *Thermochim*. *Acta* **2000**, *343*, 19-25.

(85) Baitalow, F.; Baumann, J.; Wolf, G.; Jaenicke-Rößler, K.; Leitner, G. *Thermochim*. *Acta* **2002**, *391*, 159-168.

(86) Baumann, J.; Baitalow, F.; Wolf, G. *Thermochim*. *Acta* **2005**, *430*, 9-14.

(87) Wang, J. S.; Geanangel, R. A. *Inorganica Chim*. *Acta* **1988**, *148*, 185-190.

(88) Shaw, W. J.; Linehan, J. C.; Szymczak, N. K.; Heldebrant, D. J.; Yonker, C.; Camaioni, D. M.; Baker, R. T.; Autrey, T. *Angew*. *Chem*. *Int*. *Ed*. **2008**, *47*, 7493-7496.

(89) Richardson, T.; de Gala, S.; Crabtree, R. H.; Siegbahn, P. E. M. *J*. *Am*. *Chem*. *Soc*. **1995**, *117*, 12875-12876.

(90) Cramer, C. J.; Gladfelter, W. L. *Inorg*. *Chem*. **1997**, *36*, 5358-5362.

(91) Popelier, P. L. A. *J*. *Phys*. *Chem*. *A* **1998**, *102*, 1873-1878.

(92) Morrison, C. A.; Siddick, M. M. *Angew*. *Chem*. *Int*. *Ed*. **2004**, *43*, 4780-4782.

(93) Mo, Y.; Song, L.; Wu, W.; Zhang, Q. *J*. *Am*. *Chem*. *Soc*. **2004**, *126*, 3974-82.

(94) Aijaz, A.; Karkamkar, A.; Choi, Y. J.; Tsumori, N.; Rönnebro, E.; Autrey, T.; Shioyama, H.; Xu, Q. *J*. *Am*. *Chem*. *Soc*. **2012**, *134*, 13926-13929.

(95) Stephens, F. H.; Baker, R. T.; Matus, M. H.; Grant, D. J.; Dixon, D. A. *Angew*. *Chem*. *Int*. *Ed*. **2007**, *46*, 746-749.

(96) Ewing, W. C.; Marchione, A.; Himmelberger, D. W.; Carroll, P. J.; Sneddon, L. G. *J*. *Am*. *Chem*. *Soc*. **2011**, *133*, 17093-17099.

(97) Blaquiere, N.; Diallo-Garcia, S.; Gorelsky, S. I.; Black, D. A.; Fagnou, K. *J*. *Am*. *Chem*. *Soc*. **2008**, *130*, 14034-14035.

(98) Paul, A.; Musgrave, C. B. *Angew*. *Chem*. *Int*. *Ed*. **2007**, *46*, 8153-8156.

(99) Keaton, R. J.; Blacquiere, J. M.; Baker, R. T. *J*. *Am*. *Chem*. *Soc*. **2007**, *129*, 1844-1845.

(100) Chapman, A. M.; Haddow, M. F.; Wass, D. F. *J*. *Am*. *Chem*. *Soc*. **2011**, *133*, 8826-8829.

(101) Kim, Y.; Baek, H.; Lee, J. H.; Yeo, S.; Kim, K.; Hwang, S.-J.; Eun, B.; Nam, S. W.; Lim, T.-H.; Yoon, C. W. *Phys*. *Chem*. *Chem*. *Phys*. **2013**, *15*, 19584-19594.

(102) Tang, Z.; Chen, X.; Chen, H.; Wu, L.; Yu, X. *Angew*. *Chem*. *Int*. *Ed*. **2013**, *52*, 5832-5835.

(103) Pal, A.; Vanka, K. *Chem*. *Comm*. **2011**, *47*, 11417-11419.

(104) Uhl, W.; Abel, T.; Hagemeier, E.; Hepp, A.; Layh, M.; Rezaeirad, B.; Luftmann, H. *Inorg*. *Chem*. **2011**, *50*, 325-335.

(105) Collodi, G.; Wheeler, F. *Chem*. *Eng*. *Trans*. **2010**, *19*.

(106) Kuriakose, N.; Kadam, S.; Vanka, K. *Inorg*. *Chem*. **2012**, *51*, 377-385.

(107) Kunkes, E. L.; Simonetti, D. A.; West, R. M.; Serrano-Ruiz, J. C.; Gärtner, C. A.; Dumesic, J. A. *Science* **2008**, *322*, 417-421.

(108) Navarro, R. M.; Peña, M. A.; Fierro, J. L. G. *Chem*. *Rev*. **2007**, *107*, 3952-91.

(109) Palo, D. R.; Dagle, R. A.; Holladay, J. D. *Chem*. *Rev*. **2007**, *107*, 3992-4021.

(110) Mattos, L. V.; Jacobs, G.; Davis, B. H.; Noronha, F. B. *Chem*. *Rev*. **2012**, *112*, 4094-4123.

(111) Piscina, P. R. d. l.; Homs, N. *Chem*. *Soc*. *Rev*. **2008**, *37*, 2459-2467.

(112) Sun, J.; Wang, Y. *ACS Catal*. **2014**, *4*, 1078-1090.

(113) Luo, X. L.; Crabtree, R. H. *J*. *Am*. *Chem*. *Soc*. **1989**, *111*, 2527-2535.

(114) Matarasso-Tchiroukhine, E. *J*. *Chem*. *Soc*., *Chem*. *Comm*. **1990**, 681-682.

(115) Schubert, U.; Lorenz, C. *Inorg*. *Chem*. **1997**, *36*, 1258-1259.

(116) Chang, S.; Scharrer, E.; Brookhart, M. *J. Mol. Catal. A: Chemical* **1998**, *130*, 107-119.

(117) Blackwell, J. M.; Foster, K. L.; Beck, V. H.; Piers, W. E. *J. Org. Chem.* **1999**, *64*, 4887-4892.

(118) Brunel, J. M. *Int. J. Hydrogen Energy* **2010**, *35*, 3401-3405.

(119) Sattler, W.; Parkin, G. *J. Am. Chem. Soc.* **2012**, *134*, 17462-17465.

(120) Choi, E.; Lee, C.; Na, Y.; Chang, S. *Org. Lett.* **2002**, *4*, 2369-2371.

(121) Chauhan, B. P. S.; Sarkar, A.; Chauhan, M.; Roka, A. *Appl. Organomet. Chem.* **2009**, *23*, 385-390.

(122) John, J.; Gravel, E.; Hagège, A.; Li, H.; Gacoin, T.; Doris, E. *Angew. Chem. Int. Ed.* **2011**, *50*, 7533-7536.

(123) Ison, E. A.; Corbin, R. A.; Abu-Omar, M. M. *J. Am. Chem. Soc.* **2005**, *127*, 11938-11939.

(124) Corbin, R. A.; Ison, E. A.; Abu-Omar, M. M. *Dalton Trans.* **2009**, 2850-2855.

(125) Aliaga-Lavrijsen, M.; Iglesias, M.; Cebollada, A.; Garcés, K.; García, N.; Sanz Miguel, P. J.; Fernández-Alvarez, F. J.; Pérez-Torrente, J. J.; Oro, L. A. *Organometallics* **2015**, *10.1021/om5011726*.

(126) Tan, S. T.; Kee, J. W.; Fan, W. Y. *Organometallics* **2011**, *30*, 4008-4013.

(127) Rivard, E.; Power, P. P. *Dalton Trans.* **2008**, 4336-4343.

(128) Rodriguez, R.; Gau, D.; Contie, Y.; Kato, T.; Saffon-Merceron, N.; Baceiredo, A. *Angew. Chem. Int. Ed.* **2011**, *50*, 11492-11495.

(129) Fang, H.; Ling, Z.; Brothers, P. J.; Fu, X. *Chem. Comm.* **2011**, *47*, 11677-79.

(130) Choong, S. L.; Woodul, W. D.; Schenk, C.; Stasch, A.; Richards, A. F.; Jones, C. *Organometallics* **2011**, *30*, 5543-5550.

(131) Takagi, N.; Sakaki, S. *J. Am. Chem. Soc.* **2013**, *135*, 8955-8965.

(132) Hadlington, T. J.; Hermann, M.; Frenking, G.; Jones, C. *J. Am. Chem. Soc.* **2014**, *136*, 3028-3031.

(133) Pineda, L. W.; Jancik, V.; Starke, K.; Oswald, R. B.; Roesky, H. W. *Angew. Chem. Int. Ed.* **2006**, *45*, 2602-2605.

(134) Jana, A.; Ghoshal, D.; Roesky, H. W.; Objartel, I.; Schwab, G.; Stalke, D. *J. Am. Chem. Soc.* **2009**, *131*, 1288-1293.

(135) Jana, A.; Roesky, H. W.; Schulzke, C. *Dalton Trans.* **2010**, *39*, 132-138.

(136) Jana, A.; Tavcar, G.; Roesky, H. W.; John, M. *Dalton Trans.* **2010**, *39*, 9487-9489.

(137) Mandal, S. K.; Roesky, H. W. *Acc*. *Chem*. *Res*. **2012**, *45*, 298-307.

(138) Nagendran, S.; Roesky, H. W. *Organometallics* **2008**, *27*, 457-492.

(139) So, C.-W.; Roesky, H. W.; Magull, J.; Oswald, R. B. *Angew*. *Chem*. *Int*. *Ed*. **2006**, *45*, 3948-3950.

(140) Sen, S. S.; Roesky, H. W.; Stern, D.; Henn, J.; Stalke, D. *J*. *Am*. *Chem*. *Soc*. **2010**, *132*, 1123-1126.

(141) Sen, S. S.; Hey, J.; Herbst-Irmer, R.; Roesky, H. W.; Stalke, D. *J*. *Am*. *Chem*. *Soc*. **2011**, *133*, 12311-12316.

(142) Ghadwal, R. S.; Roesky, H. W.; Merkel, S.; Henn, J.; Stalke, D. *Angew*. *Chem*. *Int*. *Ed*. **2009**, *48*, 5683-5686.

(143) Filippou, A. C.; Chernov, O.; Schnakenburg, G. *Angew*. *Chem*. *Int*. *Ed*. **2009**, *48*, 5687-5690.

(144) Denk, M.; Lennon, R.; Hayashi, R.; West, R.; Belyakov, A. V.; Verne, H. P.; Haaland, A.; Wagner, M.; Metzler, N. *J*. *Am*. *Chem*. *Soc*. **1994**, *116*, 2691-2692.

(145) Kira, M.; Ishida, S.; Iwamoto, T.; Kabuto, C. *J*. *Am*. *Chem*. *Soc*. **1999**, *121*, 9722-9723.

(146) Tokitoh, N.; Okazaki, R. *Coord*. *Chem*. *Rev*. **2000**, *210*, 251-277.

(147) Mizuhata, Y.; Sasamori, T.; Tokitoh, N. *Chem*. *Rev*. **2009**, *109*, 3479-3511.

(148) Haaf, M.; Schmedake, T. A.; West, R. *Acc*. *Chem*. *Res*. **2000**, *33*, 704-714.

(149) Hill, N. J.; West, R. *J*. *Organomet*. *Chem*. **2004**, *689*, 4165-4183.

(150) Lee, G.-H.; West, R.; Muller, T. *J*. *Am*. *Chem*. *Soc*. **2003**, *125*, 8114-8115.

(151) Haaf, M.; Schmiedl, A.; Schmedake, T. A.; Powell, D. R.; Millevolte, A. J.; Denk, M.; West, R. *J*. *Am*. *Chem*. *Soc*. **1998**, *120*, 12714-12719.

(152) Li, W.; Hill, N. J.; Tomasik, A. C.; Bikzhanova, G.; West, R. *Organometallics* **2006**, *25*, 3802-3805.

(153) Lappert, M. F.; Rowe, R. S. *Coord*. *Chem*. *Rev*. **1990**, *100*, 267-292.

(154) Gehrhus, B.; Lappert, M. F. *J*. *Organomet*. *Chem*. **2001**, *617-618*, 209-223.

(155) Gehrhus, B.; Lappert, M. F.; Heinicke, J.; Boese, R.; Bläser, D. *J*. *Chem*. *Soc*., *Chem*. *Comm*. **1995**, 1931-1932.

(156) Gehrhus, B.; Hitchcock, P. B.; Lappert, M. F.; Heinicke, J.; Boese, R.; Bläser, D. *J*. *Organomet*. *Chem*. **1996**, *521*, 211-220.

(157) Gynane, M. J. S.; Harris, D. H.; Lappert, M. F.; Power, P. P.; Riviere, P.; Riviere-Baudet, M. *J*. *Chem*. *Soc*., *Dalton Trans*. **1977**, 2004-2009.

(158) Jiménez-Pérez, V. M.; Muñoz-Flores, B. M.; Roesky, H. W.; Schulz, T.; Pal, A.; Beck, T.; Yang, Z.; Stalke, D.; Santillan, R.; Witt, M. *Eur*. *J*. *Inorg*. *Chem*. **2008**, *2008*, 2238-2243.

(159) Ding, Y.; Roesky, H. W.; Noltemeyer, M.; Schmidt, H.-G.; Power, P. P. *Organometallics* **2001**, *20*, 1190-1194.

(160) Rekken, B. D.; Brown, T. M.; Fettinger, J. C.; Tuononen, H. M.; Power, P. P. *J*. *Am*. *Chem*. *Soc*. **2012**, *134*, 6504-6507.

(161) Driess, M.; Yao, S.; Brym, M.; van Wüllen, C.; Lentz, D. *J*. *Am*. *Chem*. *Soc*. **2006**, *128*, 9628-9629.

(162) Yao, S.; Xiong, Y.; Driess, M. *Organometallics* **2011**, *30*, 1748-1767.

(163) Driess, M.; Yao, S.; Brym, M.; van Wüllen, C. *Angew*. *Chem*. *Int*. *Ed*. **2006**, *45*, 4349-4352.

(164) Kira, M. *J*. *Organomet*. *Chem*. **2004**, *689*, 4475-4488.

(165) Asay, M.; Inoue, S.; Driess, M. *Angew*. *Chem*. *Int*. *Ed*. **2011**, *50*, 9589-9592.

(166) Alder, R. W.; Allen, P. R.; Murray, M.; Orpen, A. G. *Angew*. *Chem*. *Int*. *Ed*. *Eng*. **1996**, *35*, 1121-1123.

(167) Jutzi, P.; Mix, A.; Rummel, B.; Schoeller, W. W.; Neumann, B.; Stammler, H.-G. *Science* **2004**, *305*, 849-851.

(168) Jutzi, P.; Leszczyńska, K.; Neumann, B.; Schoeller, W. W.; Stammler, H.-G. *Angew*. *Chem*. *Int*. *Ed*. **2009**, *48*, 2596-2599.

(169) Jutzi, P.; Leszczyńska, K.; Mix, A.; Neumann, B.; Rummel, B.; Schoeller, W.; Stammler, H.-G. *Organometallics* **2010**, *29*, 4759-4761.

(170) Inoue, S.; Leszczyńska, K. *Angew*. *Chem*. *Int*. *Ed*. **2012**, *51*, 8589-8593.

(171) Rekken, B. D.; Brown, T. M.; Fettinger, J. C.; Lips, F.; Tuononen, H. M.; Herber, R. H.; Power, P. P. *J*. *Am*. *Chem*. *Soc*. **2013**, *135*, 10134-10148.

(172) Becerra, R.; Goldberg, N.; Cannady, J. P.; Almond, M. J.; Ogden, J. S.; Walsh, R. *J*. *Am*. *Chem*. *Soc*. **2004**, *126*, 6816-6824.

(173) Chu, J. O.; Beach, D. B.; Estes, R. D.; Jasinski, J. M. *Chem*. *Phys*. *Lett*. **1988**, *143*, 135-139.

(174) Becerra, R.; Walsh, R. *J*. *Am*. *Chem*. *Soc*. **2000**, *122*, 3246-3247.

(175) Becerra, R.; Boganov, S. E.; Egorov, M. P.; Faustov, V. I.; Promyslov, V. M.; Nefedov, O. M.; Walsh, R. *Phys*. *Chem*. *Chem*. *Phys*. **2002**, *4*, 5079-5087.

(176) Becerra, R.; Boganov, S. E.; Egorov, M. P.; Faustov, V. I.; Krylova, I. V.; Nefedov, O. M.; Promyslov, V. M.; Walsh, R. *Phys*. *Chem*. *Chem*. *Phys*. **2004**, *6*, 3370-3382.

(177) Heaven, M. W.; Metha, G. F.; Buntine, M. A. *J*. *Phys*. *Chem*. *A* **2001**, *105*, 1185-1196.

(178) So, S. P. *J*. *Phys*. *Chem*. *A* **2001**, *105*, 4988-4991.

(179) So, S. P.; Li, W.-K. *J*. *Phys*. *Chem*. *A* **2004**, *108*, 4002-4007.

(180) Becerra, R.; Bowes, S.-J.; Steven Ogden, J.; Pat Cannady, J.; Adamovic, I.; Gordon, M. S.; Almond, M. J.; Walsh, R. *Phys*. *Chem*. *Chem*. *Phys*. **2005**, *7*, 2900.

(181) Becerra, R.; Cannady, J. P.; Walsh, R. *J*. *Phys*. *Chem*. *A* **2003**, *107*, 11049-56.

(182) Nowek, A.; Leszczynski, J. *J*. *Phys*. *Chem*. *A* **1997**, *101*, 3784-3788.

(183) Becerra, R.; Cannady, J. P.; Walsh, R. *J*. *Phys*. *Chem*. *A* **2002**, *106*, 4922-27.

(184) Ghadwal, R. S.; Sen, S. S.; Roesky, H. W.; Granitzka, M.; Kratzert, D.; Merkel, S.; Stalke, D. *Angew*. *Chem*. *Int*. *Ed*. **2010**, *49*, 3952-3955.

(185) Sen, S. S.; Tavčar, G.; Roesky, H. W.; Kratzert, D.; Hey, J.; Stalke, D. *Organometallics* **2010**, *29*, 2343-2347.

(186) Tomasik, A. C.; Mitra, A.; West, R. *Organometallics* **2009**, *28*, 378-381.

(187) Yao, S.; Brym, M.; van Wüllen, C.; Driess, M. *Angew*. *Chem*. *Int*. *Ed*. **2007**, *46*, 4159-4162.

(188) Protchenko, A. V.; Birjkumar, K. H.; Dange, D.; Schwarz, A. D.; Vidovic, D.; Jones, C.; Kaltsoyannis, N.; Mountford, P.; Aldridge, S. *J*. *Am*. *Chem*. *Soc*. **2012**, *134*, 6500-6503.

(189) Protchenko, A. V.; Schwarz, A. D.; Blake, M. P.; Jones, C.; Kaltsoyannis, N.; Mountford, P.; Aldridge, S. *Angew*. *Chem*. *Int*. *Ed*. **2013**, *52*, 568-571.

Chapter 2

Theoretical Methods and Computational Aspects

Abstract

As discussed in chapter 1, our aim is to model important chemical reactions using density functional theory. This chapter deals with the theoretical background for the various methods used in our calculations. We begin Section 2.1 with a brief introduction to the non-relativistic Schrödinger equation and the Born-Oppenheimer approximation. Section 2.2 provides a summary of density functional theory along with the Thomas-Fermi model, Hohenberg-Kohn theorems, Kohn-Sham equations and the different exchange-correlations functionals. Section 2.3 depicts the energetic span model which is employed to calculate the turn over frequency (TOF) from the theoretically obtained energy profile. The following sections also briefly describe the free volume correction for translational entropy in Section 2.4, the spin component scaled MP2 approach in Section 2.5, the RI-J and MARI-J approximations implemented in Turbomole software to improve the computational expediency in Section 2.6 and the methods taken into account for the solvent corrections in Section 2.7.

2.1 The Schrödinger Equation

An N-electronic atomic or molecular system can be determined by solving the Schrödinger equation. The time independent non-relativistic Schrödinger equation[1] is given by,

$$\hat{H}\Psi = E\Psi \tag{2.1}$$

where E is the electronic energy, $\Psi = \Psi(x_1, x_2, ..., x_N)$ is the wave function and $\hat{H}$ is the Hamiltonian operator for a system of nuclei and electrons described by the position vectors R_A and r_i, respectively. The Hamiltonian operator in atomic units can be written as

$$\hat{H} = -\sum_{i=1}^{N}\frac{1}{2m}\Delta_i^2 - \sum_{A=1}^{M}\frac{1}{2M_A}\Delta_A^2 - \sum_{i=1}^{N}\sum_{A=1}^{M}\frac{Z_A}{r_{iA}} + \sum_{i=1}^{N}\sum_{j>i}^{N}\frac{1}{r_{ij}} + \sum_{A=1}^{M}\sum_{B>A}^{M}\frac{Z_A Z_B}{R_{AB}} \tag{2.2}$$

In the above equation, the first two terms represent the kinetic energy operator of electrons with mass m and nuclei with mass M_A, respectively. The third term corresponds to the coulomb attraction between electrons and nuclei separated by a distance r_{iA}. The fourth and fifth term respectively give the repulsion between the electrons and the repulsion between nuclei where r_{ij} is the distance between the ith and jth electron and R_{AB} is the distance between the Ath nucleus and the Bth nucleus.

2.1.1 The Born-Oppenheimer Approximation

Nuclei are much heavier than electrons and therefore the movement of nuclei is very slow in comparison to electrons.[2] Based on this, the Born-Oppenheimer approximation was proposed, suggesting that the electrons in a molecule can be approximated as to be moving in the field of fixed nuclei. This approximation allows the simplification of equation 2.2, in which the kinetic energy of the nuclei can be neglected and the repulsion between the nuclei can be considered as a constant, which, in turn, separates the Hamiltonian with respect to the electronic and nuclear coordinates. The electronic Hamiltonian which depends parametrically on the nuclear coordinates can be written as

$$\hat{H}_{ele} = -\sum_{i=1}^{N}\frac{1}{2}\Delta_i^2 - \sum_{i=1}^{N}\sum_{A=1}^{M}\frac{Z_A}{r_{iA}} + \sum_{i=1}^{N}\sum_{j>i}^{N}\frac{1}{r_{ij}} \tag{2.3}$$

In order to solve the many-electron problem, it is necessary to get approximate solutions to the electronic Schrödinger equation. Many quantum mechanical methods such as the

Hartree-Fock approximation and the methods beyond Hartree-Fock approach such as Møller-Plesset (MP) perturbation theory,[3] configuration interaction (CI)[4] and coupled cluster (CC)[5] provide approximate solutions to the electronic Schrödinger equation. However, density functional theory (DFT) suggests that the ground state properties of a many-electron system can be obtained from its electron density. This provides as easy and computationally cheaper solution to replace other *ab initio* methods.

2.2 Density Functional theory

Density functional theory (DFT)[6] allows one to move away from the complicated N-electron wave function and the associated Schrödinger wave equation by replacing it with a much simpler electron density $\rho(r)$ and the associated calculation scheme. The initial contributions in the field of DFT began with the works of Thomas[7] and Fermi[8,9] in the 1920s. In their model, they proposed statistical considerations to approximate the electron distribution in an atom.

2.2.1 Thomas Fermi Model

According to the Thomas-Fermi[7-9] model, electrons are uniformly distributed in the six-dimensional phase space for the motion of an electron at the rate of two for each h^3 volume space and there is an effective potential field determined by the nuclear charge and the distribution of electrons. In this method, the kinetic energy is approximated as an explicit functional of density, idealized as non-interacting electrons in a homogeneous gas with a density equal to the local density at the given point. Based on these assumptions, the energy functional for an electron in terms of electron density is derived as,

$$E_{TF}[\rho(r)] = C_F \int \rho^{5/3}(r)dr - Z\int \frac{\rho(r)}{r}dr + \frac{1}{2}\iint \frac{\rho(r_1)\rho(r_2)}{r_1 - r_2}dr_1 dr_2 \qquad (2.4)$$

where the Thomas-Fermi coefficient C_F is equal to 2.871.

In this equation, the first term corresponds to the electronic kinetic energy derived in terms of the density $\rho(r)$ and the second and third term correspond to the classical electrostatic energies of electron-nuclear attraction and electron-electron repulsion by neglecting the exchange and correlation terms. An important aspect of the theory is that for the ground state of an atom, the energy density minimizes the energy functional under the constraint

$$N = N[\rho(r)] = \int \rho(r)dr \tag{2.5}$$

The constrained variation using the method of Lagrange multipliers yields the equation (2.6), which, in turn, yields the Euler-Lagrange equation (2.7)

$$\delta\left\{E_{TF}[\rho] - \mu_{TF}\left(\int \rho(r)dr - N\right)\right\} = 0 \tag{2.6}$$

$$\mu_{TF} = \frac{\delta E_{TF}[\rho]}{\delta\rho(r)} = \frac{5}{3}C_F\rho^{2/3}(r) - \phi(r) \tag{2.7}$$

$$\phi(r) = \frac{Z}{r} - \int \frac{\rho(r_2)}{|r - r_2|}dr_2 \tag{2.8}$$

where $\phi(r)$ is the electrostatic potential at point 'r' due to the nucleus and the entire electron distribution.

According to the Thomas-Fermi model, solving equation (2.7) in conjunction with (2.5) and inserting the resulting electron density in equation (2.4) provides the total energy. However, the accuracy of the calculated values are low and therefore, this model is considered as an oversimplified model and an approximation to the exact density functional theory.

2.2.2 Hohenberg-Kohn theorem

Modern density functional theory is based on the two theorems of Hohenberg and Kohn.[10]

The first Hohenberg-Kohn theorem (Hohenberg and Kohn 1964)[10] states that "the external potential is determined, within a trivial additive constant, by the electron density $\rho(r)$". This theorem legitimizes the use of electron density $\rho(r)$, in place of the total number of electron *N* and the external potential $\upsilon(r)$, as a basic variable for the calculation of the ground state properties of a system. The first theorem proves that there cannot be two different υ which give the same ρ for their ground states. That is, ρ determines N and υ and hence the ground state properties of a system.

Hence, the energy functional can be written as

$$E_\upsilon[\rho] = T[\rho] + V_{ne}[\rho] + V_{ee}[\rho] \tag{2.9}$$

$$= \int \rho(r)\upsilon(r)dr + F_{HK}[\rho] \tag{2.10}$$

$$\text{where} \quad F_{HK}[\rho] = T[\rho] + V_{ee}[\rho] \tag{2.11}$$

The electrostatic repulsion term in equation (2.11) can be written as,

$$V_{ee}[\rho] = J[\rho] + \text{nonclassical term} \tag{2.12}$$

where $J[\rho]$ is the classical repulsion and the nonclassical term involves the major part of the exchange-correlation energy.

The second Hohenberg-Kohn theorem[10] is analogous to the variation principle for wave functions which states that "For a trial density $\tilde{\rho}(r)$, such that $\tilde{\rho}(r) \geq 0$ and $\int \tilde{\rho}(r)dr = N$,

$$E_0 \leq E_v[\tilde{\rho}] \tag{2.13}$$

where $E_v[\tilde{\rho}]$ is the energy functional and the constrained minimization using the method of Lagrange multipliers gives

$$\delta\left\{E_\upsilon[\rho] - \mu\left[\int \rho(r)dr - N\right]\right\} = 0 \tag{2.14}$$

$$\mu = \frac{\delta E_\upsilon[\rho]}{\delta\rho(r)} = \upsilon(r) + \frac{\delta F_{HK}[\rho]}{\delta\rho(r)} \tag{2.15}$$

μ is the chemical potential and $F_{HK}[\rho]$ is a universal functional of $\rho(r)$. The exact form of $F_{HK}[\rho]$ leads the equation (2.14) an exact equation for the ground electron density. Among the all possible solutions of (2.15) the one which minimizes the energy functional $E_\upsilon[\rho]$ can provide the ground state energy of a system.

The Thomas-Fermi model provides an approximate model for $T[\rho]$ and $V_{ee}[\rho]$. However, it is necessary to calculate the kinetic energy more accurately since it constitutes the leading part of the total energy. Kohn and Sham[11] proposed introducing orbitals for the accurate computation of $T[\rho]$ with a small residual correction that is handled separately.

2.2.3 Kohn-Sham Equations

For a system of non-interacting electrons the kinetic energy is

$$T_s[\rho] = \sum_i^N \left\langle \psi_i \left| -\tfrac{1}{2}\Delta^2 \right| \psi_i \right\rangle \tag{2.16}$$

and the electron density is

$$\rho(r) = \sum_{i}^{N} \sum_{s} |\psi_i(r,s)|^2 \tag{2.17}$$

In the Kohn-Sham method,[6,11] the interacting many-body problem is replaced by a non-interacting system moving in an effective potential. The energy functional in terms of *N* orbitals can be written as

$$E[\rho] = T_s[\rho] + J[\rho] + E_{xc}[\rho] + \int \upsilon(r)\rho(r)dr \tag{2.18}$$

$$= \sum_{i}^{N} \sum_{s} \int \psi_i^*(x)(-\tfrac{1}{2}\Delta^2)\psi_i(x)dr + J[\rho] + E_{xc}[\rho] + \int \upsilon(r)\rho(r)dr \tag{2.19}$$

In equation (2.19), the first term is the kinetic energy of electrons in a model non–interacting system which has the same electron density as the real system. The second term is the Coulomb interaction between the electrons and the third term is the exchange-correlation energy, which includes the difference in the kinetic energy of the non-interacting and the interacting system ($T[\rho] - T_s[\rho]$) and the nonclassical part of $V_{ee}[\rho]$. Fourth term gives the Coulomb potential due to electron-nucleus attraction.

The variation of the Kohn-Sham (KS) energy functional with respect to electron density gives the minimum of the KS functional and this leads to *N* KS equations.

$$[-\tfrac{1}{2}\nabla^2 + \upsilon_{eff}]\psi_i = \varepsilon_i\psi_i \tag{2.20}$$

$$\rho(r) = \sum_{i}^{N} \sum_{s} |\psi_i(r,s)|^2 \tag{2.21}$$

Here ε_i are eigenvalues, ψ_i are KS orbitals and $\upsilon_{eff}(r)$ is the KS effective potential. The KS effective potential can be defined by

$$\upsilon_{eff}(r) = \upsilon(r) + \frac{\delta J[\rho]}{\delta\rho(r)} + \frac{\delta E_{xc}[\rho]}{\delta\rho(r)} \tag{2.22}$$

$$= \upsilon(r) + \int \frac{\rho(r')}{|r-r'|}dr' + \upsilon_{xc}(r) \tag{2.23}$$

where $\upsilon_{xc}(r)$ is the exchange-correlation potential. KS equations are non-linear and must be solved iteratively. Here, the total electronic energy is not the sum of the orbital energies. The total energy can be determined from

$$E = \sum_{i}^{N} \varepsilon_i - \frac{1}{2}\int \frac{\rho(r)\rho(r')}{|r-r'|}drdr' + E_{xc}[\rho] + \int \upsilon_{xc}(r)\rho(r)dr \tag{2.24}$$

Better approximations to $E_{xc}[\rho]$ would give exact ρ and *E*.

2.2.4 Exchange-Correlation Functional

The development of an accurate exchange-correlation functional ($E_{xc}[\rho]$) is the greatest challenge in DFT. In this domain, the simplest approximation is the local density approximation (LDA) for the exchange and correlation energy proposed by Kohn and Sham.[11] The LDA exchange-correlation functional is based on the assumption that the exchange-correlation energy for a non-uniform system can be obtained by applying uniform electron gas results to infinitesimal portions of the non-uniform electron distribution and then summing over all individual contributions. It is given by

$$E_{xc}^{LDA}[\rho] = \int \rho(r)\varepsilon_{xc}[\rho(r)]dr \tag{2.25}$$

Where $\varepsilon_{xc}(\rho)$ is the exchange and correlation energy per particle of a uniform electron gas of density $[\rho(r)]$. The corresponding exchange-correlation potential can be written as

$$\upsilon_{xc}^{LDA}(r) = \frac{\delta E_{xc}^{LDA}}{\delta\rho(r)} = \varepsilon_{xc}(\rho(r)) + \rho(r)\frac{\delta\varepsilon_{xc}(\rho)}{\delta\rho} \tag{2.26}$$

And the corresponding KS equations are given by

$$\left[-\frac{1}{2}\Delta^2 + \upsilon(r) + \int \frac{\rho(r')}{|r-r'|}dr' + \upsilon_{xc}^{LDA}(r)\right]\psi_i = \varepsilon_i\psi_i \tag{2.27}$$

The self-consistent solution of equation (2.27) provides the Kohn Sham-local density approximation (LDA method). This method is applicable for the system with slowly varying densities and not well defined for highly inhomogeneous systems such as atoms and molecules. In this method the major source of error is observed in the exchange energy. Further modifications in the exchange-correlation functional leads to the generalized gradient approximation (GGA). This considers the gradient of electron density and replaces $\rho(r)$ of the exchange hole by $\partial\rho(r)/\partial r$. The exchange-correlation energy functional in GGA can be written as

$$E_{xc}^{GGA}[\rho(r)] = \int \rho(r)F[\rho(r), \nabla\rho(r)]dr \tag{2.28}$$

The exchange part of $E_{xc}^{GGA}[\rho(r)]$ was proposed by Perdew and Wang (PW86)[12] in 1986 and subsequently by Becke in 1988 (B88).[13] Gradient corrections to the correlation part were proposed in 1986 by Perdew (P86)[14], in 1988 by Lee, Yang and Parr (LYP),[15] in 1991 by Perdew and Wang (PW91)[16] and in 1996 by Perdew, Burke and Ernzerhof

(PBE)[17]. In our DFT calculations, we have mainly used the PBE[17] GGA functional. For the calculations provided in chapter 3A, we have used the B3-LYP GGA functional.

2.3 Energetic Span Model

The turn over frequency (TOF) provides the efficiency of a catalytic cycle. It can be defined as the rate of reaction of a catalytic cycle, and is measured as the number of cycles per time and total catalytic concentration. There is no straightforward method to calculate the TOF of a catalytic cycle from the energy profiles (E-representation) obtained from computational calculations. In this regard, the Energetic Span Model (ESM) proposed by Kozuch and Shaik[18-25] provides a way to calculate the efficiency of a catalytic cycle, that is, its TOF from a theoretically obtained energy profile (E-representation). ESM is derived based on three conditions: i) the transition state theory (TST) is valid, ii) the steady state approximation is applicable and iii) the intermediates undergo fast relaxation. According to ESM, the TOF for the catalytic cycle is

$$TOF = \frac{k_B T}{h} \frac{e^{-\Delta G_r/RT} - 1}{\sum_{i,j}^{N} e^{\left(T_i - I_j - \delta G'_{i,j}\right)/RT}} \tag{2.29}$$

where ΔG_r is the total Gibbs reaction energy. T_i and I_j are the calculated free energies of each transition state (TS) and intermediate. $\delta G'_{ij}$ can be specified as

$$\delta G'_{i,j} = \begin{cases} \Delta G_r & \text{if } i \geq j \\ 0 & \text{if } i < j \end{cases} \tag{2.30}$$

This equation gives the E-representation of the TOF as opposed to the k-representation (rate-constant representation) of the experimentalist. If only one TS and one intermediate is significant for the TOF, namely, TDTS (TOF determining TS) and TDI (TOF determining intermediate), the equation 2.29 can be approximated as

$$TOF \approx \frac{k_B T}{h} e^{-\delta E/RT} \tag{2.31}$$

where δE is the energetic span, which is the apparent activation energy of the whole catalytic cycle. The energetic span can be estimated as

$$\delta E = \begin{cases} T_{TDTS} - I_{TDI} & \text{if the TDTS appears after the TDI} \\ T_{TDTS} - I_{TDI} + \Delta G_r & \text{if the TDTS appears before the TDI} \end{cases} \tag{2.32}$$

TDTS and TDI are the states which maximize δE. The expression for the apparent activation energy (δE) differs depending on whether the TDTS follows the TDI or precedes it. The TOF determining states can be located from the "degree of TOF control (X_{TOF})": a tool to quantify the influence of these determining states on the TOF.[18-25] The transition state and intermediate with highest X_{TOF} correspond to the TDTS and TDI.

$$X_{\mathrm{TOF},T_i} = \frac{\sum_{j=1}^{N} e^{(T_i - I_j - \delta G'_{i,j})/RT}}{\sum_{i,j=1}^{N} e^{(T_i - I_j - \delta G'_{i,j})/RT}} \tag{2.33}$$

$$X_{\mathrm{TOF},I_j} = \frac{\sum_{i=1}^{N} e^{(T_i - I_j - \delta G'_{i,j})/RT}}{\sum_{i,j=1}^{N} e^{(T_i - I_j - \delta G'_{i,j})/RT}} \tag{2.34}$$

where equation 2.33 corresponds to the degree of TOF of TS and 2.34 for that of the intermediate. Equation 2.29 is more accurate in the case of a catalytic cycle where the X_{TOF} value is significant (>0.2) for more than one TS or one intermediate.

According to the ESM, if the catalytic cycle has competing mechanisms with shared transitions state as well as intermediates, the calculation of relative TOFs for the mechanisms leads to an error.[21,26] Therefore, it is necessary to compare and obtain a single pathway from the competing cycles with respect to the stable intermediate and TS since the TDTS and TDI are shared states for all cycles. If one accessible intermediate state has very low energy, it will be the TOF determining intermediate (TDI) for all the mechanisms. This is also true when it comes to evaluating the TOF determining transition state (TDTS) for the ESM calculations.

2.4 Free Volume Correction for Translational Entropy

Theoretical methods estimate the changes in entropy that accompany the aggregation of rigid particles by calculating separately four components of the total entropy i.e., the translational, rotational, vibrational, and conformational components.

Traditionally, the translational entropy is calculated by the Sackur-Tetrode equation[27]

$$S_{trans} = R \ln \left[\left(\frac{10^{-15/2}}{N_A^4 [X]} \right) \left(\frac{2\pi MRTe^{5/3}}{h^2} \right)^{3/2} \right] \tag{2.35}$$

where (T, K) is temperature, (M, g/mol) is the mass of the particle, [X] (mol/L) is the concentration of the particles, h (J s^2), Plank's constant, Boltzmann constant, k (J/mol/K), the fundamental constant e (unitless), and Avogadro's number N_A (unitless). The first numerical term $10^{-15/2}$, converts units of m^3 and kg into L and g, respectively. This equation predicts the translational entropy of monoatomic gases successfully. However, for the molecules in the solution phase (molecules dissolved in solution at 1.0 mol/L) the translational entropy is significantly lower than the estimated value using equation 2.35. This is because the Sackur-Tetrode equation ignores the molecular volume, V_{molec} in a liquid, which comprises the major portion of the total volume, the volume enclosed by the van der Waals surface of the molecule. Such an uncertainty in rotational and vibrational entropy is negligible in comparison to the translational entropy, and for rigid particles, the fourth component S_{conf} is zero, by definition. Therefore, out of the four components, the translational entropy requires substantial improvement.

Mammen *et. al.*[28] proposed a theoretical model to provide the translational entropy correction to the values of S_{trans} (sol) of molecules in solution that are based on the Sackur-Tetrode equation.[27] This has been provided by an extended model of the free volume theory which assumes the liquid as a regular array of hard cubes (or spheres, or other shapes), where the volume of each cube is equal to the molecular volume, V_{molec}. The proposed model is valid for infinitely dilute solutions of the solute. According to this model, the correction can be calculated using equation 2.36 which contains the experimental concentration of analyte, [analyte] (mol/L), and the free volume of the solvent $V_{free}^{solvent}$ (L). The equation for estimating translational entropy correction in the condensed phase is given by

$$S_{trans} = R\ln\left[\left(\frac{10^{-15/2}V_{free}^{solvent}}{N_0^4[analyte]}\right)\left(\frac{2\pi MRTe^{5/3}}{h^2}\right)^{3/2}\right] \tag{2.36}$$

$$= 11.1 + 12.5\ln(T) + 12.5\ln(M) + 8.3\ln V_{free}^{solvent} \tag{2.37}$$

$$V_{free}^{solvent} = C_{free}\left(\sqrt[3]{\left(\frac{10^{27}}{[X]N_0}\right)} - \sqrt[3]{V_{molec}}\right)^3 \tag{2.38}$$

where $C_{free} = 8$ for hard cubes.

2.5 Spin component scaled MP2

A correction to improve the second-order Møller–Plesset perturbation theory (MP2)[3] calculations is provided by the spin component scaled MP2 method (SCS-MP2).[29-31] In the MP2 method there is an equal contribution from the spin-parallel (E_t) and spin-antiparallel (E_s) electron pair components to the correlation energy E_c. However, by employing different scaling to the two components the MP2 calculations can be improved. In the SCS-MP2 approach, the different scaling towards the electronic correlation energy ($E_c = p_sE_s + p_tE_t$) is brought about with the scaling factors p_s and p_t having the values of of 6/5 and 1/3 respectively.

2.6 RI-J and MARI-J approximations

RI-J (resolution of identity)[32-37] and MARI-J (multipole accelerated resolution of identity)[38] approximations help to evaluate the electronic Coulomb integral for both molecular and periodic systems with computational expediency. These approximations employ atom centred auxiliary basis functions to solve the algebraic equations. The MARI-J method implemented in the Turbomole software partition the Coulomb problem into two, a far field part comprising the majority of interactions including long range interactions that are evaluated using multipole expansions and a computationally dominant near field part which takes care of near field interactions through direct integration of the four-center electron repulsion integrals

$$\iint \frac{\mu(r)\nu(r)\kappa(r')\lambda(r')}{|r-r'|}drdr' = (\mu\nu\,|\,\kappa\lambda) \tag{2.39}$$

where μ,ν,κ,λ are the basis functions.

Application of the RI-J (density fitting) approximation to the near field part helps to reduce the four-center electron repulsion integrals to a three center integral. In RI approximation, the electron density ρ is approximated as a linear combination $\tilde{\rho}$ of auxiliary basis functions α,

$$\rho(r) \approx \tilde{\rho}(r) = \sum_{\alpha} c_{\alpha}\alpha(r) \tag{2.40}$$

where c_α is the expansion coefficient and can be evaluated using a positive definite two-electron operator 'g'

$$c_\alpha = \iint [\rho(r) - \tilde{\rho}(r)] g(r, r') [\rho(r') - \tilde{\rho}(r')] dr dr' \quad (2.41)$$

A combined application of RI-J and MARI-J approximations respectively on the near field and far field parts increases the computational efficiency significantly.

2.7 Solvent Correction

The solvent effects incorporated in the calculations mainly employ the Conductor-like Screening Model (COSMO).[39,40] It is a continuum solvation model (CSM). In COSMO, the solvent is treated as a dielectric continuum of permittivity ε and the solute molecule forms a cavity within the dielectric continuum. The charge distribution of the solute leads to polarization of the dielectric medium and the corresponding response of the medium towards the solute charge distribution generates a screening charges on the interface between the cavity and the dielectric namely, the 'solvent accessible surface' (SAS). In order to obtain the screening charges, the boundary condition of vanishing electrostatic potential for a conductor is used in COSMO, which is equivalent to the electrostatically ideal solvent with $\varepsilon = \infty$. For solvents with a finite dielectric constant, the screening charges are scaled by a factor.

$$\mathrm{q}^* = f(\varepsilon)\, \mathrm{q} \quad (2.42)$$

$$f(\varepsilon) = \frac{\varepsilon - 1}{\varepsilon + \frac{1}{2}} \quad (2.43)$$

The energy of the interaction between the solvent and the solute molecule can be calculated from the solvent screening charges and the known charge distribution of the molecule. Half of the solute-solvent interaction energy gives the dielectric energy and the total free energy of the solvated molecule is obtained from the sum of the energy of the isolated system calculated with the solvated wave function and the dielectric energy.

$$E = E(\psi^{solv}) + E_{diel} \quad (2.44)$$

2.8 References

(1) Schrödinger, E. *Ann*. *Phys*. **1926**, *384*, 361-376.

(2) Born, M.; Oppenheimer, R. *Ann*. *Phys*. **1927**, *389*, 457-484.

(3) Møller, C.; Plesset, M. S. *Phys*. *Rev*. **1934**, *46*, 618-622.

(4) David Sherrill, C.; Schaefer III, H. F. In *Adv*. *Quantum Chem*.; Academic Press: 1999; Vol. Volume 34, p 143-269.

(5) Bartlett, R. J. *J*. *Phys*. *Chem*. **1989**, *93*, 1697-1708.

(6) Parr, R. G.; Yang, W. *Density-Functional Theory of Atoms and Molecules*; Oxford University Press, USA, 1989.

(7) Thomas, L. H. *Mathematical Proceedings of the Cambridge Philosophical Society* **1927**, *23*, 542-548.

(8) Fermi, E. *Zs*. *f*. *Phys*. **1926**, *36*, 902.

(9) Fermi, E. *Rendiconti Lincei* **1927**, *6*, 602-607.

(10) Hohenberg, P.; Kohn, W. *Phys*. *Rev*. **1964**, *136*, B864-B871.

(11) Kohn, W.; Sham, L. J. *Phys*. *Rev*. **1965**, *140*, A1133-A1138.

(12) Perdew, J. P.; Yue, W. *Phys*. *Rev*. *B* **1986**, *33*, 8800-8802.

(13) Becke, A. D. *Phys*. *Rev*. *A* **1988**, *38*, 3098-3100.

(14) Perdew, J. P. *Phys*. *Rev*. *B* **1986**, *33*, 8822-8824.

(15) Lee, C.; Yang, W.; Parr, R. G. *Phys*. *Rev*. *B* **1988**, *37*, 785.

(16) Perdew, J. P.; Wang, Y. *Phys*. *Rev*. *B* **1992**, *45*, 13244-13249.

(17) Perdew, J. P.; Burke, K.; Ernzerhof, M. *Phys*. *Rev*. *Lett*. **1996**, *77*, 3865-3868.

(18) Kozuch, S.; Shaik, S. *J*. *Am*. *Chem*. *Soc*. **2006**, *128*, 3355-3365.

(19) Kozuch, S.; Shaik, S. *J*. *Phys*. *Chem*. *A* **2008**, *112*, 6032-6041.

(20) Kozuch, S.; Lee, S. E.; Shaik, S. *Organometallics* **2009**, *28*, 1303-1308.

(21) Kozuch, S.; Shaik, S. *Acc*. *Chem*. *Res*. **2010**, *44*, 101-110.

(22) Kozuch, S.; Shaik, S. *J*. *Mol*. *Catal*. *A: Chem*. **2010**, *324*, 120-126.

(23) Kozuch, S.; Martin, J. M. L. *ACS Catal*. **2011**, *1*, 246-253.

(24) Uhe, A.; Kozuch, S.; Shaik, S. *J*. *Comp*. *Chem*. **2011**, *32*, 978-985.

(25) Kozuch, S. In *Understanding Organometallic Reaction Mechanisms and Catalysis*; Wiley-VCH Verlag GmbH & Co. KGaA: 2015, p 217-248.

(26) Kuriakose, N.; Kadam, S.; Vanka, K. *Inorg*. *Chem*. **2012**, *51*, 377-385.

(27) Gurney, R. W. *Introduction to statistical mechanics*; 1st ed.; McGraw Hill, 1949.

(28) Mammen, M.; Shakhnovich, E. I.; Deutch, J. M.; Whitesides, G. M. *J*. *Org*. *Chem*. **1998**, *63*, 3821-3830.

(29) Hellweg, A.; Grun, S. A.; Hattig, C. *Phys*. *Chem*. *Chem*. *Phys*. **2008**, *10*, 4119-4127.

(30) Goumans, T. P. M.; Ehlers, A. W.; Lammertsma, K.; Würthwein, E.-U.; Grimme, S. *Chem*. *–Eur*. *J*. **2004**, *10*, 6468-6475.

(31) Grimme, S. *J*. *Chem*. *Phys*. **2003**, *118*, 9095-9102.

(32) Eichkorn, K.; Treutler, O.; Öhm, H.; Häser, M.; Ahlrichs, R. *Chem*. *Phys*. *Lett*. **1995**, *240*, 283-290.

(33) Burow, A. M.; Sierka, M.; Mohamed, F. *J*. *Chem*. *Phys*. **2009**, *131*, 214101.

(34) Whitten, J. L. *J*. *Chem*. *Phys*. **1973**, *58*, 4496-4501.

(35) Vahtras, O.; Almlöf, J.; Feyereisen, M. W. *Chem*. *Phys*. *Lett*. **1993**, *213*, 514-518.

(36) Dunlap, B. I.; Connolly, J. W. D.; Sabin, J. R. *J*. *Chem*. *Phys*. **1979**, *71*, 3396-3402.

(37) Eichkorn, K.; Weigend, F.; Treutler, O.; Ahlrichs, R. *Theor*. *Chem*. *Acc*. **1997**, *97*, 119-124.

(38) Sierka, M.; Hogekamp, A.; Ahlrichs, R. *J*. *Chem*. *Phys*. **2003**, *118*, 9136-9148.

(39) Klamt, A.; Schuurmann, G. *J*. *Chem*. *Soc*. *Perkin Trans*. *2* **1993**, 799-805.

(40) *User's Manual, Turbomole Version 6.4* **2012**.

Chapter 3
Small Molecule Activation Using Homogeneous Transition Metal Complexes

Transition metal complexes play an important role in homogeneous catalytic processes. Therefore, the development of efficient metal based catalytic compounds is an important area of research. The current chapter discusses our computational investigation to modify existing transition metal based catalyst complexes for important chemical reactions. Here, we have considered two catalytic processes: i) the homogeneous water gas shift reaction (WGSR), and ii) the homogeneous olefin metathesis reaction. These reactions deal with the activation or cleavage of chemical bonds in small molecules such as H_2O, CO and alkenes. Well studied catalytic complexes for these respective reactions are $Fe(CO)_5$ and the second generation Grubbs' catalyst, ($C_{46}H_{65}Cl_2N_2PRu$). Our motivation has been to investigate various possibilities for improving these catalytic complexes either by the modification of the metal centre or the attached ligands. This chapter is divided into two parts, Chapter 3A and Chapter 3B. Chapter 3A showcases the role of metal-metal cooperativity to improve the WGS reaction, for which the quantum mechanical calculations have been performed using the DFT and ESM approach, described in Chapter 2. Chapter 3B discusses the potential of the allene ligand to act as an effective leaving group in catalytic processes. Here, we have demonstrated the use of the allene ligand as an efficient leaving group for the olefin metathesis reaction with Grubbs' catalysts.

Chapter 3A

The Role of Metal-Metal Cooperativity in the Homogeneous Water Gas Shift Reaction

Abstract

The possibility of metal-metal cooperativity in improving the yield of the homogeneous Water Gas Shift reaction (WGSR) has been investigated through full quantum mechanical (QM) density functional theory (DFT) calculations. The calculations indicate that bi-metallic catalysts would be likely to be more highly active than mono-nuclear metal based catalysts for the WGSR. The results have implications for the design of improved WGSR catalysts in the future.

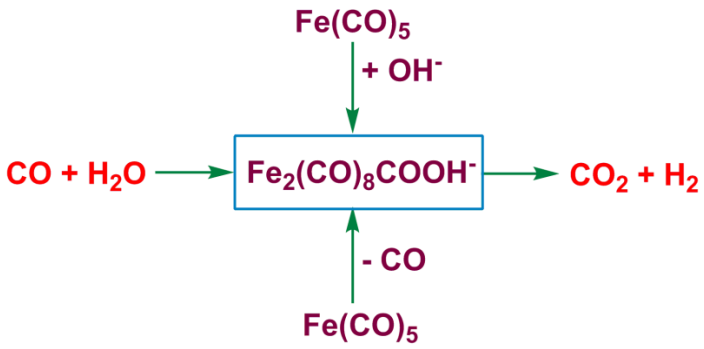

3A.1 Introduction

The presence of two metal centers in an organometallic complex can give rise to interesting new chemistry because of the interaction and cooperativity between the metal centers. This has led to a conscious effort in recent years to create bi-nuclear metal complexes and investigate their impact on important catalytic reactions such as olefin polymerization[1], C-H activation[2] and alkyne/methylene coupling reactions[3]. However, the fact that binuclear complexes confer advantages in homogeneous catalysis systems due to metal-metal cooperativity leads to an important question: is it possible that reactions that have been considered to date to occur at mono-nuclear metal centers *could be happening instead at bi-nuclear centers, the bi-nuclear species being formed during the homogeneous catalysis process?*

An interesting reaction in this regard is the homogeneous Water Gas Shift Reaction (WGSR)[4-10]. As mentioned in Chapter 1, the WGSR has significance in industrial applications because it improves the hydrogen content of water gas, thereby enhancing the steam reforming process as shown in equations (1) and (2). The homogeneous catalysis of WGSR is important because it requires milder conditions[14], with water being present as a liquid, than the heterogeneous catalysis systems, which have been traditionally used in industry. Therefore, there has been considerable interest in recent years towards understanding the mechanism of the WGSR for homogeneous catalysis systems. Transition metal carbonyls[14,15], such as $Cr(CO)_6$ and $Mo(CO)_6$ have been employed as homogeneous catalysts of WGSR, but it is $Fe(CO)_5$ that has been used in almost all experimental and computational studies that have focused on understanding the mechanism of the WGSR. Several groups have proposed different mechanistic cycles for the $Fe(CO)_5$ catalyzed WGSR.

$$CH_4 + H_2O \longrightarrow CO + H_2 + CO_2 \quad (1)$$

$$CO + H_2O \longrightarrow CO_2 + H_2 \quad (2)$$

From experimental observations, gas phase $Fe(CO)_5$ catalyzed WGSR was initially proposed to proceed through a catalytic cycle as shown in Scheme 3A.1, which included the experimentally substantiated individual reactions[16]. Subsequent modifications to the mechanism were proposed by Sunderlin and Squires[17], who suggested a $Fe(CO)_4COOH^-$ intermediate[18], based on new experimental observations. Torrent *et al*.[19] investigated this

mechanism through a theoretical approach and proposed a $[H_2O]$-$[Fe(CO)_4H^-]$ adduct followed by OH^- desorption to yield the $Fe(CO)_4H_2$ species (see Scheme 3A.2).

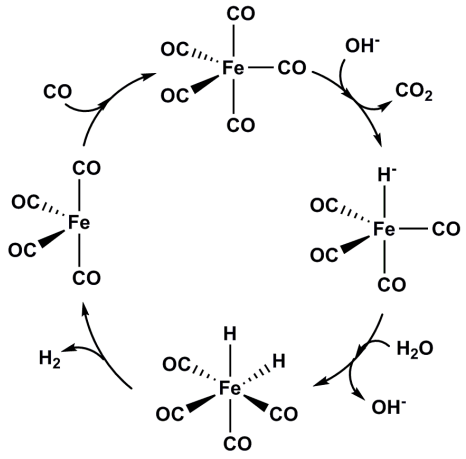

Scheme 3A.1. The mechanism initially proposed for $Fe(CO)_5$ catalyzed WGSR.

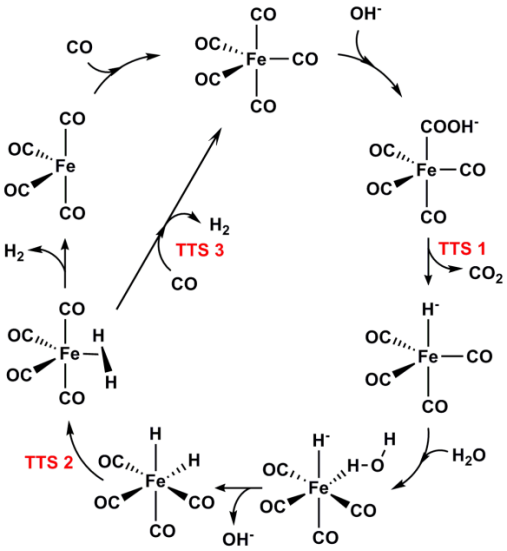

Scheme 3A.2. The mechanism proposed by Torrent *et al*. for a $Fe(CO)_5$ catalyzed WGSR.

Since this OH^- desorption step was found to have a high energy barrier, S. E. Barrows[20] suggested a further modification that avoided this step by having the $Fe(CO)_4COOH^-$ species directly convert to $Fe(CO)_4CHO^-$ and back to $Fe(CO)_4COOH^-$ (see Scheme 3A.3). However, since the Barrows mechanism avoided the experimentally observed $Fe(CO)_4H^-$ species, Rozanska and Vuilleumier[21] proposed a new mechanism that included the $Fe(CO)_4H^-$ species and also excluded the OH^- desorption step (see Scheme 3A.4). Subsequent to this, Zhang[22] *et al*. have done a theoretical revisit of the mechanism, examining other new possible pathways for the WGSR (see Scheme 3A.5).

As the schemes 3A.1-3A.5 indicate, what all the proposed WGSR mechanisms have in common is a mono-nuclear metal catalyst that does the conversion of CO and H_2O to CO_2 and H_2. However, it is of interest to note that binuclear intermediates having the formula $Fe_2(CO)_8OH^-$ (potentially $Fe_2(CO)_7COOH^-$), have been observed during gas phase experimental studies on the $Fe(CO)_5$ catalyzed WGSR, at increased flow rates of $Fe(CO)_5$[18]. It is possible that the mono-nuclear $Fe(CO)_5$ species can form bi-nuclear intermediates and, due to the consequent possibilities of metal-metal cooperativity, this may lead to a mechanistic cycle for the WGSR that is more energetically favorable.

Indeed metal-metal cooperativity leading to the WGSR has been observed for bi-metallic ruthenium based systems[23,24]. These considerations have led us to propose a new mechanism for the WGSR that incorporates metal-metal cooperativity and bi-nuclear intermediates during the reaction cycle. This mechanism is shown in Scheme 3A.6 below. As the scheme indicates, two $Fe(CO)_5$ molecules and OH^- can combine to form $Fe_2(CO)_8COOH^-$ which can then decarboxylate to yield $Fe_2(CO)_8H^-$, followed by addition of H_2O and the loss of H_2 to yield the $Fe_2(CO)_7COOH^-$ intermediate, which upon addition of CO would give back the $Fe_2(CO)_8COOH^-$ species and complete the cycle.

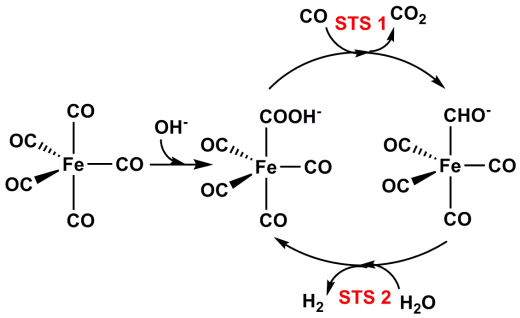

Scheme 3A.3. The mechanism proposed by S. E. Barrows for a $Fe(CO)_5$ catalyzed WGSR.

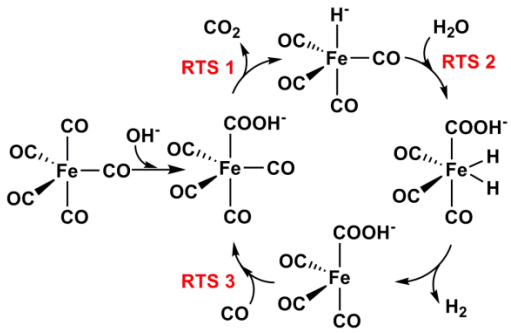

Scheme 3A.4. The mechanism proposed by Rozanska *et al*. for a $Fe(CO)_5$ catalyzed WGSR.

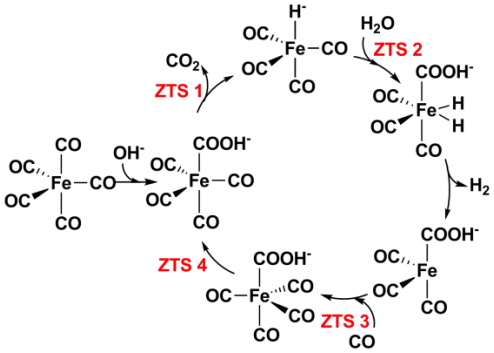

Scheme 3A.5. The mechanism proposed by Fuli Zhang *et al*. for a $Fe(CO)_5$ catalyzed WGSR.

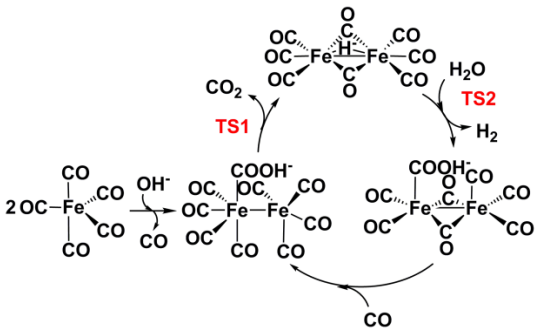

Scheme 3A.6. The newly proposed mechanism for a homogeneous $Fe(CO)_5$ catalyzed WGSR, describing a bi-metallic pathway.

Our objective in this work has been to evaluate all the steps of this mechanistic cycle through full gas phase quantum mechanical calculations using density functional theory (DFT). Furthermore we calculated all the intermediates and transition states

pertaining to all the previous WGSR mechanisms proposed by Torrent *et al*.[19], Barrows[20], Rozanska *et al*.[21] and Zhang *et al*.[22], shown in the schemes 3A.2-3A.5. This has been done in order to evaluate the efficiency of our mechanism in comparison to the other proposed mechanisms, at the same level of theory. Moreover, the "Energetic Span Model" (ESM) developed by Shaik and co-workers[25-27] has been employed to determine the relative Turn-over Frequencies (TOFs) for the different mechanisms. This has been done as a further index for comparing our proposed mechanism with the others in order to evaluate the one with the highest efficiency, that is, the one that would give the highest TOF. This is a more reliable way of comparing the different mechanisms because it takes into account not only the principal rate determining transition state, but also the other, potentially rate influencing transition states and intermediates during the catalysis process[25].

In addition to the gas phase calculations, we have also studied all mechanisms after incorporating solvent effects. This is because it is possible that a reaction mechanism that is calculated to be energetically unfavorable in the gas phase could be found to be favorable in the solvent phase. This is due to the possibility of differential energy stabilization of the solvent on the charged dissociated ion pair intermediates and transition states. Such differences in energy stabilization can potentially alter the energetics of the different mechanistic cycles and cause one mechanism that was less significant in the gas phase to become more predominant in the solvent phase. The possibility of this occurring has been speculated in the past[21,28]. In order to determine the relative efficacies of the different reaction mechanisms, the Energetic Span Model has also been employed with the results obtained from for the solvent phase calculations, for different solvent combinations of water and methanol. Finally, based on the insights gained from our mechanistic studies, we have discussed the possibility of developing new bi-metallic systems for the homogeneous catalysis of the WGSR.

3A.2 Computational Details

Geometry optimizations and vibrational frequency calculations were performed at the level of DFT-B3LYP[29,30] in Gaussian 09[31]. The basis set employed was 6-31++g(d,p)[32]. Previous reports[20] on WGSR mechanisms have employed this functional and basis set combination. As shown in Table 3A.1, the results obtained from the present calculations

on the previously reported mechanisms accurately match the reported ΔE values. Further validity for the chosen basis set was provided by full geometry optimizations done for a set of structures with the 6-311++g(2df,2pd). As shown in Table 3A.2, it was found that there was no change in the bond lengths and the bond angles between the different structures obtained from the geometry optimizations done with the 6-31++g(d,p) and the 6-311++g(2df,2pd) basis set, thus indicating that the geometries obtained from the 6-31++g(d,p) basis set are reliable. With regard to the energies, a comparison to the experimentally observed ΔH values[17] for a given set of reactions, collected in Table 3A.3, indicated that the ΔH values calculated with the 6-31++g(d,p) basis set corresponded better with the experimental values than the ΔH values obtained with the 6-311++g(2df,2pd) bases set. Hence the 6-31++g(d,p) basis set, employed for all the calculations, was seemed to be appropriate for obtaining both reliable structures and potential energy surfaces.

Table 3A.1. The comparison of the B3LYP/6-31++G(d,p) calculated energies (ΔE values in kcal/mol) with the ΔE values reported previously in Reference (17); [a] Numbers in parentheses include ZPE corrections.

Reaction	ΔE B3LYP/6-31++G(d,p) (Torrent)	ΔE B3LYP/6-31++G(d,p) (SE Barrows)	ΔE B3LYP/6-31++G(d,p) (current)
$Fe(CO)_5 + OH^- \rightarrow (CO)_4FeCOOH^-$	-70.5 (-65.8)[a]	-71.8 (-67.6)[a]	-71.8 (-67.6)[a]
$(CO)_4FeCOOH^- \rightarrow (CO)_4FeH^- + CO_2$	-3.9 (-7.3)	-1.6 (-5.0)	-1.6 (-4.9)
$(CO)_4FeH^- + H_2O \rightarrow (CO)_4FeH^- - H_2O$	-7.0 (-3.4)	-7.5 (-5.9)	-7.5 (-5.99)
$(CO)_4FeH^- - H_2O \rightarrow (CO)_4FeH_2 + OH^-$	82.6 (78.5)	84.3 (80.5)	84.3 (80.6)
$(CO)_4FeH_2 \rightarrow (CO)_4FeH_2$	7.9 (7.7)	6.4 (6.6)	6.4 (6.6)
$(CO)_4FeH_2 \rightarrow (CO)_4Fe + H_2$	17.5 (13.2)		18.2 (13.6)
$(CO)_4Fe + CO \rightarrow Fe(CO)_5$	-37.9 (-35.1)		-39.3 (-36.4)

Table 3A.2. The comparison of the bond lengths and bond angles of the optimized geometries, using the 6-31++G(d,p) and the 6-311++G(2df,2pd) basis sets for the three molecules $Fe(CO)_5$, $Fe(CO)_4COOH^-$ and $Fe(CO)_4H^-$. [a]Bond length is in A^0 unit and [b]bond angle is in the degree unit.

$Fe(CO)_5$	6-31++G(d,p)	6-311++G(2df,2pd)
$Fe\text{-}C_{axial}$	1.828[a]	1.828
$Fe\text{-}C_{equitorial}$	1.819	1.819
$C_{ax}\text{-}O_{ax}$	1.148	1.148
$C_{eq}\text{-}O_{eq}$	1.152	1.152
$C_{ax}\text{-}Fe\text{-}C_{eq}$	90.0[b]	90.0[b]
$C_{eq}\text{-}Fe\text{-}C_{eq}$	120.0	120.0
$Fe(CO)_4COOH^-$	6-31++G(d,p)	6-311++G(2df,2pd)
$Fe\text{-}C_{axial}$	1.789a	1.789a
$Fe\text{-}C_{eq1}$	1.799	1.799
$Fe\text{-}C_{eq2}$	1.788	1.788
$C_{ax}\text{-}O_{ax}$	1.164	1.164
$C_{eq1}\text{-}O_{eq1}$	1.161	1.161
$C_{eq2}\text{-}O_{eq2}$	1.168	1.168
Fe-C=O	129.4b	129.4b
C-O-H	105.9	105.9
$C_{eq1}\text{-}Fe\text{-}C_{eq2}$	126.8	126.8
$C_{eq2}\text{-}Fe\text{-}C_{eq3}$	116.1	116.1
$Fe(CO)4H^-$	6-31++G(d,p)	6-311++G(2df,2pd)
$Fe\text{-}C_{axial}$	1.787a	1.787a
$Fe\text{-}C_{equitorial}$	1.774	1.774
$C_{ax}\text{-}O_{ax}$	1.168	1.168
$C_{eq}\text{-}O_{eq}$	1.171	1.171
$H\text{-}Fe\text{-}C_{eq}$	81.1b	81.1b
$C_{eq}\text{-}Fe\text{-}C_{eq}$	117.6	117.6
$C_{eq}\text{-}Fe\text{-}C_{ax}$	98.9	98.9
[a]Bond length is in A^0 unit and [b]bond angle is in the degree unit.		

Table 3A.3. The comparison of the calculated ΔH values, obtained for a set of reactions with different basis sets and with and without dispersion corrections, with the experimentally reported ΔH values (reference 17) for the same set of reactions.

Reaction	Experimental	B3LYP/ 6-31g++ (d,p)	B3LYP/6-311++g (2df,2pd)	DFT-D3/ Zero Damping	DFT-D3/ B-J Damping
$Fe(CO)_5+OH^- \rightarrow (CO)_4FeCOOH^-$	-60.0	-69.0	-65.2	-68.0	-64.7
$(CO)_4FeCOOH^- \rightarrow (CO)_4FeH^- + CO_2$	-4.0	-4.7	-8.5	-5.9	-12.2
$(CO)_4FeH^- + H_2O \rightarrow (CO)_4FeH_2 + OH^-$	72.0	74.4	72.6	74.7	75.6
$(CO)_4FeH_2 \rightarrow (CO)_4Fe + H_2$	26.0	22.3	21.3	21.7	19.6
$(CO)_4Fe+CO \rightarrow Fe(CO)_5$	-42.0	-37.3	-35.9	-36.7	-32.4

A further correction that was considered for the energies was a DFT-D3 dispersion correction,[33,34] done as a single point correction to the final geometry optimized structures. DFT-D3 dispersion corrections with zero damping and Becke-Johnson damping were considered. As shown in Table 3A.3, the dispersion corrected ΔH values for a given set of reactions corresponded better with the experimental ΔH values in comparison to the uncorrected values, in some cases. However, in many cases, the uncorrected ΔH values corresponded better with experiment than the dispersion corrected ΔH values, for both the types of dispersion corrections considered. Therefore, the DFT-D3 dispersion corrections have not been included for the results for the potential energy surfaces obtained for the different reactions discussed in the thesis.

Solvent corrections were included with the help of the PCM-SMD[35] model. The parameters that were employed when using this model were taken from the database by Truhlar and co-workers.[35, 36] The values are shown in Table 3A.4 below. It is to be noted that the database provides parameters only for pure solvents. Each of the seven parameters for the methanol-water mixtures has been calculated as the weighted average of corresponding parameters of the methanol and water from the Truhlar's database. The contributions of internal energy and entropy were further obtained from frequency calculations done on the DFT structures at 298.15 K: thus, the energies reported in the figures of the paper are the ΔG values. Care has been taken to ensure that all the transition states had only one negative frequency. In this regard, it is noted that, for the solvent

corrected calculations, a correction factor in the shape of an additional 1.89 kcal/mol was added to the free energy values, in order to account for the standard solute concentration in solvent, which is 1 M, or equivalently, 24 atm[37,38]. The potential energy surfaces of the mechanisms described in the thesis can be obtained for low catalyst concentrations - corresponding to 1 atm – by the subtraction of this correction factor from all the reactant, intermediate and product species in each of the energy profiles.

Table 3A.4. The weighted averages for the parameters for different water-methanol compositions, the parameters for pure water and methanol having been taken from Truhlar's database.

Parameters	water	methanol	25% methanol	50% methanol	75% methanol
n	1.333	1.328	1.332	1.331	1.329
α	0.820	0.430	0.723	0.625	0.528
β	0.350	0.470	0.380	0.410	0.440
γ	0.000	31.770	7.943	15.885	23.828
E	78.355	32.613	66.919	55.484	44.049
Φ	0.000	0.000	0.000	0.000	0.000
ψ	0.000	0.000	0.000	0.000	0.000

The efficiency of a catalytic cycle can be analyzed through the determination of TOFs. Shaik and co-workers[25] have proposed an ESM in order to calculate the TOF from theoretically obtained energy profiles. According to this model, the TOF-determining transition state and the TOF determining intermediate can be located from a catalytic cycle by the evaluation of the degree of TOF control (X_{TOF})[25]. The TOF can be calculated by the following equation.

$$TOF = \frac{K_B T}{h} e^{\frac{-\delta E}{RT}}$$

Where δE , the energetic span can be defined as

$$\delta E = \begin{cases} T_{TDTS} - T_{TDI} & \text{if TDTS appears after TDI} \\ T_{TDTS} - T_{TDI} + \Delta G_r & \text{if TDTS appears before TDI} \end{cases}$$

This model has been employed to calculate the TOFs for the free energy profiles obtained for the different mechanisms discussed in the thesis. The theoretical details of ESM is provided in Chapter 1.

3A.3 Results and Discussion

3A.3.1 Proposed Bi-nuclear mechanism: Shown in Figure 3A.1 below is the energy profile for our proposed bi-nuclear mechanism in the gas phase (shown in the brackets) as well as for the reaction occurring in for a solvent consisting of a 50% methanol-water mixture (values shown outside the brackets). Our mechanism shows the possibility of the formation of the binuclear intermediate $Fe_2(CO)_8COOH^-$ from two mono-nuclear $Fe(CO)_5$ species reacting with OH^-. The formation of $Fe_2(CO)_8COOH^-$ is envisaged to occur through the following two steps: (i) formation of the $Fe(CO)_4COOH^-$ species through the reaction of $Fe(CO)_5$ with OH^-, as described in all the previously proposed mechanisms (see the Schemes 3A.2-3A.5) followed by (ii) the reaction of $Fe(CO)_4COOH^-$ with another $Fe(CO)_5$ to produce $Fe_2(CO)_8COOH^-$, releasing a molecule of CO in the process. As Figure 3A.1 indicates, the reaction is endothermic by 6.0 kcal/mol (ΔG value) in the solvent phase, while it is favorable by 44.0 kcal/mol (ΔG value) in the gas phase. The greater stabilization of the OH^- reactant species by the solvent leads to the reduced favorability of the reaction in the solvent phase. The formed $Fe_2(CO)_8COOH^-$ species can subsequently decarboxylate to produce the bi-nuclear hydride species, $Fe_2(CO)_8H^-$, after passing through the transition state labeled as TS1 in Figure 3A.1. The formation of a bi-nuclear hydride intermediate species has been proposed in the past for the WGSR for the mono-nuclear $Ru(CO)_5$ species[14]. The transition state structure of TS1 is shown in Figure 3A.2(a). The addition of water to the bi-nuclear hydride $Fe_2(CO)_8H^-$ would yield $Fe_2(CO)_7COOH^-$ along with the formation of H_2 is the step with the highest activation barrier in the cycle, passing through a barrier of 41.6 kcal/mol in the solvent phase and of 43.4 kcal/mol in the gas phase. The transition state structure (TS2) for this process is shown in Figure 3A.2(c). Further addition of CO to $Fe_2(CO)_7COOH^-$ would give back the $Fe_2(CO)_8COOH^-$ species and complete the catalytic cycle. As mentioned in the Introduction, we have also determined the free energy profiles for the reaction mechanisms proposed by Torrent *et al*.[19], Barrows[20], Rozanska *et al*.[21] and Zhang *et al*.[22], and they are shown in the Figures 3A.3, 3A.4, 3A.5 and 3A.6 respectively. Like in the case of Figure 3A.1, the values inside and outside the parentheses indicate the ΔG values obtained in the gas and solvent phases respectively, the solvent, as before, being the 50% mixture of water and methanol. A perusal of the obtained ΔG values for the other mechanisms and their comparison to the values that have been obtained for our proposed bi-nuclear mechanism indicates that the two barriers, TS1 and TS2, in our mechanism, are

lower than the corresponding barriers in all the other proposed mechanisms. For the TS1 case: the transition state prior to the release of CO_2, the ΔG value for the barrier calculated in the gas (19.1 kcal/mol) and solvent phase (19.2 kcal/mol) for the bi-nuclear mechanism is lower than the corresponding, CO_2 producing reaction barriers in the gas and solvent phases for mechanism proposed by Torrent *et al*. (29.9 kcal/mol: gas phase, 31.6 kcal/mol: solvent phase), by the Barrows mechanism (31.7 kcal/mol: gas phase, 27.9 kcal/mol: solvent phase), by Rozanska *et al*. (29.9 kcal/mol: gas phase, 31.6 kcal/mol: solvent phase) and by Zhang *et al*. (29.9 kcal/mol: gas phase, 31.6 kcal/mol: solvent phase) (see Figures 3A.1 and 3A.3-3A.6). Likewise, for TS2, the bi-nuclear mechanism, the values (43.4 kcal/mol: gas phase, 41.6 kcal/mol: solvent phase) are lower than the values obtained for the H_2 formation step, the step with the highest activation barrier, by Torrent *et al*. (101.2 kcal/mol: gas phase, 48.8 kcal/mol: solvent phase), by the Barrows mechanism (52.4 kcal/mol: gas phase, 55.6 kcal/mol: solvent phase), by Rozanska *et al*. (49.7 kcal/mol: gas phase, 51.3 kcal/mol: solvent phase) and by Zhang *et al*. (49.7 kcal/mol: gas phase, 51.3 kcal/mol: solvent phase) (see Figures 3A.1 and 3A.3-3A.6).

The reason why the bi-nuclear mechanism provides more facile transformations through lower barriers is explained by the metal-metal cooperativity between the two iron centers. Figure 3A.2 shows the structures of the transition states that have been obtained from the bi-nuclear mechanism: TS1 (Figure 3A.2a) and TS2 (Figure 3A.2c) as well as the corresponding transition state structures 2(b) and 2(d) obtained from the mono-nuclear Zhang mechanism, indicated as ZTS1 and ZTS2 and shown for the purpose of comparison. A comparison of TS1 and ZTS1 shows that the presence of two iron centers in TS1 makes a five membered ring, which is less sterically crowded and therefore more favorable than the more highly strained four membered ring formed in the case of ZTS1. Similarly, TS2 is a more sterically favored six membered ring structure in comparison to the more encumbered five membered ring ZTS2 structure. The formation of a five membered transition state leading to a more facile reaction for a bi-metallic species in comparison to a mono-nuclear one has been observed earlier, for the case of alkene insertion into the C-H bond, for a Y-based catalyst[39]. The formation of the bi-nuclear species thus alleviates ring strain in both the transition states and leads to lower barriers. It appears that it is this steric advantage conferred by metal-metal cooperativity that is the principal cause of the lower barriers for the bi-nuclear mechanism: a Natural Bond Orbital (NBO)[40] analysis, conducted for the intermediates and transition states for both

the bi-nuclear and the Zhang mechanism did not reveal any significant differences in the essential nature of the bonding between the atoms in the intermediates and the transition states. The charges obtained from the NBO analysis for the intermediates and transition states TS2 and ZTS2 are shown in the Table 3A.5.

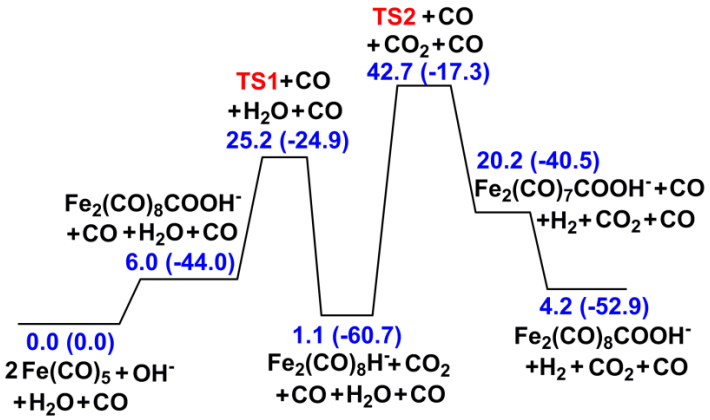

Figure 3A.1. The free energy profile for the newly proposed mechanism using $Fe(CO)_5$ as the catalyst; solvent corrections considered are for the 50% methanol-water mixture case, gas phase values are given in parentheses; all values are in kcal/mol.

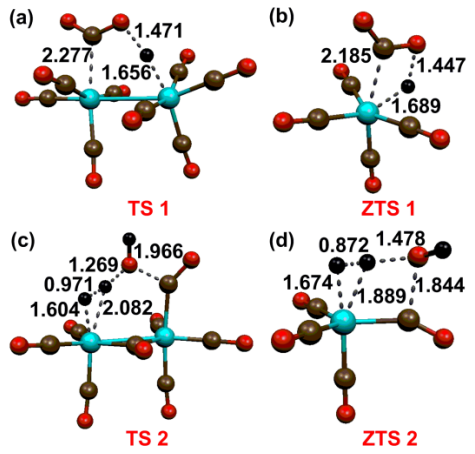

Figure 3A.2. The optimized structures for the transition states (a) TS 1 (b) ZTS 1 (c) TS 2 (d) ZTS 2; the color scheme is as follows: iron-green, carbon-brown, oxygen-red, and hydrogen-black.

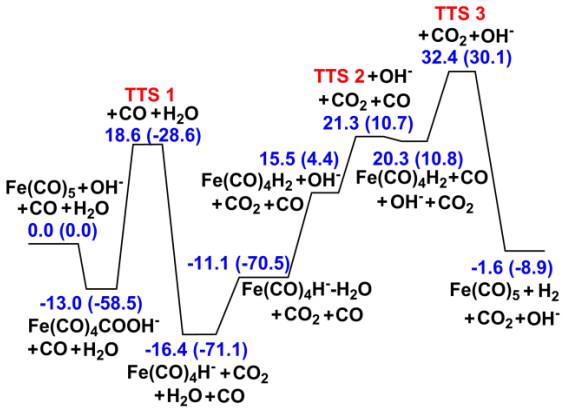

Figure 3A.3. The free energy profile for the Torrent mechanism; solvent corrections considered are for the 50% methanol-water mixture case; gas phase values are given in parentheses; all values are in kcal/mol.

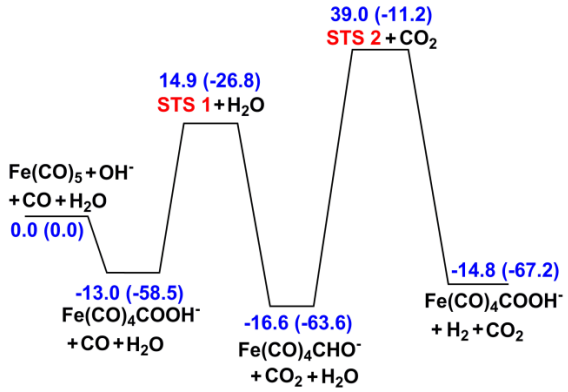

Figure 3A.4. The free energy profile for the Barrows mechanism; solvent corrections considered are for the 50% methanol-water mixture case; gas phase values are given in parentheses; all values are in kcal/mol.

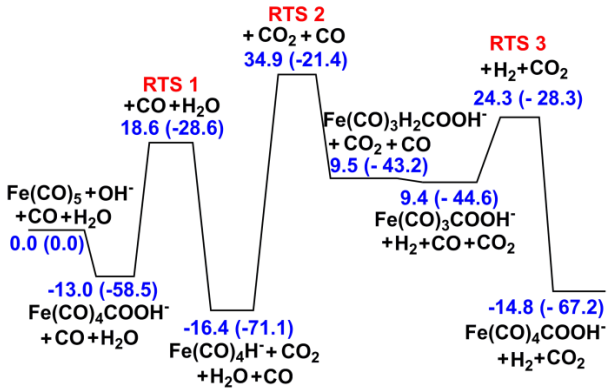

Figure 3A.5. The free energy profile for the Rozanska mechanism; solvent corrections considered are for the 50% methanol-water mixture case; gas phase values are given in parentheses; all values are in kcal/mol.

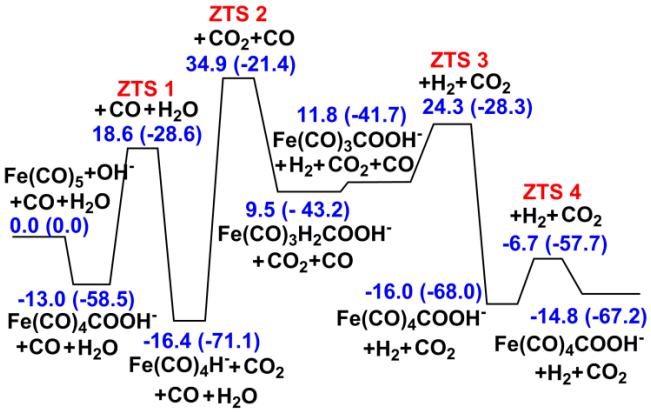

Figure 3A.6. The free energy profile for the Zhang mechanism, solvent corrections considered are for the 50% methanol-water mixture case; gas phase values are given in parentheses; all values are in kcal/mol.

Table 3A.5. The natural charges obtained from the NBO analysis, for the transition state and the intermediate of the rate determining step for the Zhang and the newly proposed bi-nuclear mechanism.

Atom	$Fe(CO)_4H^-$	$Fe_2(CO)_8H^-$	ZTS 2	TS 2
Fe (1)	-2.30254	-2.04764	-1.88276	-1.77439
Fe (2)	-	-2.04764	-	-1.77341
H	0.21020	0.30474	0.06426	0.04385
H (H_2O)	0.48823	0.48823	0.30803	0.39335
O (H_2O)	-0.97647	-0.97647	-0.97731	-0.84525

3A.2.2 Comparison of the efficiency of the different mechanisms using the energetic span model: As discussed in the Introduction, the efficiency of the different mechanisms has been further compared with the help of TOF calculations done with the aid of the energetic span model (ESM)[25]. This is a more reliable way of comparing the different mechanisms because it takes into account not only the principal rate determining transition state, but also the other, potentially rate influencing transition states and intermediates during the catalysis process. Discussed in this section are the TOFs calculated for the different reaction mechanisms, not only in the gas phase but also in the solvent phase for different methanol-water mixture combinations.

A perusal of the mechanistic cycles shown in the Figures 3A.3-3A.6 indicates that the mono-nuclear mechanisms have shared intermediates and transition states. Moreover, all the mechanisms shown in the Figures 3A.1 and 3A.3-3A.6 compare mechanistic routes starting from the same catalyst: $Fe(CO)_5$. Therefore, according to the ESM, if one accessible state has very low energy, it will be the TOF determining intermediate (TDI) for *all* the mechanisms. This is also true when it comes to evaluating the TOF determining transition state (TDTS) for the ESM calculations. Therefore, it is necessary to compare the energy profiles for all the mechanisms, both in the gas as well as in the solvent phase, in order to find the TDI and TDTS for each case. Figure 3A.7 below shows the different energy profiles for the mechanistic cycles, considered in the gas phase. Shown in blue are the lowest lying intermediate and transition state for the gas phase calculations, which would be the TDI and the TDTS for the WGSR in the gas phase when using the $Fe(CO)_5$ catalyst. As Figure 3A.7 indicates, both the TDI and TDTS correspond to the Zhang Mechanism. The newly proposed bi-nuclear mechanism has a lower

difference between its intermediates and transition states (barrier heights), as shown in the previous section, but it does not yield the lowest intermediate or transition state along the potential energy surface. Therefore, even though the effects of metal-metal cooperativity enable the bi-nuclear mechanism to have lower barriers in the mechanistic cycle, the fact that the intermediates and transition states in this mechanistic cycle lie slightly higher than for the competing mono-nuclear mechanistic cycles leads to it not being the predominant mechanism for the $Fe(CO)_5$ catalyst and thus not contributing to the TDI or TDTS in the ESM TOF calculations. We have analyzed the effect of 25%, 50% and 75% methanol-water mixtures computationally using Truhlar's database[36]. The same results are obtained when considering the potential energy surfaces for the solvent corrected potential energy surfaces for the different mechanistic cycles. Shown in Figure 3A.8 is a comparison of the potential energy surfaces of the intermediates and transition states for the different WGSR mechanisms for the solvent corrected energies pertaining to the case of the 50% water-methanol mixture solvent. For this case (as well as for the 25% and 75% water-methanol mixture cases), it is the mono-nuclear Torrent Mechanism that was found to yield the TDI and TDTS (shown in blue – see Figure 3A.8).

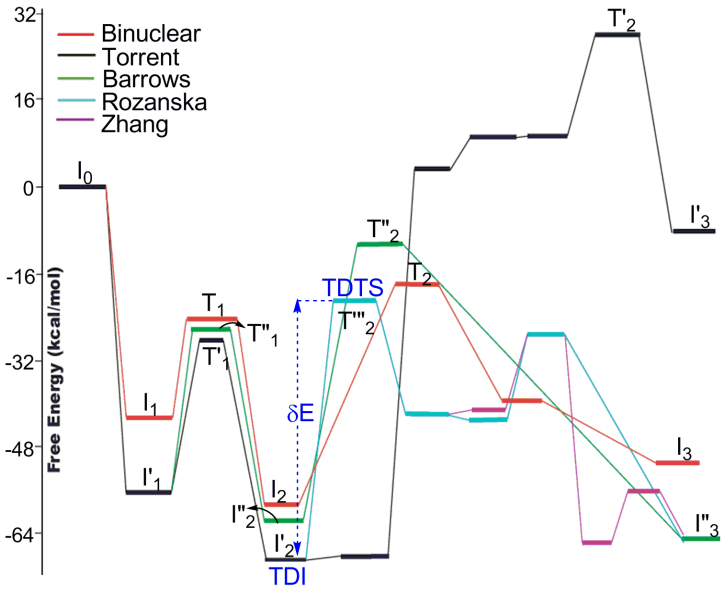

Figure 3A.7. The combined free energy profile of all the $Fe(CO)_5$ catalyzed mechanisms in the gas phase.

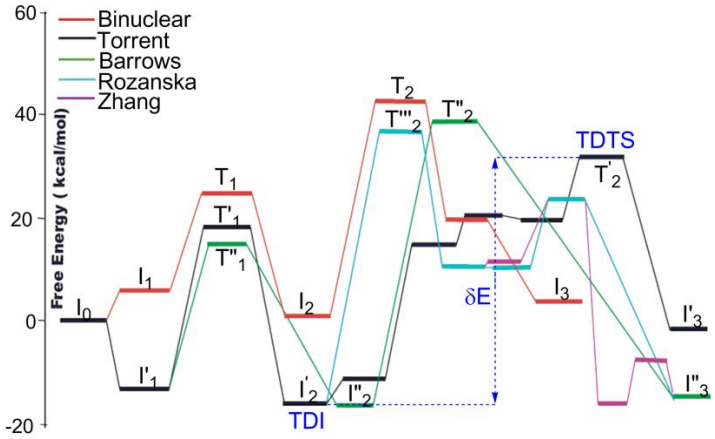

Figure 3A.8. The solvent corrected combined free energy profile of all the $Fe(CO)_5$ catalyzed mechanisms, for the case of the 50% methanol-water mixture, all values are in kcal/mol.

The calculated free energy profiles for the 25% and 75% methanol-water mixtures have been provided in Figures 3A.9-3A.13.

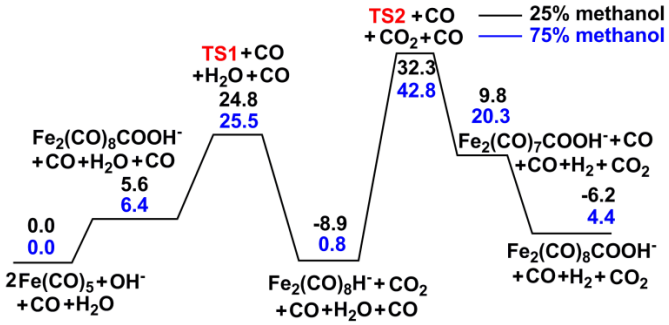

Figure 3A.9. The free energy profile for the newly proposed mechanism, with 25% and 75% methanol-water mixtures as the two solvent cases; all values are in kcal/mol.

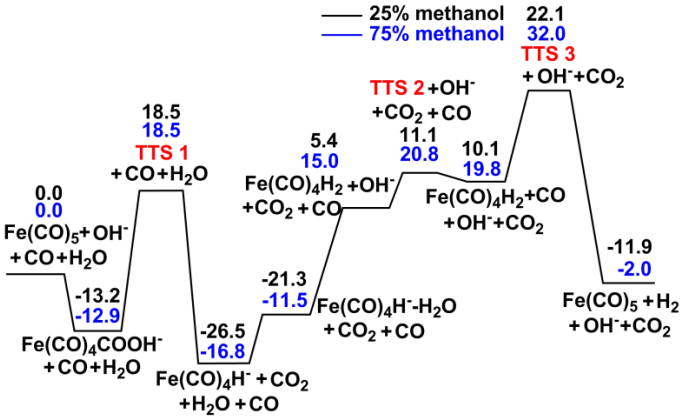

Figure 3A.10. The free energy profile for the Torrent mechanism, with 25% and 75% methanol-water mixtures as the two solvent cases; all values are in kcal/mol.

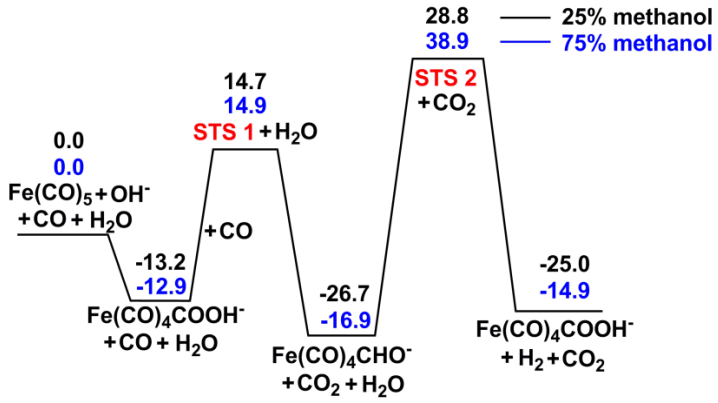

Figure 3A.11. The free energy profile for the S. E. Barrows mechanism, with 25% and 75% methanol-water mixtures as the two solvent cases; all values are in kcal/mol.

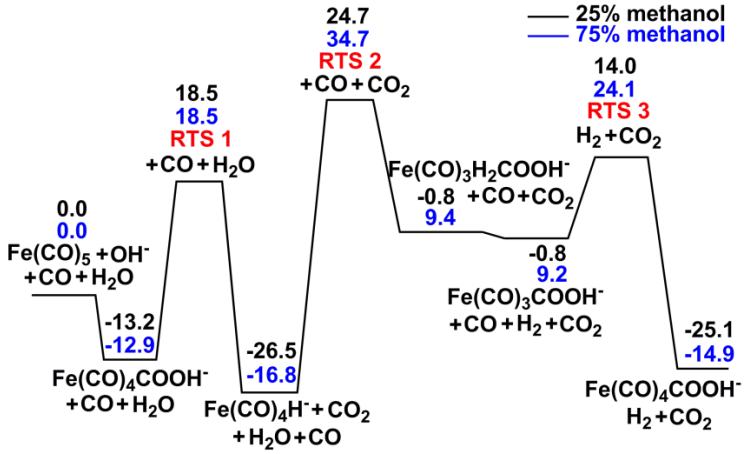

Figure 3A.12. The free energy profile for the Rozanska mechanism, with 25% and 75% methanol-water mixtures as the two solvent cases; all values are in kcal/mol.

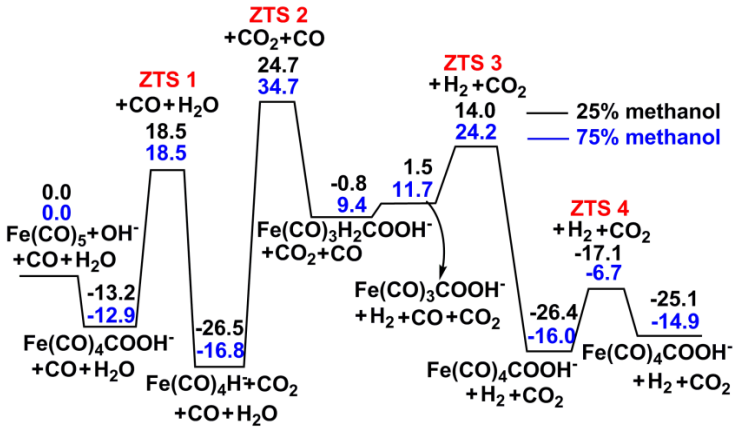

Figure 3A.13. The free energy profile for the Zhang mechanism, with 25% and 75% methanol-water mixtures as the two solvent cases; all values are in kcal/mol.

In this regard, it is to be noted that for the TDI, the Barrows Mechanism does have a slightly lower intermediate – lower by only 0.2 kcal/mol - than the Torrent mechanism intermediate that has been chosen for the TDI. However, the Barrows Mechanism intermediate has not been considered as the TDI because this does not connect to the TDTS (obtained from the Torrent Mechanism) through a shared pathway. Since the difference between the Torrent intermediate and the Barrows intermediate is small enough (0.2 kcal/mol) to fall within the bounds of systematic calculation error, the Torrent Mechanism intermediate has been considered the TDI for the ESM calculations. Again, as for the gas phase results, the newly proposed bi-nuclear mechanism, despite having lower barrier heights did not contribute to the TDI or TDTS, since its intermediates and transition states were found to lie higher in energy than the corresponding intermediates and transition states for the Torrent mechanism.

Having determined the TDI and TDTS for the different gas phase and solvent phase (25%, 50% and 75% methanol-water mixtures) cases, the TOF calculations were then done for each case. The results are collected in Table 3A.6. The first row of TOF values in Table 3A.6 shows the absolute values of the calculated TOFs for the overall mechanistic cycles derived for the gas phase and the different solvent mixture cases. As seen in Table 3A.6, the absolute TOF values are of the order of 10^{-20}, but this is likely due to the sensitivity of the method to error when comparing exponential terms. It is, however, to be noted that the value of the ESM TOF calculations lies in comparing the *relative* TOF values, rather than *absolute* TOF numbers, especially (as in the current calculations), when all the values for the barrier heights and the energies of the intermediates have been calculated at the same level of theory. The errors arising from comparing exponential terms are compensated for when doing relative TOF comparisons[25]. The relative TOF values, shown in the second row of Table 3A.6, were obtained by dividing all the entries for the absolute TOF values by the smallest TOF value: 7.5×10^{-21} h^{-1}, obtained for the gas phase calculation.

Table 3A.6. The absolute and relative TOF values (h^{-1}) obtained for the mono-nuclear mechanism using $Fe(CO)_5$ as the catalyst.

	Gas phase	25% methanol	50% methanol	75% methanol
Absolute TOF	7.5×10^{-21}	4.8×10^{-20}	3.5×10^{-20}	3.5×10^{-20}
Relative TOF	1	6.4	4.7	4.7

As seen in Table 3A.6, the comparison of the relative TOF values for the different cases provides some useful insights into the nature of the mechanisms for the WGSR. These are discussed point-wise below:

(i) As was mentioned in the Introduction, one of the reasons for incorporating solvent corrections was to determine whether certain mechanistic cycles that had been found to be less significant in the gas phase would become more important once solvent effects were introduced. As seen from the composite mechanism derived from the different mechanisms for the solvent case shown in Figure 3A.8 (50% methanol-water mixture), this is indeed true for the Torrent mechanism, which is seen to provide the TDI and the TDTS for the ESM calculations in the solvent phase, while the transition states for the same Torrent mechanism in the gas phase were found to be lying significantly higher in energy than for the other competing mechanisms (see Figure 3A.7). The reason for this is because the Torrent mechanism is the only one among all the proposed mechanisms that involves desorption of OH^- in one of the intermediate stages (see Scheme 3A.2 and Figure 3A.3). While desorption of OH^- is a highly endothermic process in the gas phase (75.5 kcal/mol), it is much more favored in the solvent phase (31.9 kcal/mol for the case of the 50% methanol-water mixture), due to the greater degree of stabilization of the small OH^- ion by the solvent. Thus, the results validate the need to check all the proposed mechanisms, even ones that had been found to be very poor in the gas phase, once solvent corrections had been added.

(ii) The absolute, as well as the relative TOF values, calculated for the WGSR mechanisms in the different solvent mixture cases, indicates that the efficiency of the WGSR decreases with the increase of the % of methanol in the methanol-water mixtures (see Table 3A.6): the relative TOF value is 6.4 for the 25% methanol-water mixture while it is 4.7 for both the 50% and 75% methanol-water mixtures. This appears to contradict experimental observations: different methanol-water mixtures have been experimentally studied by King and co-workers[9], who have found that the efficiency of the WGSR improved at higher methanol-water ratios. This discrepancy between the experimental and computational results can be explained by the fact that methanol acts not only as a solvent, but also as a reactant for the WGSR, providing the OH^- ions that are necessary for the formation of the important $Fe(CO)_4COOH^-$ intermediate species in the mono-nuclear mechanism and the $Fe_2(CO)_8COOH^-$ intermediate species in the proposed bi-

nuclear mechanism. As a solvent, increased methanol in the methanol-water mixtures would reduce the dielectric constant of the solvent and thus act to reduce the stabilization of the ionic intermediates and transition states, which gets reflected in the lower TOF values shown in Table 3A.6. However, as a reactant, increased methanol in the methanol-water mixtures would improve the efficiency of the WGSR and lead to increased TOF, because of the increased availability of OH^- during the reaction. Thus, the experimentally observed favorable effect of increased methanol in methanol-water mixtures[9] suggests that methanol in its role as a reactant has a greater influence on the WGSR than in its role as the solvent.

(iii) Finally, a perusal of the energy profiles in the Figures 3A.7 and 3A.8, as well as the fact that the composite mechanism determined for the gas phase and solvent mixture cases does not include any TDI or TDTS from the newly proposed bi-nuclear mechanism shows that the effects of metal-metal cooperativity would not have an impact on the rate or the TOF for the WGSR when using the $Fe(CO)_5$ catalyst. The reason for this is the fact that the first step of the bi-nuclear mechanism involves a dimerization process: the reaction of two $Fe(CO)_5$ molecules with OH^- to form the $Fe_2(CO)_8COOH^-$ species. Such a process is entropically disfavored, and this is reflected in the higher energy of the first intermediate in comparison to the other intermediates in the other mechanisms. This entropic unfavorability may provide an explanation for why the bi-nuclear species having the formula $Fe_2(CO)_8OH^-$ (likely to be $Fe_2(CO)_7COOH^-$) has only been experimentally observed at increased flow rates of $Fe(CO)_5$[18]. What is important to note, however, is that the problem of entropic unfavorability would not exist for Fe-based catalysts *that are bi-nuclear to begin with*. In such a situation, the first unfavorable dimerization step is automatically avoided, and then one might see the advantages of metal-metal cooperativity leading to significant improvements in the TOF. This is discussed further in the next section.

3A.3.3 Designing improved catalysts for the WGSR: As pointed out at the end of the previous section, the true potential of metal-metal cooperativity in improving the yield from the WGSR can be realized if one designed bi-metallic systems, thereby eliminating the entropically unfavorable dimerization step necessary for the bi-nuclear mechanism when employing mono-metallic catalysts. This point is made more clear through the example of the bi-nuclear complex $Fe_2(CO)_9$ considered as the catalyst for the WGSR.

Shown in Figure 3A.14 below is the free energy profile for the gas and solvent (50% methanol-50% water) phase catalysis of the WGSR by $Fe_2(CO)_9$. As the figure indicates, the formation of the $Fe_2(CO)_8COOH^-$ species for this case is now an exergonic process in both the gas phase (ΔG = -73.6 kcal/mol, 29.6 kcal/mol more stable than for the bi-nuclear mechanism with the $Fe(CO)_5$ catalyst) as well as in the solvent phase (ΔG = -16.9 kcal/mol, 22.9 kcal/mol more stable than for the bi-nuclear mechanism with the $Fe(CO)_5$ catalyst). This leads to a significantly increased overall energetic favorability for the entire reaction cycle: the completion of the cycle is now exergonic by 82.5 kcal/mol in the gas phase comparison to it being only exergonic by 52.9 kcal/mol for the bi-nuclear mechanism with the $Fe(CO)_5$ catalyst. It is noted here that $Fe_2(CO)_9$ is only used as an example: its insolubility in methanol makes it an unlikely candidate for a bi-nuclear WGSR catalyst. It is also to be noted that the bi-metallic catalyst to be employed for the WGSR should be resistant to dissociation to yield mono-nuclear species during the WGSR catalysis, because this would again lead to the predominance of mono-nuclear mechanisms over the bi-nuclear mechanism, as has been shown in the Figures 3A.7 and 3A.8 earlier. A comparison of the TDI and TDTS for the bi-metallic $Fe_2(CO)_9$ catalyst to the TDI and TDTS obtained for the mono-nuclear $Fe(CO)_5$ catalyst in the gas phase (Figure 3A.15) and solvent phase (50% methanol-water mixture - Figure 3A.16), suggests that the bi-metallic catalyst would perform significantly better. This is also true for the other two solvent mixture cases considered: the 25% methanol-water mixture and the 75 % methanol-water mixture cases, the free energy profiles of the bi-metallic mechanism for which have been included as the Figure 3A.17. The superior performance of the bi-metallic catalyst is further illustrated from the calculation of the relative TOF values for the gas phase and the different solvent mixture cases that have been collected and shown in Table 3A.7. The relative TOF values were calculated by dividing the absolute TOF values obtained for the bi-metallic $Fe_2(CO)_9$ catalyst by the corresponding absolute TOF value obtained for the mono-nuclear $Fe(CO)_5$ catalyst for each of the cases considered (the absolute TOF values for each case are provided in Table 3A.8). It is clear from the relative TOF values obtained that the bi-metallic catalyst species would provide a performance that would be at least two orders of magnitude better than the mono-metallic species (see Table 3A.7). Thus, the advantages of metal-metal cooperativity in reducing the barriers for the WGSR that have been uncovered through the work discussed here provide a guide for the design of improved WGSR catalysts in the future.

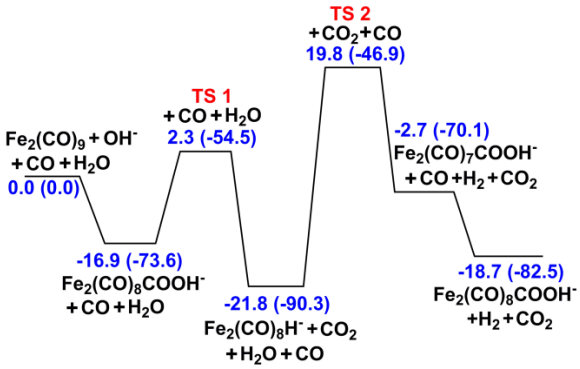

Figure 3A.14. The free energy profile for the newly proposed mechanism for the bi-metallic $Fe_2(CO)_9$ catalyst, with the 50% methanol-water mixture as the solvent; gas phase values are given in parentheses; all values are in kcal/mol.

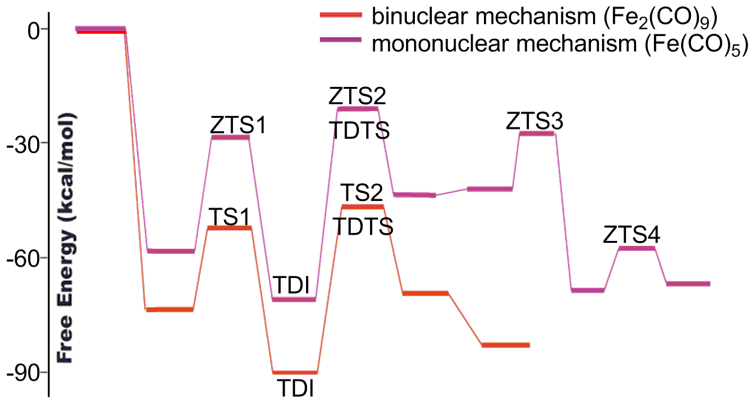

Figure 3A.15. The comparison of the free energy profiles in the gas phase obtained with $Fe(CO)_5$ and $Fe_2(CO)_9$ as the catalysts.

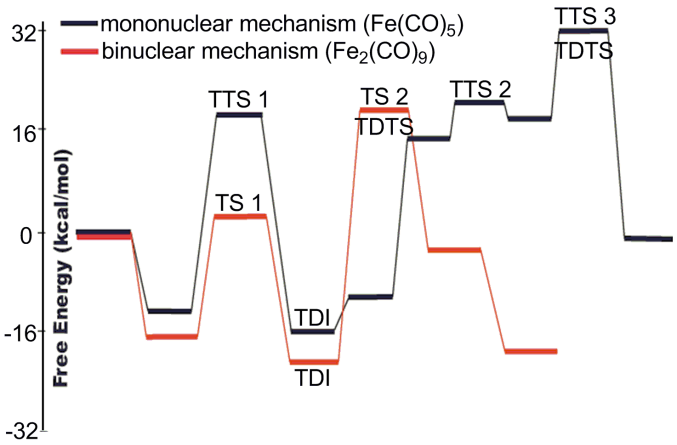

Figure 3A.16. The comparison of the free energy profiles obtained for the case of the 50% methanol-water mixture, with $Fe(CO)_5$ and $Fe_2(CO)_9$ as the catalysts.

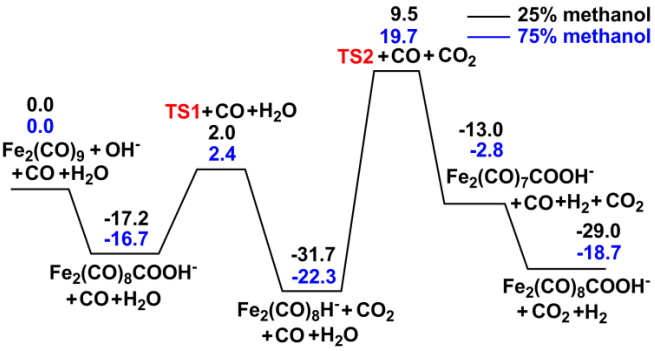

Figure 3A.17. The free energy profile for the newly proposed mechanism using $Fe_2(CO)_9$ catalyst, with 25% and 75% methanol-water mixtures as the two solvent cases; all values are in kcal/mol.

Table 3A.7. The relative TOF values, obtained for the mono-nuclear $Fe(CO)_5$ and the bi-nuclear $Fe_2(CO)_9$ catalysts, in the gas phase and for the different solvent mixture cases.

Mechanism	Gas phase	25% methanol	50% methanol	75% methanol
mono-nuclear $Fe(CO)_5$ catalyst	1	1	1	1
Bi-nuclear $Fe_2(CO)_9$ catalyst	4.3×10^4	2.7×10^5	1.9×10^5	9.7×10^4

Table 3A.8. The absolute values for the TOF (h^{-1}) obtained for all the mechanisms, for the cases of the mono-nuclear $Fe(CO)_5$ and the bi-nuclear $Fe_2(CO)_9$ catalysts.

Mechanism	Gas phase	25% methanol	50% methanol	75% methanol
mono-nuclear $Fe(CO)_5$ catalyst	7.5×10^{-21}	4.8×10^{-20}	3.5×10^{-20}	3.5×10^{-20}
Bi-nuclear $Fe_2(CO)_9$ catalyst	3.2×10^{-16}	1.3×10^{-14}	6.6×10^{-15}	3.4×10^{-15}

3A.4 Conclusions

Computational studies employing density functional theory (DFT) have been done in order to investigate a bi-nuclear mechanism for the homogeneous water gas shift Reaction (WGSR). This represents the first mechanistic computational investigations of metal-

metal cooperativity for the WGSR. A bi-nuclear mechanism has been proposed for the WGSR with the $Fe(CO)_5$ catalyst, and compared with full quantum mechanical (QM) calculations with all the previously suggested mechanisms[19-22] in the literature. The calculations indicate that the bi-nuclear mechanism leads to lower barriers in comparison to the previously proposed mono-nuclear mechanisms. While the comparison of the free energy profiles, as well as the predicted turn over frequencies (TOFs), with the aid of the recently developed energetic span model,[25] indicates that the bi-nuclear mechanism would not be the predominant mechanism if one were to start from a mono-nuclear catalyst, calculations indicate that one would achieve much higher TOFs if a bi-metallic rather than a mono-nuclear catalyst were to be employed for the WGSR. While the calculations have been done with iron based catalysts, a natural extension of the results obtained here is the prediction that metal-metal cooperativity would be likely to render other bi-metallic catalysts, such as bi-ruthenium systems, for instance, more effective than their mono-nuclear counterparts in catalyzing the WGSR. The calculations thus provide a recipe for the design of better WGSR catalysts in the future: soluble bi-metallic complexes that can exploit metal-metal cooperativity in order to increase the efficiency of the WGSR catalysis.

3A.5 References

(1) Motta, A.; Fragala, I. L.; Marks, T. J. *J. Am. Chem. Soc.* **2009**, *131*, 3974-3984.

(2) Torkelson, J. R.; Antwi-Nsiah, F. H.; McDonald, R.; Cowie, M.; Pruis, J. G.; Jalkanen, K. J.; DeKock, R. L. *J. Am. Chem. Soc.* **1999**, *121*, 3666-3683.

(3) Wigginton, J. R.; Chokshi, A.; Graham, T. W.; McDonald, R.; Ferguson, M. J.; Cowie, M. *Organometallics* **2005**, *24*, 6398-6410.

(4) Miller, A. E. S.; Beauchamp, J. L. *J. Am. Chem. Soc.* **1991**, *113*, 8765-8770.

(5) Kang, H. C.; Mauldin, C. H.; Cole, T.; Slegeir, W.; Cann, K.; Pettit, R. *J. Am. Chem. Soc.* **1977**, *99*, 8323-8325.

(6) King, A. D.; King, R. B.; Yang, D. B. *J. Am. Chem. Soc.* **1981**, *103*, 2699-2704.

(7) King, R. B.; Frazier, C. C.; Hanes, R. M.; King, A. D. *J. Am. Chem. Soc.* **1978**, *100*, 2925-2927.

(8) Reppe, J. W.; Reindl, E. *Liebigs Ann. Chem.* **1953**, *582*, 121-124.

(9) King, A. D.; King, R. B.; Yang, D. B. *J. Am. Chem. Soc.* **1980**, *102*, 1028-1032.

(10) Lane, K. R.; Sallans, L.; Squires, R. R. *Organometallics* **1985**, *4*, 408-410.

(11) Kunkes, E. L.; Simonetti, D. A.; West, R. M.; Serrano-Ruiz, J. C.; Gartner, C. A.; Dumesic, J. A. *Science* **2008**, *322*, 417-421.

(12) Serrano-Ruiz, J. C.; West, R. M.; Dumesic, J. A. *Annu. Rev. Chem. Biomol. Eng.* **2010**, *1*, 79-100.

(13) Huber, G. W.; Shabaker, J. W.; Dumesic, J. A. *Science* **2003**, *300*, 2075-2077.

(14) Ford, P. C. *Acc. Chem. Res.* **1981**, *14*, 31-37.

(15) King, A. D.; King, R. B.; Yang, D. B. *J.C.S. Chem. Comm.* **1980**, 529-530.

(16) Grice, N.; Kao, S. C.; Pettit, R. *J. Am. Chem. Soc.* **1979**, *101*, 1627-1628.

(17) Sunderlin, L. S.; Squires, R. R. *J. Am. Chem. Soc.* **1993**, *115*, 337-343.

(18) Lane, K. R.; Lee, R. E.; Sallans, L.; Squires, R. R. *J. Am. Chem. Soc.* **1984**, *106*, 5767-5772.

(19) Torrent, M.; Sola , M.; Frenking, G. *Organometallics* **1999**, *18*, 2801-2812.

(20) Barrows, S. E. *Inorg. Chem.* **2004**, *43*, 8236-8238.

(21) Rozanska, X.; Vuilleumier, R. *Inorg. Chem.* **2008**, *47*, 8635-8640.

(22) Zhang, F.; Zhao, L.; Xu, C.; Chen, Y. *Inorg. Chem.* **2010**, *49*, 3278-3281.

(23) Majumdar, M.; Sinha, A.; Ghatak, T.; Patra, S. K.; Sadhukhan, N.; Rahaman, S. M. W.; Bera, J. K. *Chem. – Eur. J.* **2010**, *16*, 2574-2585.

(24) Sinha, A.; Ghatak, T.; Bera, J. K. *Dalton Trans.* **2010**, *39*, 11301-11313.

(25) Kozuch, S.; Shaik, S. *Acc. Chem. Res.* **2010**, *44*, 101-110.

(26) Kozuch, S.; Martin, J. M. L. *ACS Catal.* **2011**, *1*, 246-253.

(27) Uhe, A.; Kozuch, S.; Shaik, S. *J. Comput. Chem.* **2010**, *32*, 978-985.

(28) Amovilli, C.; Floris, F. M.; Sola , M.; Tomasi, J. *Organometallics* **2001**, *20*, 1310-1316.

(29) Axel, D. B. *J. Chem. Phys.* **1993**, *98*, 5648-5652.

(30) Lee, C.; Yang, W.; Parr, R. G. *Phys. Rev. B* **1988**, *37*, 785.

(31) Frisch, M. J. T., G. W.; Schlegel, H. B.; Scuseria, G. E.;; Robb, M. A. C., J. R.; Scalmani, G.; Barone, V.; Mennucci, B.;; Petersson, G. A. N., H.; Caricato, M.; Li, X.; Hratchian, H. P.;; Izmaylov, A. F. B., J.; Zheng, G.; Sonnenberg, J. L.; Hada, M.;; Ehara, M. T., K.; Fukuda, R.; Hasegawa, J.; Ishida, M.; Nakajima,; T.; Honda, Y. K., O.; Nakai, H.; Vreven, T.; Montgomery, J. A., Jr.;; Peralta, J. E. O., F.; Bearpark, M.; Heyd, J. J.; Brothers, E.; Kudin,; K. N.; Staroverov, V. N. K., R.; Normand, J.; Raghavachari, K.;; Rendell, A. B., J. C.; Iyengar, S. S.; Tomasi, J.; Cossi, M.; Rega,; N.; Millam, J. M. K., M.; Knox, J. E.; Cross, J. B.; Bakken, V.;; Adamo, C. J., J.; Gomperts, R.; Stratmann, R. E.; Yazyev, O.;; Austin, A. J. C., R.; Pomelli, C.; Ochterski, J. W.; Martin, R. L.;; Morokuma,

K. Z., V. G.; Voth, G. A.; Salvador, P.;; Dannenberg, J. J. D., S.; Daniels, A. D.; Farkas, O.; Foresman, J. B. O., J. V.; Cioslowski, J.; Fox, D. J., Gaussian 09, revision. B.01; *Gaussian, Inc., Wallingford, CT, 2009*.

(32) Ditchfield, R.; Hehre, W. J.; Pople, J. A. *J. Chem. Phys.* **1971**, *54*, 724-728.

(33) Stefan, G.; Jens, A.; Stephan, E.; Helge, K. *J. Chem. Phys.* **2010**, *132*, 154104.

(34) Grimme, S.; Ehrlich, S.; Goerigk, L. *J. Comput. Chem.* **2011**, *32*, 1456-1465.

(35) Marenich, A. V.; Cramer, C. J.; Truhlar, D. G. *J. Phys. Chem. B* **2009**, *113*, 6378-6396.

(36) Winget, P.; Dolney, D.M.; Giesen, D.J.; Cramer, C.J.; Truhlar, D.G. *Minnesota Solvent Descriptor Database* Version date:July 9,1999;updated:June 6,**2010**.

(37) Harvey, J. N. *Faraday Discus.*, **2009**, *145*, 487-505.

(38) Ho, J.; Klamt, A.; Coote, M. L. *J. Phys. Chem. A*, **2010**, *114*, 13442-13444.

(35) Luo, Y.; Hou, Z. *Organometallics* **2006**, *25*, 6162-6165.

(36) NBO Version 3.1, Glendening, E. D.; Reed, A. E.; Carpenter, J. E. and F. Weinhold.

Chapter 3B

Substituted Allenes as Highly Efficient Leaving Groups in Catalytic Processes

Abstract

There is considerable interest presently in the chemistry of allenes. The current chapter looks into the possibility of employing allenes and their derivatives as leaving groups. As is well known, leaving groups are significant in catalytic processes for generating the active site. A full quantum mechanical study using density functional theory (DFT) shows that allenes and their derivatives can function as excellent leaving groups. Indeed, the calculations show that they can be several orders of magnitude more effective than existing ligands for this purpose. The modification of second Generation Grubbs' catalysts with these ligands suggests that the allene ligand cases that would be most effective are those having electron withdrawing groups, especially those that have the potential for supramolecular interactions between the substituent groups in the free state.

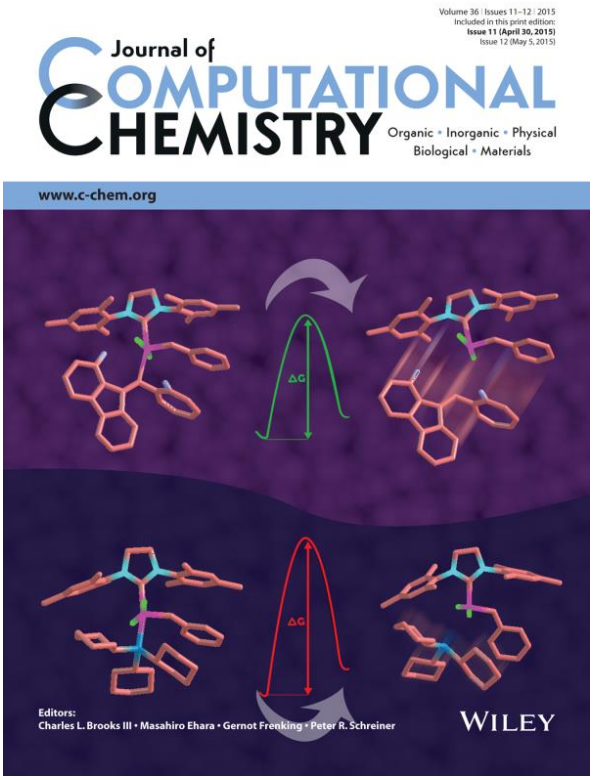

3B.1 Introduction

The multifaceted nature of a ligand makes it an indispensable candidate for homogeneous transition metal based catalytic processes. A high degree of regio[1-3] and enantioselectivity[4] has been obtained by certain metal complexes due to the ability of some ligands to influence a favourable positioning of the substrate relative to the catalytic centre. In other catalytic processes, the ligand can act as hemilabile,[5,6] cooperative[7-9] or both[10] in order to stabilize the reactive intermediates, to activate small molecules[11,12] or to take part in reversible ligand assisted processes in chemical reactions.[10] To attain these characteristics in metal complexes, appropriate ligands have been selected based on the charge, size, functional groups, denticity or hapticity. However, while the different roles of the ligand mentioned above are important, one of the most important functions of the ligand is to perform as a "leaving group": generate an active catalyst species by dissociating in a facile manner from the metal complex. This ability of the ligand to act as a leaving group is important in several well known catalytic processes, such as olefin metathesis,[13] hydrogenation of the olefin by Wilkinson's catalyst,[14] and the hydroformylation reaction.[15] The desired property of the ligand in such cases is the ability to make a labile bond with the metal centre. This allows them to dissociate in an energetically feasible manner in the presence of a substrate. The development of ligands that possess such a lability in the corresponding metal complexes is one of the important areas of research in homogeneous catalysis.

In this context, we feel that a family of ligands that holds special promise is that of the allenes. Allenes are organic compounds in which a carbon atom has two double bonds with each of its two neighbouring carbon centers, i.e. they are compounds of the type: $R_2C=C=CR_2$ (R = H). Some substituted allenes with different –R groups differ from the classical allene in that the C=C=C angle is more acute. While classical allenes have an orthogonal arrangement of the substituent groups on the carbons attached to the central carbon atom, this arrangement is disturbed in the substituted allenes, leading to a more distorted bent structure.[16] Thus, in the distorted allene structures having a bent angle, the symmetry point group is reduced from D_{2d} to C_2.[16] Indeed, as shown in recent studies, when the allenes are bent to a sufficient degree, they can be considered as systems with carbone character – systems that can bind strongly to the metal center.[17-34] If one considers an allene ligand where the C=C=C angle is less acute, it may lead to a weak

metal-ligand bond in the complex in comparison with the highly bent carbone ligand cases, because of the greater delocalization of electron density into the C=C=C backbone in such systems. Therefore, such ligands can be used as leaving groups in catalytic processes where the dissociation of a labile ligand is necessary in order to generate the active catalytic centre. Allenes have generally been considered as a substrate for many catalytic reactions. However they have never been considered as leaving groups in catalytic processes. Therefore, it is necessary to consider their potential to act as effective leaving groups.

In our current work, we have considered the use of substituted allenes with a less acute C=C=C angle as leaving groups in catalytic systems, employing density functional theory (DFT). Different derivatives have been generated by the introduction of substituents (shown as "X" and "Y" in Figure 3B.1 below) in the parent allenic system "**A**", leading to the systems "**B**". **A** is a classical allene that has a fluorenyl and a heptenyl carbene attached to the central carbon atom. This classical allenic system has been considered because Frenking and co-workers have shown in a recent theoretical study that **A** is an allene which does not show any carbone behaviour[35]– therefore it would be a good allenic system to consider in terms of being an effective leaving group. While difficulties have been faced in synthesizing **A**, analogous compounds with non-planar heptenyl ring derivatives have been successfully synthesized.[36,37]

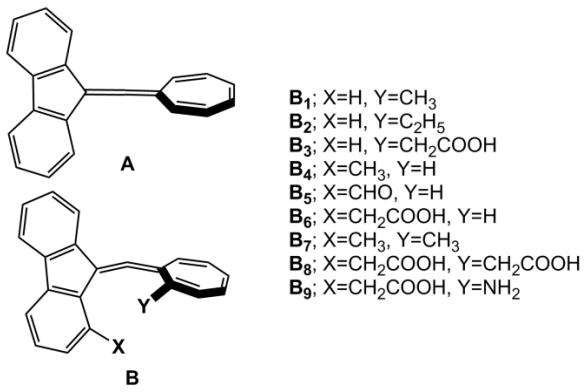

Figure 3B.1. The classical allene "**A**", having a fluorenyl and a heptenyl carbene attached to the central carbon, and other allenes "**B**", having substitutions in the fluorenyl and heptenyl rings.

Other substituted allenes that have been considered are modifications to **A** *via* the introduction of electron donating and electron withdrawing groups. All the substituted

allene ligands: **B_1** to **B_9**, that have been considered in the current study, are indicated in Figure 3B.1. An interesting subset of the substituted allenes that has been considered are those with groups that can bind supramolecularly to each other through hydrogen bonding (cases **B_8** and **B_9** in Figure 3B.1). This is because supramolecularly bound leaving groups are more water soluble, which is an important attribute, allowing an easy removal of the dissociated ligand from the reaction medium,[38,39] either by chemical trapping[40] or by phase transfer into an orthogonal solvent.[41]

In the current work, we have considered the potential ability of the allene (**A**) and their derivatives (**B_1-B_9**) to act as good leaving groups, for the specific case of the Grubbs' olefin metathesis catalyst system. The system considered is the 2nd Generation Grubbs' catalyst ($C_{46}H_{65}Cl_2N_2PRu$) shown in Figure 3B.2. "X" in Figure 3B.2 refers to the different allene systems that have been employed as leaving groups. Also considered, as a reference, is PCy_3 as X, which is the standard 2nd Generation Grubbs' metathesis catalyst. The selection of the Grubbs' system in order to test the leaving group ability of the allenes is because it is one of the most important homogeneous catalyst systems of the present day.[42-50] Mechanistic studies with the Grubbs' systems have revealed the presence of a monophosphine coordinated metal intermediate in the reaction process,[45,46] which suggests that one of the ancillary ligands has to be labile for improved catalytic activation. In other words, the presence of a good leaving group is vital to the efficiency of the Grubbs' metathesis systems, which makes them a good target for our current studies. It is also to be noted that the allenes, if used as leaving groups, would be present in catalytic amounts - therefore, the dissociated allene ligand would not be competitive in olefin metathesis reactions. Furthermore, as will be shown in the Results and Discussion section, the involvement of allenes in the metathesis reaction is also a kinetically unfavourable process.

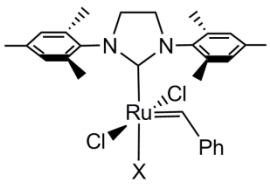

1

Figure 3B.2. 2nd Generation Grubbs' catalyst systems, the X refers to PCy_3 or substituted allene ligands, studied as leaving groups in the current investigation.

The current full quantum chemical calculations with density functional theory (DFT) have compared the energy of dissociation of the ligands from the metal centre with the corresponding energy required to dissociate the PCy_3 ligand from the ruthenium complex. Furthermore, the influence of supramolecular interactions, as well as that of the electron donating and withdrawing groups on the substituted allene ligands has been investigated. The results provide interesting insights about the potential of the allene systems to act as leaving groups in homogeneous catalysis systems.

3B.2 Computational Details

All the calculations have been carried out with Turbomole 6.4,[51] using the TZVP basis set and the PBE[52] functional. The basis set includes relativistic effective core potentials (ECP) for ruthenium. Dispersion corrections have been included in all the geometry optimization calculations. For the dispersion correction calculation, an empirical dispersion correction, DFT-D proposed by Grimme has been employed.[53] Solvent effects have been incorporated through full optimization with COSMO,[54] with water (epsilon = 80.0) as the solvent for all the calculations, except the AuCl coordination and proton affinity calculations of **A**, $\mathbf{B_8}$ and $\mathbf{B_9}$. The resolution of identity (RI),[55] along with the multipole accelerated resolution of identity (marij)[56] approximations have been employed for an accurate and efficient treatment of the electronic Coulomb term in the DFT calculations. The values reported are ΔG values, with zero point energy, internal energy and entropic contributions included through frequency calculations on the optimized minima, with the temperature and pressure taken to be 298.15 K and 1 atm respectively. The molecular orbitals HOMO and HOMO-2 have been obtained by the single point calculation at PBEPBE/TZVP//PBE/TZVP level using Gaussian 09.[57]

3B.3 Results and discussion

3B.3.1 Allene as a leaving droup in the Grubbs' catalyst system: The values of the C=C=C angle obtained for the different allene and the allene derivatives considered in the current study (**A** and $\mathbf{B_1}$-$\mathbf{B_9}$) are shown in Table 3B.1 below. The values suggest that the substituents distort the classical allene "**A**" to the allenes "**B**". In **A**, the C=C=C angle is 180.0˚, which changes slightly, ranging from a change of 0.2 degrees to 4.9 degrees in the absence of hydrogen bonding in the systems $\mathbf{B_1}$ to $\mathbf{B_7}$ (see Table 3B.1). However, in the hydrogen bonded system $\mathbf{B_8}$, the C=C=C angle is more bent. Here, the value is 165.8˚,

indicating a change of 14.2 degrees. However, interestingly, for the case of **B_9**, the C=C=C angle is again higher: 175.3˚, even though substituents (-CH_2COOH and -NH_2) that can bind supramoleculary were considered in this case. The reason for this is that the lowest energy conformation of **B_9** was found to be a non-hydrogen bonded structure.

Table 3B.1. The C=C=C angle of the allene and their derivative systems discussed in the Chapter 3B.

Ligands	C=C=C angle (˚)	Ligands	C=C=C angle (˚)
A	180.0	**B_5**	175.1
B_1	178.3	**B_6**	177.5
B_2	176.4	**B_7**	179.8
B_3	177.8	**B_8**	165.8
B_4	179.6	**B_9**	175.3

The small change in the C=C=C angle in most of the substituted allene cases suggests that they are not able to bind to the metal as strongly as in the case of carbones and can act as leaving groups in the Grubbs' metathesis systems, as discussed in the Introduction. The coordination of the compounds to the ruthenium complex was therefore considered next. The corresponding complexes: **M-A** and **M-B_1** to **M-B_9** are indicated in Figure 3B.3. It is to be noted that for each case, three different conformational possibilities have been considered: (i) the central carbon (C_1) of the allene and the substituted allene coordinated in an η^1 fashion with the ruthenium, (ii) the central carbon and the adjoining carbon of the heptenyl group (C_h) coordinated in an η^2 fashion with the ruthenium and (iii) the central carbon and the adjoining carbon of the fluorenyl group (C_f) coordinated in an η^2 fashion with the ruthenium. The relative electronic energies for the different modes of coordination have been provided in Table 3B.2. Of the three possibilities, only the lowest energy conformer has been indicated in Figure 3B.3. It is interesting to note that the η^1 coordination is the preferred mode of binding for all the cases, except for **M-B_5** and **M-B_6**, where possibility (ii) is found to be preferred. The reason for this is that these are the only two cases where there is an electron withdrawing group on the fluorenyl ring and none on the heptenyl. This combination would lead to electron density being more concentrated in the C-C bond of the central carbon and the

carbon of the heptenyl ring, thus encouraging the η^2 coordination. The lowest energy conformers obtained for each case have been considered in the subsequent calculations.

Table 3B.2. The relative electronic energy for the different modes of coordination of allene and bent allene ligand towards ruthenium metal centre; all values are in kcal/mol.

System	$\eta^1 C_1$	$\eta^2(C_1\text{-}C_h)$	$\eta^2(C_1\text{-}C_{hf})$
A	0.0	0.8	8.0
$\mathbf{B_1}$	0.0	4.5	22.2
$\mathbf{B_2}$	0.0	-	21.5
$\mathbf{B_3}$	0.0	1.9	20.3
$\mathbf{B_4}$	0.0	2.9	3.8
$\mathbf{B_5}$	0.0	-3.3	1.2
$\mathbf{B_6}$	0.0	-0.4	2.4
$\mathbf{B_7}$	0.0	4.7	11.1
$\mathbf{B_8}$	0.0	-	30.1
$\mathbf{B_9}$	0.0	1.4	9.1

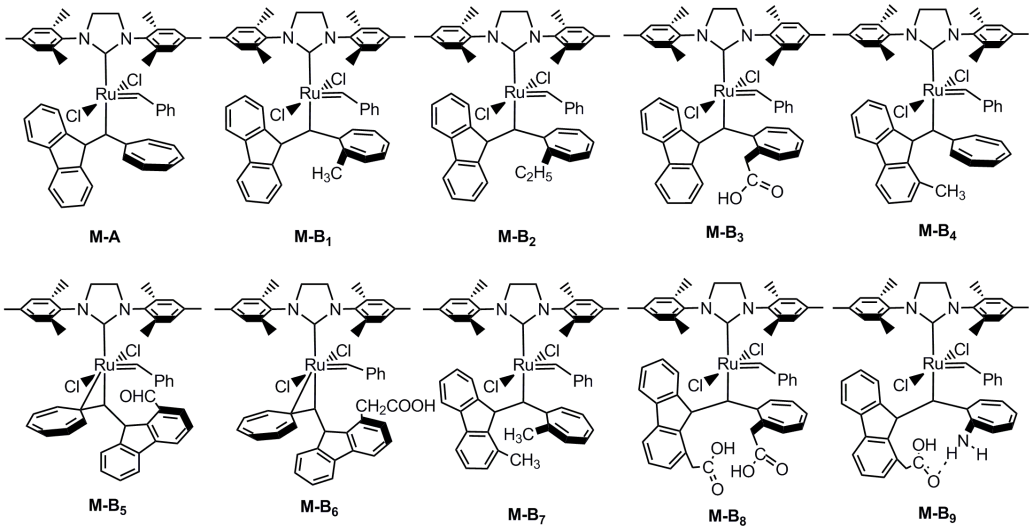

Figure 3B.3. The lowest energy conformers of the modified 2nd Generation ruthenium based Grubbs' systems that have been considered in the present study.

The optimized geometry of the 2nd Generation Grubbs' catalyst **1-PCy$_3$** is shown in Figure 3B.4. The calculated values of the selected bond parameters at the PBE/TZVP level are in good agreement with the corresponding experimental values.

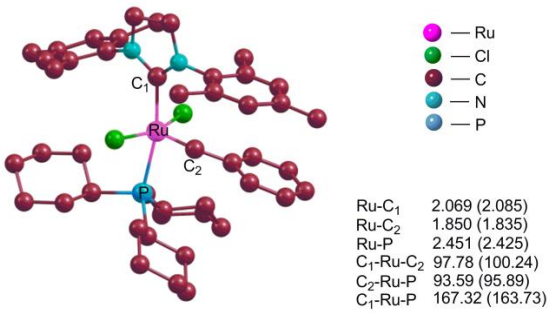

Figure 3B.4. The optimized geometry of **1-PCy$_3$** with selected bond lengths (A^0) and bond angles (^{0}); the experimental values are given inside the parenthesis; H atoms have been omitted for clarity.

Considered next was the energy of dissociation of the corresponding allene ligands from the complexes **M-A** and **M-B$_1$** to **M-B$_9$**, i.e., for the reaction shown in Equation 1. The results are given in Table 3B.3. For the purpose of comparison, the energy of dissociation of PCy_3 from the complex **1-PCy$_3$** was also considered. The gas phase electronic binding energy for **1-PCy$_3$** has been reported as 36.9±2.3 kcal/mol in the previous experimental and computational studies.[58-60] Our calculations suggest the corresponding gas phase electronic energy to be 37.6 kcal/mol. However, the values reported in the current work include both solvent and dispersion corrections, and these corrected values are also in very good agreement with the recent computational studies involving olefin metathesis for the 2nd Generation Grubb's catalyst.[61] As the values in Table 3B.3 indicate, for all the cases considered, the dissociation of the allene ligands were found to be considerably more favorable than for the PCy_3 case. The difference in the dissociation energy values between PCy_3 and the proposed allene cases lies in the range 4.7-20.2 kcal/mol. By considering the equation $\Delta G = -RT \ln K$, the results suggest that the systems that we have considered, having the allenes and allene derivatives as ligands, would be 1806.6 to 4.3×10^{14} times more effective as leaving groups in comparison to PCy_3. This result shows the significance of considering the allene and its derivative ligands as alternatives to PCy_3 as potential leaving groups in Grubbs' olefin metathesis systems.

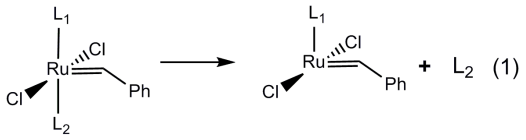

Table 3B.3. The energy of dissociation of the ligand PCy_3, **A**, and of $\mathbf{B_{1\text{-}9}}$, from the corresponding ruthenium complexes, according to Equation (1); all values are in kcal/ mol.

Ruthenium complexes	ΔE	ΔG
1-PCy$_3$	30.9	9.8
M-A	25.0	3.1
M-B$_1$	26.3	3.2
M-B$_2$	26.6	4.7
M-B$_3$	24.8	1.7
M-B$_4$	19.0	-4.7
M-B$_5$	22.0	-1.3
M-B$_6$	16.7	-1.7
M-B$_7$	16.5	-6.9
M-B$_8$	13.8	-10.4
M-B$_9$	21.6	-2.1

In these systems, the dissociation energy of the ligand from the metal centre has been found to depend on many factors (i) the effect of substituent when it is on the heptenyl ring, (ii) the effect of substituent when it is on the fluorenyl ring, (iii) the mode of coordination of the ligand towards the metal centre (η^1 or η^2), and (iv) the supramolecular interaction between the substituents on the ligand.

The ruthenium complexes **M-B$_1$** to **M-B$_3$** correspond to cases where (i) is pertinent, i.e., the substituents are on the heptenyl ring. As seen from Table 3B.3, the calculated dissociation energies for the three cases are 3.2 kcal/mol, 4.7 kcal/mol and 1.7 kcal/mol respectively. While **M-B$_1$** and **M-B$_2$** have electron donating groups as substituents (-CH_3 and –C_2H_5 respectively), **M-B$_3$** contains an electron withdrawing group: –CH_2COOH, which leads to the Ru-C_1 bond being slightly stronger in these systems. However, the dissociation of the ligand is still favourable in comparison with the

PCy_3 dissociation from the metal centre in the Grubbs' catalyst. We have confirmed this by calculating the activation barrier for the **M-B$_2$** case, a system that, thermodynamically, has a higher dissociation energy (see Table 3B.3). The free energy of activation for the dissociation of **B$_2$** from the ruthenium centre in **M-B$_2$** is 19.1 kcal/mol and the corresponding value for **1-PCy$_3$** is 21.4 kcal/mol, which suggests that the dissociation of **B$_2$** is favourable by 2.3 kcal/mol. The optimized geometries of the transition states structures are shown in Figure 3B.5.

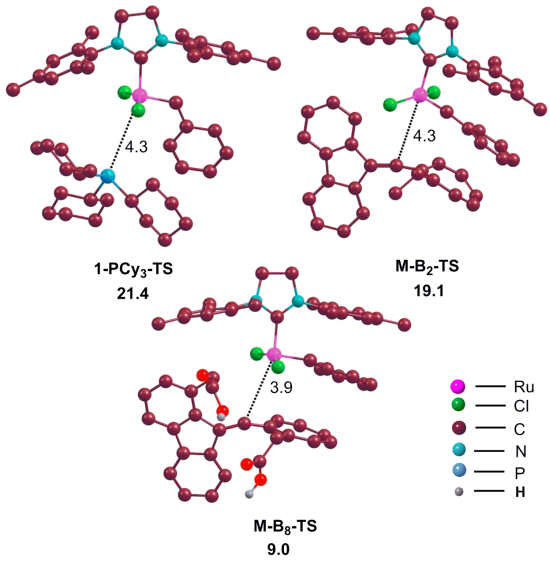

Figure 3B.5. The optimized geometries of the transition state structures corresponding to the dissociation of the allene ligand from the metal centre of the **1-PCy$_3$**, **M-B$_2$**, and **M-B$_8$** systems; all values are in kcal/mol; H atoms have been omitted for clarity.

The next three cases, **M-B$_4$** to **M-B$_6$**, pertain to (ii): where the substitution is on the fluorenyl ring. For these cases, the calculated dissociation energies are -4.7 kcal/mol, -1.3 kcal/mol and -1.7 kcal/mol respectively, i.e., much lower than for the **M-B$_1$**-**M-B$_3$** cases. Here, the substituents at the fluorenyl moiety are $–CH_3$, -CHO and $–CH_2COOH$ respectively. For these three cases, factor (iii) is important: the mode of coordination of allene ligand towards the metal centre. In the case of **M-B$_5$** and **M-B$_6$**, an η^2 coordination exists between the metal and the allene ligand, while the **M-B$_4$** complex displays an η^1 coordination. The consequence of this is that the coordination is found to be stronger for **M-B$_5$** and **M-B$_6$** compared to the η^1 **M-B$_4$** complex, thereby explaining the difference in the dissociation energies observed for these cases (see Table 3B.3).

For the **M-B$_7$**, **M-B$_8$** and the **M-B$_9$** cases, the substituents are present at both the fluorenyl and the heptenyl carbenes. The dissociation energy in these systems is lower in comparison to the previous cases. This can be considered as the substituent effect on the two rings. In **M-B$_7$**, the dissociation energy obtained is -6.9 kcal/mol. However, in **M-B$_8$** and **M-B$_9$** the factor (iv), the supramolecular interaction between the substituents on the ligand, plays an important role in determining ligand dissociation. This is discussed in the following section.

3B.3.2 Supramolecular interaction between the substituents on the ligand: As mentioned in the Introduction, supramolecular interactions are desirable in leaving groups because they make it easier to remove the ligand from the catalyst system. Furthermore, supramolecular interactions may aid in improving the thermodynamics of ligand removal from the metal center. This is because, in some cases where supramolecular interaction is possible between the substituents on the ligand, the said interaction may be absent when the ligand is coordinated to the metal centre. This may be due to the steric strain associated with the metal-ligand complexes. Therefore, the dissociation of the ligand from the metal center will be a more thermodynamically favorable process, due to the stabilizing supramolecular interaction that would be present in the free ligand and not in the corresponding complex. This is what is likely to occur in the case of the ruthenium complex **M-B$_8$**, where there is no supramolecular interaction between the two –CH_2COOH substituents. The optimized structure of **M-B$_8$** is shown in Figure 3B.6. On the other hand, the two local minima structures of the free ligand suggest that in the absence of metal coordination, the ligand with hydrogen bonding is more stable compared to its non-hydrogen bonded counterpart. The optimized geometries of the two local minima are shown in Figure 3B.7. The electronic energy of the hydrogen bonded ligand is 3.3 kcal/mol lower than that of the non-hydrogen bonded ligand. This added thermodynamic advantage leads to this ligand being the best leaving group compared to the other ligands. The corresponding dissociation energy obtained according to Equation (1) is -10.4 kcal/mol. The comparison with **M-B$_7$**, where the heptenyl and fluorenyl carbenes contain an electron donating group without any supramolecular interaction, indicates that the effect of hydrogen bonding is significant in lowering the dissociation energy. This also confirms the role of supramolecular interactions in stabilizing the reactive intermediates in solution. Since this system was seen to be the most favorable in terms of the thermodynamics of the ligand leaving the vicinity of the metal center, we

have looked at the corresponding kinetics for this case also. As shown in Figure 3B.5, the activation barrier in this system is 9.0 kcal/mol. Here, the energy barrier for ligand dissociation is lower by 12.4 kcal/mol in comparison with the **1-PCy$_3$** system. The low value therefore further showcases the potential of the substituted allene systems to be excellent leaving groups.

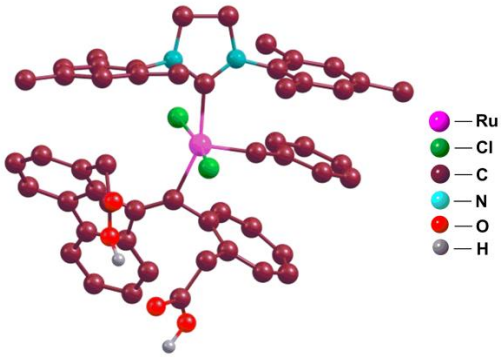

Figure 3B.6. The optimized geometry of the ruthenium complex **M-B$_8$**; H atoms have been omitted for clarity.

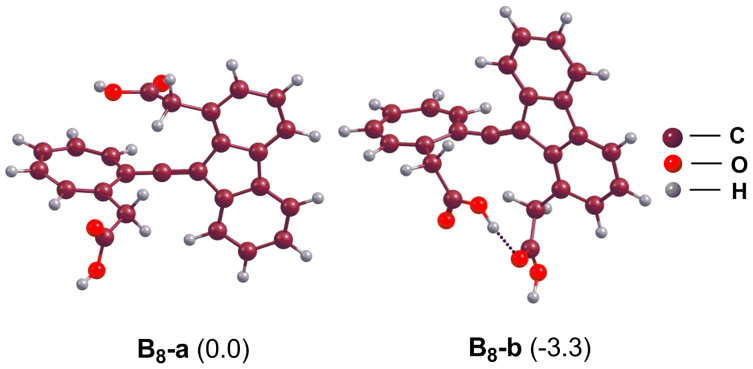

Figure 3B.7. The optimized structures of the local minima of the free ligand **B$_8$** with and without supramolecular interactions between the substituent groups; the values inside the parenthesis are in kcal/mol.

We have also considered the supramolecular interactions in the presence of electron donating groups in the case of **B$_9$**, where the electron donating group (-NH_2) is present on the heptenyl ring and the electron withdrawing group (-CH_2COOH) is on the fluorenyl skeleton. For this case, the dissociation of the ligand was found to be more feasible than for the case of the PCy_3 ligand. However, the leaving group will dissociate

less easily than the leaving group in **M-B$_8$**. The dissociation energy of **B$_9$** from **M-B$_9$** is -2.1 kcal/mol, i.e., it is higher by 8.3 kcal/mol than the dissociation of **B$_8$** from **M-B$_8$**. Unlike for **M-B$_8$**, here the hydrogen bonding is present in the ligand when it is coordinated to the ruthenium metal centre and the comparison of the local minima for the free ligand indicates that the hydrogen bonding is not present when it is in the free state. Therefore, in this case, the supramolecular interactions indicate a loss in thermodynamic favorability upon dissociation, and thus to an increase in the energy of dissociation.

3B.3.3 The possibility of hidden carbone character affecting the binding energy: It is also important to investigate whether the two cases: **B$_8$** and **B$_9$** shows any hidden carbone character, since that may also be a factor in determining the strength of the binding of the ligand to the metal center. Previous studies have demonstrated that carbones and allenes can be differentiated from each other by analysing three parameters: (a) their molecular orbitals, (b) their mode of coordination towards AuCl and (c) their proton affinity.[19] With regard to parameter (a), the molecular orbital analysis of carbones shows a σ-type and a π type lone pair orbital at the central carbon atom, while allenes show π type orbitals delocalized over the adjacent carbon atoms. The comparison of carbones and allenes for parameter (b) shows that carbones have the ability to bind with one or two AuCl molecules in an η^1 fashion, whereas allenes prefer the η^2 coordination. In a recent study, Esterhuysen and Frenking[19] have shown that the compounds with latent C(0) character will coordinate with the AuCl in more than one way, and the dominant mode will indicate the character of carbone, allene, or carbene in the molecule. Also, the value of the first and the second proton affinity (PA) {parameter (c)} is also considered as a measure of carbone behaviour.[18] The first PA is generally higher for both carbones as well as for carbenes. However, carbones possesses a higher second PA compared to carbenes. The second PA for most of the compounds which have been confirmed as carbones generally ranges between 130-300 kcal/mol.

We have studied the carbone nature of **B$_8$** and **B$_9$** by analysing the above-mentioned three parameters (a), (b) and (c). We have also studied the same for the allene **A** case for the purpose of comparison. It is to be noted that a previous study on **A** shows that it is a perfect allene without any carbone character.[19] The optimized geometries of **A** and **B$_9$** are given in Figure 3B.8.

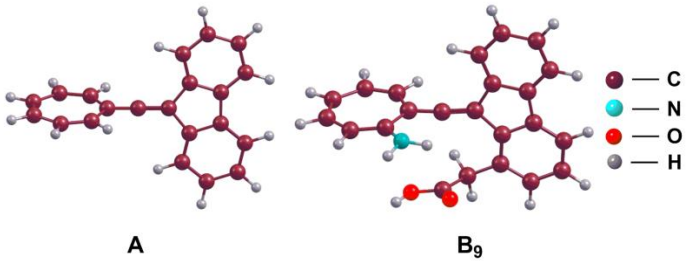

Figure 3B.8. The optimized geometries of **A** and **B9**.

(a) The molecular orbitals of the molecule **A**, **B8** and **B9** have been obtained through single point calculations at PBEPBE/TZVP//PBE/TZVP level in Gaussian 09 with the optimized structures obtained at the PBE/TZVP level in Turbomole 6.4. As shown in Figure 3B.9, the shape of the occupied orbitals HOMO and HOMO-2 are more important in analysing the carbone behaviour of the systems **A**, **B8** and **B9**. In these molecules, the bonding analysis shows the presence of π type orbitals on both HOMO and HOMO-2. HOMO and HOMO-2 are delocalized between the central carbon atom C_1 with the fluorenyl ligand and the heptenyl ligand respectively. The molecular orbital analysis indicates allenic behaviour in all the three systems.

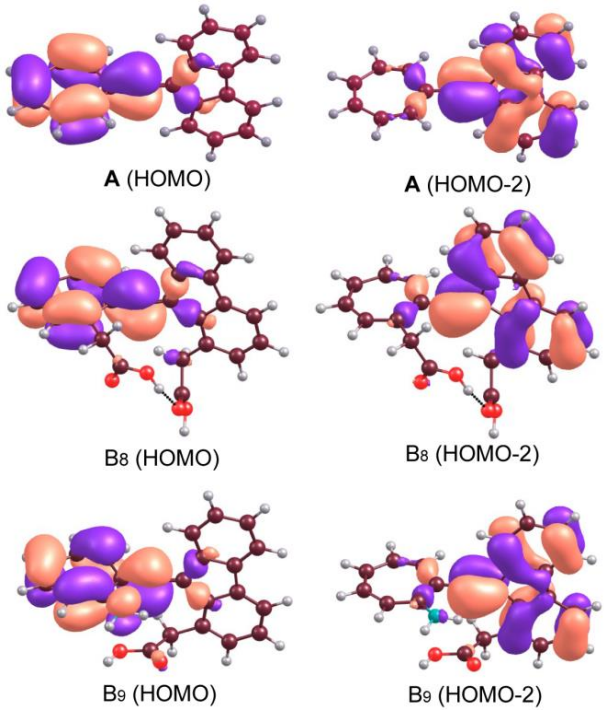

Figure 3B.9. The HOMO and HOMO-2 for **A**, **B8** and **B9**.

(b) The modes of coordination of one AuCl molecule towards the **A**, $\mathbf{B_8}$ and $\mathbf{B_9}$ ligands are given in Figure 3B.10. The relative free energies are given in parenthesis. In all the three cases, the coordination with AuCl gives two different modes of coordination: an η^2 coordination at the C_1-C_h bond and an η^2 coordination at the C_1-C_f bond. The $\eta^2(C_1$-$C_h)$ coordination was found to be lower in energy in all the cases by 3.6 kcal/mol, 2.3 kcal/mol and 7.8 kcal/mol for **A**, $\mathbf{B_8}$ and $\mathbf{B_9}$ respectively. No local minima corresponding to an η^1 coordination was obtained for any of the cases. The metal coordination behaviour of the central C_1 atom was further analysed with two AuCl moieties. The results are shown in Figure 3B.11. What was observed was that all three systems preferred an η^2 coordination on the C_1-C_f as well as the C_1-C_h bond. The results therefore suggest an allenic character in all the three systems.

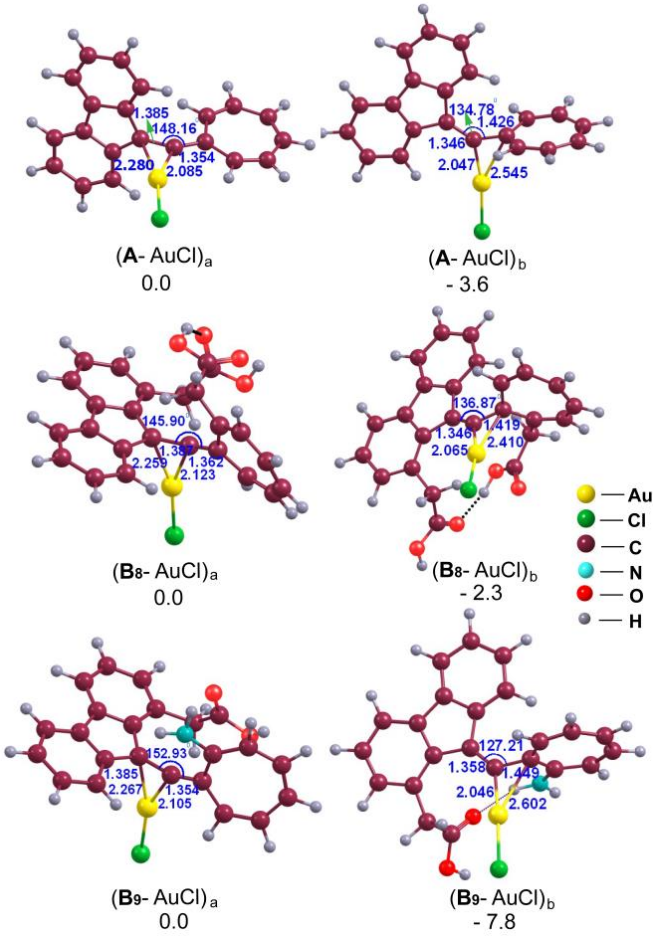

Figure 3B.10. The optimized structures of the AuCl complexes of **A**, $\mathbf{B_8}$ and $\mathbf{B_9}$, with important bond lengths (Å) and angles (°) indicated.

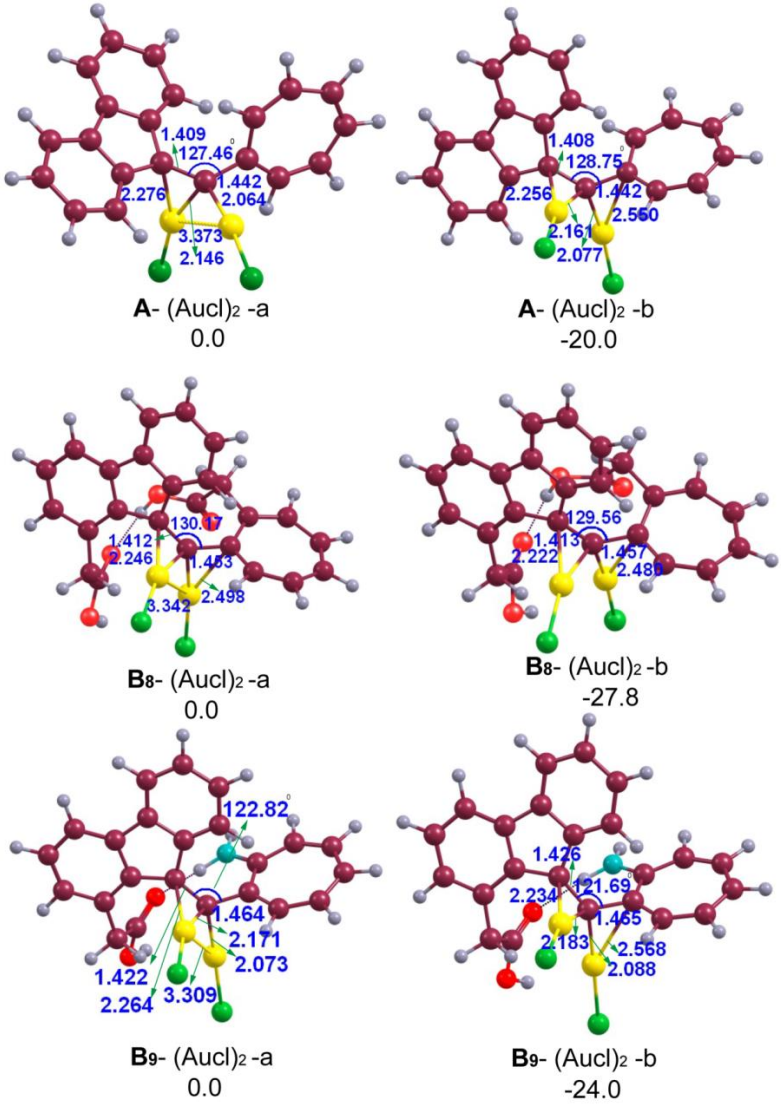

Figure 3B.11. The optimized structures of the $(AuCl)_2$ complexes of **A**, **B_8** and **B_9**, with important bond lengths (Å) and angles (°) indicated.

(c) Table 3B.4 shows the first and second proton affinities (PAs) of **A**, **B_8** and **B_9**. The first PA was calculated by taking the complexes **[$A(H^+)$]**, **[$B_8(H^+)$]** and **[$B_9(H^+)$]** and removing the proton from each of these complexes. The second PA was calculated by removing a proton from each of the complexes **[$A(H^+)_2$]**, **[$B_8(H^+)_2$]** and **[$B_9(H^+)_2$]**. This follows the procedure adopted by Esterhuysen *et al*.[19]. The results indicate that the three cases show proton affinity values between 242.3 kcal/mol to 257.8 kcal/mol for the first proton affinity and 140.6 kcal/mol to 149.1 kcal/mol for the second proton affinity. While these values are suggestive of some carbone character in the three ligands, it is to

be noted that the previous indicators: (a) the delocalization in the HOMOs and LUMOs in the three cases, as well (b) as the coordination to AuCl, suggests that the three cases **A**, **B_8** and **B_9** are allenes without carbone character. Hence, the proton affinity data appears to contradict the results from (a) and (b). However, since the delocalization in the frontier MOs can be considered a more fundamental property of the three ligands, in comparison to the proton affinity, where a reorganization of the electron density in the ligand can be envisaged to occur in the presence of the added proton, the results from (a), (b) and (c) can be interpreted to suggest that all the three cases **A**, **B_8** and **B_9**, are allenes without any hidden carbone character.

Table 3B.4. The first and second proton affinities (PAs) of **A, B_8** and **B_9**; all values are in kcal/mol.

X	$X(H^+) \rightarrow X + H^+$	$X(H^+)_2 \rightarrow X(H^+) + H^+$
A	250.2	140.6
B_8	242.3	149.1
B_9	257.8	147.8

From these studies, we can conclude that the high energy of dissociation that would be required for **B_9** in comparison to **B_8** is due the combination of the following factors: the electronic effect of the substituents, and the supramolecular interaction between substituents present in the metal complex but not in the free ligand.

3B.3.4 Competitive metathesis reaction of the allene ligand: Since the allene ligand contains two unsaturated bonds, one has to consider the possibility of the allene competing with the olefin substrate in undergoing metathesis at the metal center – a situation that would interfere with its potential role as a leaving group. This possibility has been considered for the cases of the **B_2** and **B_8** ligands. It was observed that, depending on the orientation and the binding mode of unsaturated bonds in the allene towards the ruthenium alkylidene double bond, four different pathways are possible. The products that would be obtained from these four possibilities, as well as their relative energies, are shown in Scheme 3B.1 below. Out of these possibilities, the one that would give rise to a ruthenium vinylidene species as one of the side products was found to be the most favourable - by 14.9 kcal/mol and 13.0 kcal/mol for **M-B_2** and **M-B_8** respectively (see Scheme 3B.1), which might suggest that such side-reactions could be competitive.

However, since catalytic processes usually occur over a brief period of time, it is also necessary to consider the kinetics of the metathesis process. Previous studies[62] suggest that in the olefin metathesis reaction involving unchelated ruthenium catalysts[63, 64], or a ruthenium catalyst with NHC ligands[65, 66], a bottom-bound metallacycle pathway is favoured over the side-bound approach of the olefin towards the Ru-C bond of the active catalyst. Therefore, in our current study, we have analyzed a bottom-bound metallacycle pathway. The energy profile, which is given in Scheme 3B.2, shows that the transition state (**TS 1**), which leads to the formation of a metallacyclobutane intermediate, is higher by 17.2 kcal/mol than the reactants for **M-B$_2$** and by 13.7 kcal/mol for **M-B$_8$**. Also, the metallacyclobutane intermediate is endergonic by 18.1 kcal/mol for **M-B$_2$** and 13.0 kcal/mol for **M-B$_8$** with respect to the reactant. However, the energy barrier for the formation of ruthenium vinylidene- one of the products from the cyclobutane intermediate - is 7.2 kcal/mol and 8.6 kcal/mol higher for the **M-B$_2$** and **M-B$_8$** cases respectively. This step involves a transition state **TS 2** as shown in Scheme 3B.2. Now, as mentioned in the previous section, it has been shown that the barrier for the dissociation of **B$_2$** and **B$_8$** from the ruthenium center are 19.1 kcal/mol and 9.0 kcal/mol. Therefore, there is a 6.7 kcal/mol and 9.2 kcal/mol difference in the barriers respectively for the two competing possibilities: (a) the ligand leaving the metal center or (b) participating in the metathesis reaction. This suggests that the dissociation of the ligand from the metal center would be favored by several orders of magnitude over the ligand participating in the metathesis reaction. The significant difference between the two possibilities suggests that the allene ligand behaving as a leaving group would also be the likely outcome for the other allene cases that have been considered in the current study.

The previous sections have therefore shown that allenes, substituted allenes (as well as substituted allenes with some hidden carbone character) can all function as excellent leaving groups in important homogeneous catalysis processes such as the Grubbs' metathesis reaction. In fact, the calculations have shown that such ligands would be significantly better at leaving the vicinity of the active site in comparison to existing ligands such as PCy_3.

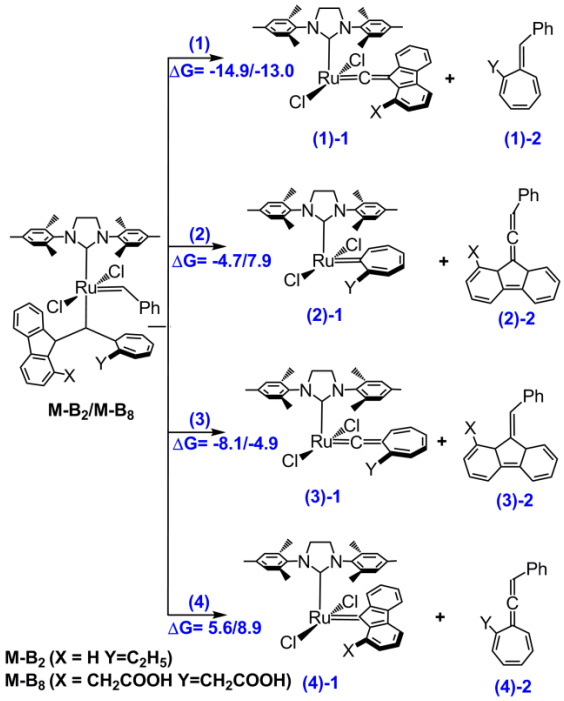

Scheme 3B.1. The products obtained from four different pathways in the competing metathesis reaction of substituted allenes, $\mathbf{B_2}$ and $\mathbf{B_8}$; all values are in kcal/mol.

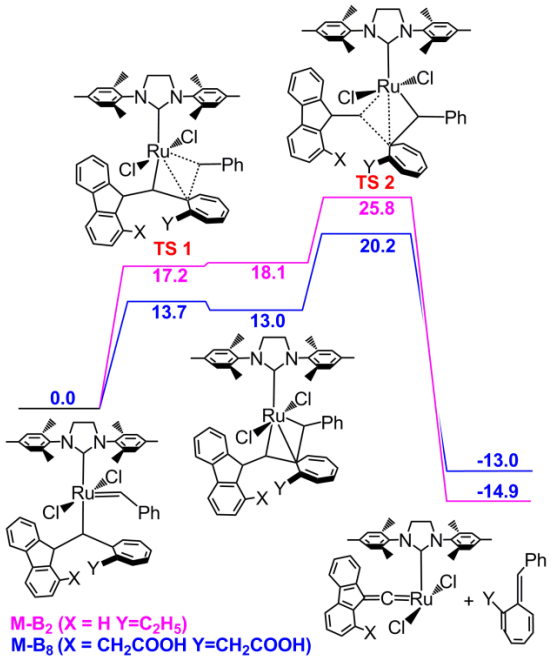

Scheme 3B.2. The free energy profile for the metathesis reaction of $\mathbf{B_2}$ and $\mathbf{B_8}$ ligand cases; all values are in kcal/mol.

3B.4 Conclusions

In many important catalytic processes of the present day, the dissociation of a ligand is necessary in order to generate an active catalytic centre. The development of improved ligands that can function as better leaving groups is therefore a very significant area of research. What we have considered in the current work using full quantum chemical calculations with density functional theory (DFT), is the possibility of allenes and substituted allenes as potential leaving groups. These are systems that have generated considerable interest in recent times.[16, 19, 22-24, 67] In order to test the ability of allenes and substituted allenes to act as leaving groups, the well known catalytic system, the Grubbs' catalyst, has been considered. Our calculations for a range of different allene and substituted allene systems show that they would all perform significantly (upto several orders in magnitude) better than the existing ligand PCy_3, that is used as a leaving group in the Grubbs' metathesis reaction. The reasons for this have been explored in the current work. An important factor that has been found to affect the ability of the substituted allenes to leave the metal center is the presence of electron withdrawing substituents on the allenes. Furthermore, an interesting aspect that has been considered is the possibility of supramolecular interactions *via* hydrogen bonding affecting the ability of the substituted allene ligand to leave the vicinity of the metal center. This is significant because of the advantages of making the leaving group water soluble,[38-41] which can be achieved through supramolecular interactions. Different cases have been considered in this regard: the ligand displaying supramolecular interactions in the metal complex but not in the free state, and *vice versa*. Overall, the current investigations display the importance of considering allenes and substituted allenes as potential leaving groups in homogeneous catalysis processes, and can be expected to serve as a guide to experimentalists working in this important area of research.

3B.5 References

(1) Šmejkal, T.; Breit, B. *Angew. Chem., Int. Ed.* **2008**, *47*, 311-315.

(2) Šmejkal, T.; Breit, B. *Angew. Chem., Int. Ed.* **2008**, *47*, 3946-3949.

(3) Grünanger, C. U.; Breit, B. *Angew. Chem., Int. Ed.* **2008**, *47*, 7346-7349.

(4) Breuil, P.-A. R.; Patureau, F. W.; Reek, J. N. H. *Angew. Chem., Int. Ed.* **2009**, *48*, 2162-2165.

(5) Braunstein, P. *J. Organomet. Chem.* **2004**, *689*, 3953-3967.

(6) Braunstein, P.; Naud, F. *Angew. Chem., Int. Ed.* **2001**, *40*, 680-699.

(7) Grützmacher, H. *Angew. Chem., Int. Ed.* **2008**, *47*, 1814-1818.

(8) Meeuwissen, J.; Sandee, A. J.; de Bruin, B.; Siegler, M. A.; Spek, A. L.; Reek, J. N. H. *Organometallics* **2010**, *29*, 2413-2421.

(9) Zweifel, T.; Naubron, J.-V.; Grützmacher, H. *Angew. Chem., Int. Ed.* **2009**, *48*, 559-563.

(10) Gunanathan, C.; Ben-David, Y.; Milstein, D. *Science* **2007**, *317*, 790-792.

(11) Gutsulyak, D. V.; Piers, W. E.; Borau-Garcia, J.; Parvez, M. *J. Am. Chem. Soc.* **2013**, *135*, 11776-11779.

(12) Milsmann, C.; Turner, Z. R.; Semproni, S. P.; Chirik, P. J. *Angew. Chem., Int. Ed.* **2012**, *51*, 5386-5390.

(13) Dias, E. L.; Nguyen, S. T.; Grubbs, R. H. *J. Am. Chem. Soc.* **1997**, *119*, 3887.

(14) Halpern, J. *Inorg. Chim. Acta* **1981**, *50*, 11-19.

(15) Heck, R. F.; Breslow, D. S. *J. Am. Chem. Soc.* **1961**, *83*, 4023-4027.

(16) Hänninen, M. M.; Peuronen, A.; Tuononen, H. M. *Chem. - Eur. J.* **2009**, *15*, 7287.

(17) Bertrand, G.; Dyker, C. A.; Lavallo, V.; Google Patents: 2009.

(18) Tonner, R.; Heydenrych, G.; Frenking, G. *ChemPhysChem* **2008**, *9*, 1474.

(19) Esterhuysen, C.; Frenking, G. *Chem. - Eur. J.* **2011**, *17*, 9944-9956.

(20) Klein, S.; Tonner, R.; Frenking, G. *Chem. - Eur. J.* **2010**, *16*, 10160.

(21) Deshmukh, M. M.; Gadre, S. R.; Tonner, R.; Frenking, G. *Phys. Chem. Chem. Phys.* **2008**, *10*, 2298-2301.

(22) Dyker, C. A.; Lavallo, V.; Donnadieu, B.; Bertrand, G. *Angew. Chem., Int. Ed.* **2008**, *47*, 3206-3209.

(23) Fürstner, A.; Alcarazo, M.; Goddard, R.; Lehmann, C. W. *Angew. Chem., Int. Ed.* **2008**, *47*, 3210-3214.

(24) Alcarazo, M.; Lehmann, C. W.; Anoop, A.; Thiel, W.; Fürstner, A. *Nat. Chem.* **2009**, *1*, 295-301.

(25) Tonner, R.; Öxler, F.; Neumüller, B.; Petz, W.; Frenking, G. *Angew. Chem., Int. Ed.* **2006**, *45*, 8038-8042.

(26) Tonner, R.; Frenking, G. *Chem. - Eur. J.* **2008**, *14*, 3260-3272.

(27) Tonner, R.; Frenking, G. *Chem. - Eur. J.* **2008**, *14*, 3273-3289.

(28) DeHope, A.; Donnadieu, B.; Bertrand, G. *J. Organomet. Chem.* **2011**, *696*, 2899.

(29) Melaimi, M.; Parameswaran, P.; Donnadieu, B.; Frenking, G.; Bertrand, G. *Angew. Chem., Int. Ed.* **2009**, *48*, 4792-4795.

(30) Fernandez, I.; Dyker, C. A.; DeHope, A.; Donnadieu, B.; Frenking, G.; Bertrand, G. *J. Am. Chem. Soc.* **2009**, *131*, 11875-11881.

(31) Lavallo, V.; Dyker, C. A.; Donnadieu, B.; Bertrand, G. *Angew. Chem., Int. Ed.* **2008**, *47*, 5411-5414.

(32) Tonner, R.; Frenking, G. *Chem. Comm.* **2008**, 1584-1586.

(33) Frenking, G.; Tonner, R.; Klein, S.; Takagi, N.; Shimizu, T.; Krapp, A.; Pandey, K. K.; Parameswaran, P. *Chem. Soc. Rev.* **2014**, *43*, 5106-5139.

(34) Soriano, E.; Fernández, I. *Chem. Soc. Rev.* **2014**, *43*, 3041-3105.

(35) Esterhuysen, C.; Frenking, G. *Dalton Trans.* **2013**, *42*, 13349-13356.

(36) Alcarazo, M. *Dalton Trans.* **2011**, *40*, 1839-1845.

(37) Alcarazo, M.; Suárez, R. M.; Goddard, R.; Fürstner, A. *Chem. - Eur. J.* **2010**, *16*, 9746-9749.

(38) Lynn, D. M.; Mohr, B.; Grubbs, R. H.; Henling, L. M.; Day, M. W. *J. Am. Chem. Soc.* **2000**, *122*, 6601-6609.

(39) Hong, S. H.; Grubbs, R. H. *J. Am. Chem. Soc.* **2006**, *128*, 3508-3509.

(40) Thompson, L. A. *Curr. Opin. Chem. Biol.* **2000**, *4*, 324-337.

(41) Xi, Z.; Bazzi, H. S.; Gladysz, J. A. *Org. Lett.* **2011**, *13*, 6188-6191.

(42) Nguyen, S. T.; Johnson, L. K.; Grubbs, R. H.; Ziller, J. W. *J. Am. Chem. Soc.* **1992**, *114*, 3974-3975.

(43) Schwab, P.; France, M. B.; Ziller, J. W.; Grubbs, R. H. *Angew. Chem., Int. Ed. Eng.* **1995**, *34*, 2039-2041.

(44) Schwab, P.; Grubbs, R. H.; Ziller, J. W. *J. Am. Chem. Soc.* **1996**, *118*, 100.

(45) Adlhart, C.; Hinderling, C.; Baumann, H.; Chen, P. *J. Am. Chem. Soc.* **2000**, *122*, 8204-8214.

(46) Hinderling, C.; Adlhart, C.; Chen, P. *Angew. Chem., Int. Ed.* **1998**, *37*, 2685-2689.

(47) Huang, J.; Stevens, E. D.; Nolan, S. P.; Petersen, J. L. *J. Am. Chem. Soc.* **1999**, *121*, 2674-2678.

(48) Scholl, M.; Trnka, T. M.; Morgan, J. P.; Grubbs, R. H. *Tetrahedron Lett.* **1999**, *40*, 2247-2250.

(49) Ackermann, L.; Fürstner, A.; Weskamp, T.; Kohl, F. J.; Herrmann, W. A. *Tetrahedron Lett.* **1999**, *40*, 4787-4790.

(50) Scholl, M.; Ding, S.; Lee, C. W.; Grubbs, R. H. *Org. Lett.* **1999**, *1*, 953.

(51) Ahlrichs, R.; Bär, Michael; Häser, M.; Horn, H.; Kölmel, C. *Chem. Phys. Lett.* **1989**, *162*, 165-169.

(52) Ansgar, S.; Christian, H.; Reinhart, A. *J*. *Chem*. *Phys*. **1994**, *100*, 5829.

(53) Grimme, S.; Antony, J.; Ehrlich, S.; Krieg, H. *J*. *Chem*. *Phys*. **2010**, *132*, 154104.

(54) Klamt, A.; Schuurmann, G. *J*. *Chem*. *Soc*., *Perkin Trans*. *2* **1993**, 799-805.

(55) Eichkorn, K.; Treutler, O.; Öhm, H.; Häser, M.; Ahlrichs, R. *Chem*. *Phys*. *Lett*. **1995**, *240*, 283-290.

(56) Sierka, M.; Hogekamp, A.; Ahlrichs, R. *J*. *Chem*. *Phys*. **2003**, *118*, 9136.

(57) Frisch, M. J. T., G. W.; Schlegel, H. B.; Scuseria, G. E.; Robb, M. A.; Cheeseman, J. R.; Scalmani, G.; Barone, V.; Mennucci, B.; Petersson, G. A.; Nakatsuji, H.; Caricato, M.; Li, X.; Hratchian, H. P.; Izmaylov, A. F.; Bloino, J.; Zheng, G.; Sonnenberg, J. L.; Hada, M.; Ehara, M.; Toyota, K.; Fukuda, R.; Hasegawa, J.; Ishida, M.; Nakajima, T.; Honda, Y.; Kitao, O.; Nakai, H.; Vreven, T.; Montgomery, Jr., J. A.; Peralta, J. E.; Ogliaro, F.; Bearpark, M.; Heyd, J. J.; Brothers, E.; Kudin, K. N.; Staroverov, V. N.; Kobayashi, R.; Normand, J.; Raghavachari, K.; Rendell, A.; Burant, J. C.; Iyengar, S. S.; Tomasi, J.; Cossi, M.; Rega, N.; Millam, J. M.; Klene, M.; Knox, J. E.; Cross, J. B.; Bakken, V.; Adamo, C.; Jaramillo, J.; Gomperts, R.; Stratmann, R. E.; Yazyev, O.; Austin, A. J.; Cammi, R.; Pomelli, C.; Ochterski, J. W.; Martin, R. L.; Morokuma, K.; Zakrzewski, V. G.; Voth, G. A.; Salvador, P.; Dannenberg, J. J.; Dapprich, S.; Daniels, A. D.; Farkas, Ö.; Foresman, J. B.; Ortiz, J. V.; Cioslowski, J.; Fox, D. J. Gaussian 09, Revision B.01, *Gaussian, Inc*., *Wallingford CT*, **2009**.

(58) Torker, S.; Merki, D.; Chen, P. *J*. *Am*. *Chem*. *Soc*. **2008**, *130*, 4808-4814.

(59) Minenkov, Y.; Occhipinti, G.; Jensen, V. R. *Organometallics* **2013**, *32*, 2099.

(60) Minenkov, Y.; Occhipinti, G.; Jensen, V. R. *J*. *Phys*. *Chem*. *A* **2009**, *113*, 11833.

(61) Poater, A.; Credendino, R.; Slugovc, C.; Cavallo, L. *Dalton Trans*. **2013**, *42*, 7271-7275.

(62) Liu, P.; Xu, X.; Dong, X.; Keitz, B. K.; Herbert, M. B.; Grubbs, R. H.; Houk, K. N. *J*. *Am*. *Chem*. *Soc*. **2012**, *134*, 1464-1467.

(63) Correa, A.; Cavallo, L. *J*. *Am*. *Chem*. *Soc*. **2006**, *128*, 13352-13353.

(64) Adlhart, C.; Chen, P. *J*. *Am*. *Chem*. *Soc*. **2004**, *126*, 3496-3510.

(65) Romero, P. E.; Piers, W. E. *J*. *Am*. *Chem*. *Soc*. **2005**, *127*, 5032-5033.

(66) Romero, P. E.; Piers, W. E. *J*. *Am*. *Chem*. *Soc*. **2007**, *129*, 1698-1704.

(67) Weber, E.; Seichter, W.; Hess, B.; Will, G.; Dasting, H.-J. *J*. *Phys*. *Org*. *Chem*. **1995**, *8*, 94-96.

Chapter 4
Homogeneous Catalytic Processes Using Main Group Compounds

Several approaches have been investigated in recent years in the area of homogeneous catalytic reactions using main group compounds. This chapter introduces new concepts in this field: that of the potential of molecular cages, containing only main group elements, towards activating small molecules, as well as the use of Group 14 hydrides in important catalytic reactions. This chapter is devided into two parts, Chapter 4A and Chapter 4B. Chapter 4A discusses quantum mechanical calculations employing DFT/SCS-MP2 methods on the Ga-N cage molecular cage compounds, and the results indicate them to be excellent candidates for mediating in important reactions such as the catalysis of ammonia borane dehydrogenation. The work discussed in this chapter therefore opens up exciting new possibilities in small molecule activation research. Chapter 4B deals with the dihydrogen generation by the protolytic cleavage of O-H bond in ROH (R=H, CH_3, C_2H_5) molecules using Ge (II) hydride compounds. Computational investigations through a predictive approach on such systems explore the potential of the Ge (II) hydride in generating dihydrogen from water and alcohols. A complete catalytic cycle can also be set up for such reactions through the use of silanes like SiF_3H. Our approach shows that this would lead to significant improvement in comparison to existing post transition metal based compounds in dihydrogen generation from ROH molecules.

Chapter 4A

Ga-N Cage Compounds for Effective Small Molecule Activation

Abstract

Several approaches have been investigated in recent years in the area of small molecule activation. This chapter introduces a new concept in this field: that of molecular cages, containing only main group elements, serving to activate small molecules. Full quantum mechanical calculations employing DFT/SCS-MP2 methods indicate that recently synthesized Ga-N cage compounds would be excellent candidates for mediating in important reactions such as the catalysis of ammonia borane dehydrogenation. The work discussed in this chapter therefore opens up exciting new possibilities in small molecule activation research.

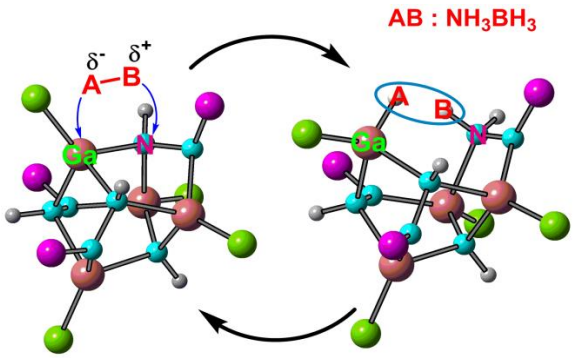

4A.1 Introduction

The activation of small molecules has become fertile ground for research in recent years. Various new strategies have been developed in order to activate the C-H, N-H and O-H bonds in small molecules, using methods as diverse as main-group containing frustrated Lewis pairs (FLPs)[1,2], metal-ligand cooperativity through aromatization/dearomatization of the ancillary ligand[3], as well as through activation of the metal-nitrogen bond in transition metal complexes[4,5]. Of these approaches, methods that employ systems that move away from transition metal complexes hold special interest, because main-group systems have the advantage of being cheaper than their metal counterparts. Therefore, new strategies for small molecule activation that can be based on main-group systems have received considerable attention recently[6,7].

We have previously shown that solid, zero dimensional (0D) cage structures have the potential to act as catalysts, due to the presence of latent Lewis acidity and basicity in the atoms of the 0D cages[8]. What is discussed in the current work is an approach towards understanding the potential of *molecular cages* towards exhibiting interesting behaviour pertaining to small molecule activation. While the 0D cages, containing conjugating phenyl rings, were computationally demonstrated to be capable of functioning more as frustrated Lewis pairs (FLPs)[8], what is discussed in this work is a strategy exploiting the "opening" and "closing" of labile bonds in molecular cages. The idea is illustrated in Figure 4A.1 below, discussing a possibility of homogeneously catalysing a dissociation process in a small molecule. When approached by the small molecule "CDEF", an existing bond in the cage, "A-B" in Figure 4A.1, can be broken and new bonds formed, thus activating CDEF, and eliminating the new molecule "D-E". The intermediate complex formed in this process would, however, also have the thermodynamic incentive to reconvert back to the original molecular cage, since the cage structure is a stable minima, and it would do so by remaking the broken "A-B" bond, and expelling a new small molecule "C-F". For instance, for the case where "C" and "F" are hydrogen atoms, the process described would be the catalysis of a dehydrogenation reaction. Thus, for appropriate cage structures having labile bonds, and for correspondingly appropriate small molecules that can attack the cage, an energetically feasible catalytic cycle would be

set up. This is the working principle that we have employed in order to test the potential for small-molecule activation by molecular cage structures such as the recently synthesized main-group gallium-nitrogen cage compounds[9].

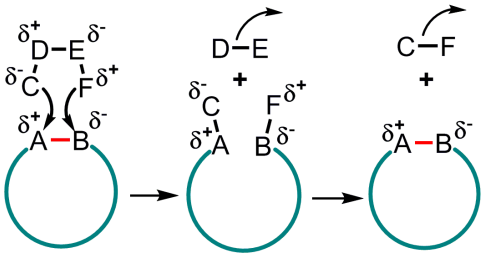

Figure 4A.1. The proposed strategy for exploiting labile bonds in molecular cages: the "opening" and "closing" of the A-B bond in the cage can lead to small molecule activation and catalysis.

Werner Uhl and coworkers have experimentally isolated the oligonuclear gallium-nitrogen cage compounds such as $(^{i}PrGa)_4(NH\text{-}NPh)_3NH$ and $(MeGa)_4(NH\text{-}N^{t}Bu)_4$ as molecular intermediates during the conversion of gallium hydrazide to gallium nitride by the thermolysis process[9]. The structural features of the Ga-N cage compound $(^{i}PrGa)_4(NH\text{-}NPh)_3NH$ have been reported to be similar to the arrangement of the phosphorous atoms in the $[P_{11}]^{3-}$ anion. The cage is reported to have six interconnected five membered rings in an envelope conformation, which accounts for its stability. The optimized geometry of the caged structure is shown in Figure 4A.2 below. The cage moiety contains four different Ga-N bonds, the bonds being distinguished from each other by the chemical environment of the gallium and the nitrogen atoms.

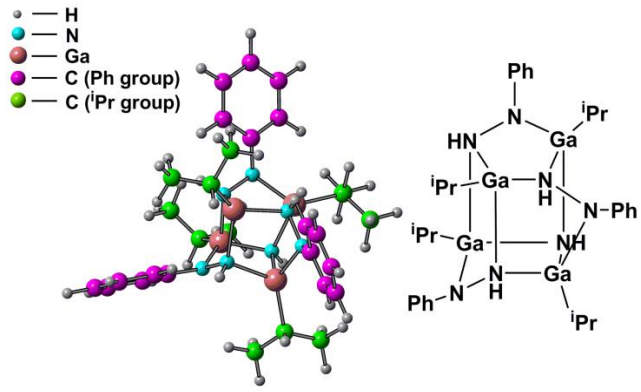

Figure 4A.2. The DFT optimized geometry of the cage $(^{i}PrGa)_4(NH\text{-}NPh)_3NH$.

Fontaine and co-workers[10] have shown that aluminium-phosphorus dimeric compounds display FLP type behavior in the presence of CO_2, upon dissociation of the dimer. Uhl and co-workers have also made dimeric aluminium-phosphorus compounds that exhibited frustrated Lewis pair behavior and could activate molecules such as CO_2 and phenyl isocyanate[11,12]. We believe that the gallium-nitrogen containing caged structure shown in Figure 4A.2 could, likewise, also display Lewis acidic and Lewis basic tendencies and thus act to activate small molecules, through the "opening" and "closing" of the Ga-N bonds in the cage, as discussed earlier. For example, for the case of the activation of the small molecule ammonia borane (AB), NH_3BH_3, the Lewis acidic gallium atom in a Ga-N bond of the cage will be susceptible to attack by the hydridic hydrogen attached to the boron of NH_3BH_3, while the Lewis basic nitrogen of the same bond approach and attack the protic hydrogen attached to the AB nitrogen, leading to the type of catalytic cycle illustrated in Figure 4A.1. Our objective in this work is to employ computational methods in order to investigate this possibility, by studying the dissociation and re-coordination of the Ga-N bonds in the Ga-N caged compound $(^{i}PrGa)_4(NH\text{-}NPh)_3NH$, when approached by ammonia borane. That our calculations represent a valid approach is shown by a computational investigation of an experimentally reported system: the dimeric aluminium-phosphorus complex, $(Me_2PCH_2AlMe_2)_2$, which has been experimentally shown to activate the small molecule: CO_2. Since several other molecular cage structures have also recently been synthesized and reported, some with gallium-nitrogen linkages[13,14] and others with aluminium-nitrogen bonds[15,16], we believe that the current computational study will open up interesting possibilities for exploiting this new class of compounds.

4A.2 Computational Details

All the calculations in this study have been performed with the aid of the Turbomole 6.0 suite of programs[17], using the PBE functional[18]. The TZVPP[19] basis set has been employed for the studies on AB dehydrogenation. For other cases, the calculations have been done at the TZVP level[19], with subsequent single point calculations done with the optimized structures with the TZVPP basis set. The resolution of identity (RI)[20], along with the multipole accelerated resolution of identity (marij)[21] approximations have been employed for an accurate and efficient treatment of the electronic Coulomb term in the DFT calculations. Solvent effects were incorporated

with single point calculations using the COSMO model[22], with toluene (ε = 2.38) as the solvent. It is to be noted that for the comparison to the experimental results of Boudreau *et al*.[10], with regard to the activation of CO_2 by the dimeric aluminium-phosphorus complex: $(Me_2PCH_2AlMe_2)_2$, the COSMO calculations were done with dichloromethane, CH_2Cl_2, (ε = 9.10) as the solvent. The values reported are ΔG values, with zero point energy, internal energy and entropic contributions included through frequency calculations on the optimized minima and transition state structures, with the temperature taken to be 298.15 K. Care has been taken to ensure that all the reported transition state structures contained only one negative frequency corresponding to the correct normal mode. In order to account for the fact that all the species are in solution, the translational entropy term in the calculated structures was corrected through a free volume correction introduced by Mammen *et al*.[23]. This free volume correction accounts for the unreasonable enhancement in translational entropy by calculating the volume through the ideal gas law, as done in the Turbomole and other softwares. Furthermore, for the case of the dehydrogenation of ammonia borane (AB) mediated by "**Bond 1**" (as specified in the Results and Discussion section) of the Ga-N model cage $(CH_3Ga)_4(NH\text{-}NPh)_3NH$, single point SCS-MP2[24,25] calculations have been done with the DFT optimized geometries for the case of all the intermediates and transition states along the potential energy surface, for the purpose of comparison with the DFT results.

4A.3 Results and Discussion

4A.3.1 Reactivity of a dimeric aluminium-phosphorus Lewis pair towards CO_2 activation: The focus is to understand the catalytic possibilities present in the activation of NH_3BH_3 by Ga-N containing molecular cages that have been synthesized by Uhl *et al*.[9]. However, as mentioned in the Introduction, calculations have also been done to investigate the potential of other Lewis pair containing structures that have been experimentally shown to activate small molecules. Specifically, we have investigated the behavior of the dimeric aluminium-phosphorus complex: $(Me_2PCH_2AlMe_2)_2$ (henceforth referred to as the "Al-P" complex), which has been shown by Boudreau *et al*. to activate CO_2[10]. As shown in Scheme 4A.1 below, one of the Al-P bonds of the dimeric Al-P complex can be activated in the presence of CO_2. This leads to a structure where the CO_2 is inserted in the Al-P bond, with the carbon coordinating to the phosphorus and the oxygen coordinating to the

aluminium. This is referred to as **Al-P-CO_2_1** in Scheme 4A.1 below, and is more stable by 1.4 kcal/mol than the Al-P complex. The barrier for this process is calculated to be 28.5 kcal/mol. Subsequent to this, a facile internal reorganization can occur, leading to the activation of the other Al-P bond, leading to the eventual formation of the structure "**Al-P-CO_2_3**" (see Scheme 4A.1). The structure **Al-P-CO_2_3** has been experimentally obtained[10], thus indicating the feasibility of the reactivity of the dimeric, ring structure, Al-P, towards CO_2. As the free energy surface shown in Scheme 4A.1 indicates, the slowest step of the reaction has a barrier of 28.5 kcal/mol, which provides the explanation as to why the reaction between CO_2 and Al-P complex is found to proceed very slowly: it takes more than 18 hours to get the species **Al-P-CO_2_3** when Al-P and CO_2 are reacted at ambient temperature. Another competing pathway, where the CO_2 inserts between the two aluminiums of the Al-P dimer, was calculated and found to have a prohibitively high barrier of 38. 3 kcal/mol (see Scheme 4A.2), thereby indicating that the pathway shown in Scheme 4A.1 is more feasible. It is also to be noted that in the presence of two equivalents of CO_2, the dimeric Al-P species (Al-P Complex) has been experimentally found to split into two $Me_2PCH_2AlMe_2$ molecules that form adduct complexes with CO_2. Calculations show that this process is facile by 14.2 kcal/mol (see Scheme 4A.3), which provides an explanation as to why the CO_2 bound monomeric structure (**Al-P-CO_2_4** in Scheme 4A.3) is observed experimentally to form within fifteen minutes under ambient conditions. Lastly, some intermediates that had been computationally investigated by Boudreau *et al*.[10] have also been optimized, and found to match well in energy (gas phase values) with the values reported by Boudreau *et al*.[10].

Overall, the calculations provide some insight into how the activation of small molecules can be done by Lewis Pair containing ring structures that have been experimentally studied. However, the experimental work shows a stoichiometric reaction between the small molecule and the studied ring structure. The real utilization of such Lewis pair containing ring or cage structures would occur if they can be made to *catalyze* transformations involving small molecule activation. That is the focus of the rest of the work, taking the example of the catalysis of ammonia borane (AB) dehydrogenation by the Ga-N cage structure, which is discussed below in the following subsections.

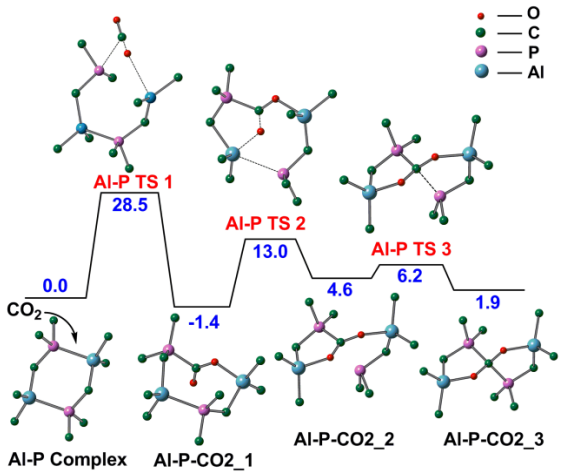

Scheme 4A.1. The free energy profile for the activation of $CO_2$with the Al-P Lewis pair $(Me_2PCH_2AlMe_2)_2$; all the structures shown are the fully optimized geometries from the DFT calculations; all values are in kcal/mol.

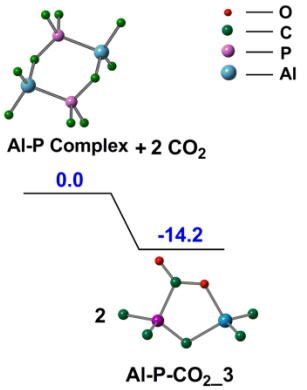

Scheme 4A.2. The free energy profile for the reaction of Al-P complex with two equivalent of CO_2; all the structures shown are the fully optimized geometries from the DFT calculations; all the values are in kcal/mol.

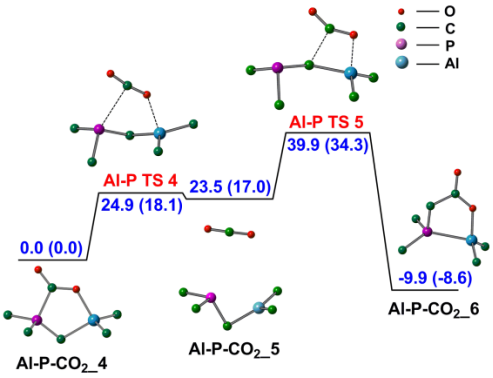

Scheme 4A.3. The free energy profile for Al-P system; all the structures shown are the fully optimized geometries from the DFT calculations; all the values are in kcal/mol.

4A.3.2 Catalysis of ammonia borane (AB) dehydrogenation by the Ga-N cage: As mentioned in the Introduction, computational studies have been done to investigate the potential of recently synthesized cage structures containing gallium and nitrogen (the "Ga-N" cage) towards small molecule activation, such as the catalysis of ammonia borane (AB) dehydrogenation. Shown in Scheme 4A.4 is the free energy profile for the dehydrogenation catalysis of AB mediated by the dissociation and recoordination of one of the bonds of the Ga-N cage. Ammonia borane, it bears

mention, is one of the most promising compounds for the chemical storage of hydrogen[26], and its catalytic dehydrogenation is an important area of research[27]. It is also to be noted that, while complexes such as $B(C_6F_5)_3$ have been employed to initiate AB dehydrogenation[28], no main-group systems have been developed to date that can catalytically dehydrogenate AB, which indicates the significance of the current studies with main-group containing cage systems. It was found that AB dehydrogenation with the Ga-N cage would follow a three-step pathway: (i) the transfer of the protic hydrogen from the nitrogen of AB to the nitrogen of the Ga-N bond of the cage, (ii) the subsequent transfer of the hydridic hydrogen from the boron of AB to the gallium of the Ga-N bond leading to the complete rupture of the Ga-N bond and the elimination of NH_2BH_2 and (iii) the reformation of the Ga-N bond by elimination of the protic and hydridic hydrogens to yield H_2, to complete the catalytic cycle. As Scheme 4A.4 indicates, step (i) leads to an intermediate that is higher in energy by 26.2 kcal/mol than the separated reactant species: the cage and AB. This is because the cage rearranges during the protic hydrogen transfer, in order to make new four and six membered rings, leading to greater ring strain and, therefore, to the unstable intermediate. Indeed, the barrier for the first reaction is almost at the same level (26.3 kcal/mol) as the intermediate. The optimized structure of the intermediate, which shows the four and six-membered rings formed more clearly, is shown in Figure 4A.3 below. It is to be noted that catalytic reaction cycles having unstable intermediates have been reported in the past[29]. The barrier for the subsequent reaction of this first intermediate species requires only 1.6 kcal/mol and will yield the second intermediate (see Scheme 4A.4). This species has only five membered rings, with the Ga-N bond completely ruptured. The final step, eliminating hydrogen, requires a barrier of 25.9 kcal/mol with respect to the separated reactant species and will regenerate the Ga-N bond. The overall process is exothermic by 4.2 kcal/mol. The three barriers obtained {26.3 kcal/mol, 1.6 kcal/mol (from the intermediate) and 25.9 kcal/mol} are in the range of AB dehydrogenation barriers obtained in transition metal catalyst systems[4,30] and the overall exothermicity of the reaction indicates that the process would be thermodynamically favorable.

As Scheme 4A.4 indicates, a further set of calculations have been done with a model system: $(CH_3Ga)_4(NH\text{-}NPh)_3NH$, made by replacing the isopropyl groups attached to the gallium atoms in $(^iPrGa)_4(NH\text{-}NPh)_3NH$ with methyl groups. The

corresponding values for the intermediates and transition states for the AB dehydrogenation with the model cage are shown in parentheses in Scheme 4A.4. A comparison of the corresponding values indicates that the model system provides results that are both qualitatively and quantitatively comparable to the real cage system. Hence, for the purposes of computational expediency, the validated model cage will be employed for subsequent investigations of Ga-N bond activation, as well as for other reactions.

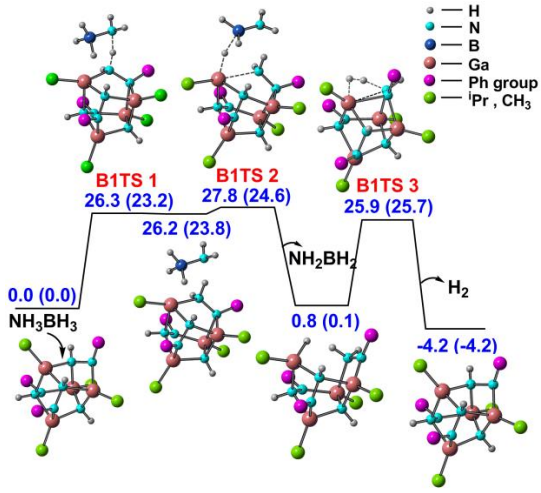

Scheme 4A.4. The free energy profile for the dehydrogenation of ammonia borane (AB) mediated by the Ga-N cage; all the structures shown are the fully optimized geometries form the DFT calculations; the values outside the parentheses are the values for the real system, $(^{i}PrGa)_4(NH\text{-}NPh)_3NH$; the values for the model system $(CH_3Ga)_4(NH\text{-}NPh)_3NH$ are given inside the perentheses; all valuesare in kcal/mol.

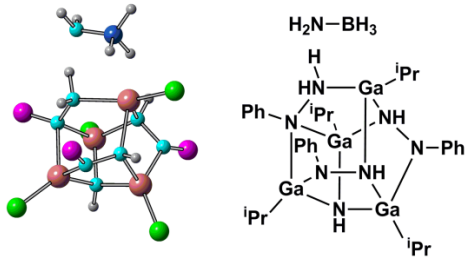

Figure 4A.3. The DFT optimized geometry of the first intermediate formed by the reaction of ammonia borane with the $(^{i}PrGa)_4(NH\text{-}NPh)_3NH$ cage.

A further study has been done in order to test the efficacy of the PBE/TZVPP DFT approach adopted here. For the model system, single point SCS-MP2 calculations (also with the RI approximation) have been done with the DFT optimized

structures, obtained along the free energy surface. Previous investigations have also considered this approach of single point MP2 calculations done on DFT optimized structures[25,31]. The ΔG values (with the internal energy and entropy contributions taken from the DFT calculations) are shown in Scheme 4A.5. The values are seen to match quite well with those obtained with the DFT calculations. Therefore, the results indicate that the prediction of the nature of the catalytic process remains the same when considering the DFT/MP2 level of theory, thus validating the PBE/TZVPP DFT approach adopted here.

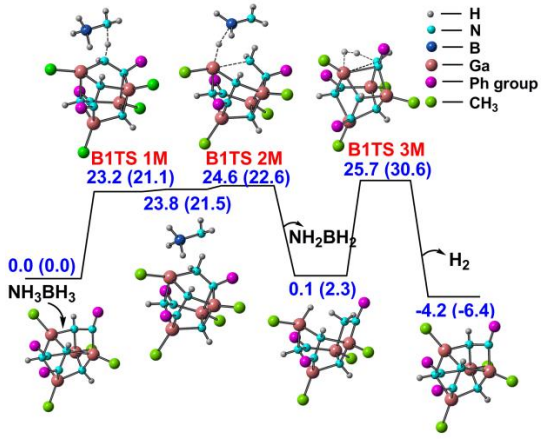

Scheme 4A.5. The free energy profiles comparing the DFT/SCS-MP2 approach to the DFT approach for the dehydrogenation of ammonia borane (AB) mediated by the Ga-N model cage $(CH_3Ga)_4(NH\text{-}NPh)_3NH$ for "**Bond 1**"; the free energies obtained at PBE/TZVPP level are given outside the parentheses and the SCS-MP2 corrected free energies are given inside the parentheses; all the structures shown are the fully optimized geometries from the DFT calculations; all the values are in kcal/mol.

It is be noted that the previous studies were done with a specific Ga-N bond in the cage structure. This is the bond corresponding to the gallium atom that is bound to three N-H groups (denoted as "**Bond_1**" in Figure 4A.4). It is also possible that the AB dehydrogenation catalysis can be mediated by other Ga-N bonds in the cage. Two other possibilities have been considered; shown as "**Bond_2**" and "**Bond_3**" in Figure 4A.4. The gallium of the two Ga-N bonds, **Bond_2** and **Bond_3**, is connected to two NH and an N-Ph group, with the nitrogen of the Ga-N bond in **Bond_2** being the N-H group and the nitrogen of the Ga-N bond in **Bond_3** being the N-Ph group (see Figure 4A.4 below). The results of the AB dehydrogenation catalysis calculations with **Bond_2** and **Bond_3** are shown in Scheme 4A.6 and Scheme 4A.7.

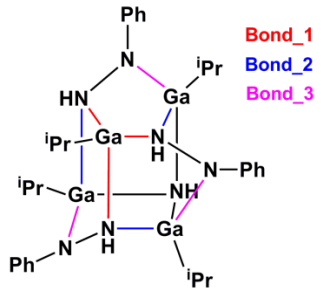

Figure 4A.4. Different Ga-N bonds studied for the reaction of ammonia borane (AB) with the $(^{i}PrGa)_4(NH\text{-}NPh)_3NH$ cage.

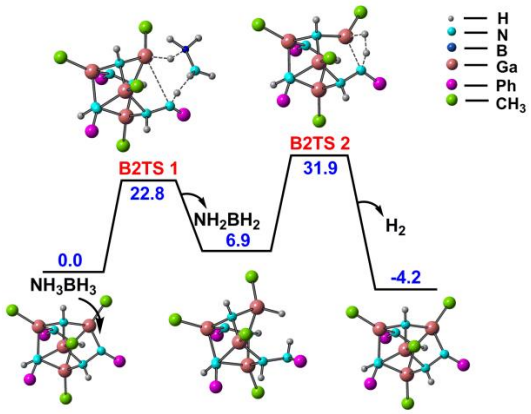

Scheme 4A.6. The free energy profile for the dehydrogenation of ammonia borane (AB) mediated by the Ga-N cage; a second, different Ga-N bond (**Bond_2**) for the model system $(CH_3Ga)_4(NH\text{-}NPh)_3NH$ has been considered in this case; all the structures shown are the fully optimized geometries from the DFT calculations; all the values are in kcal/mol.

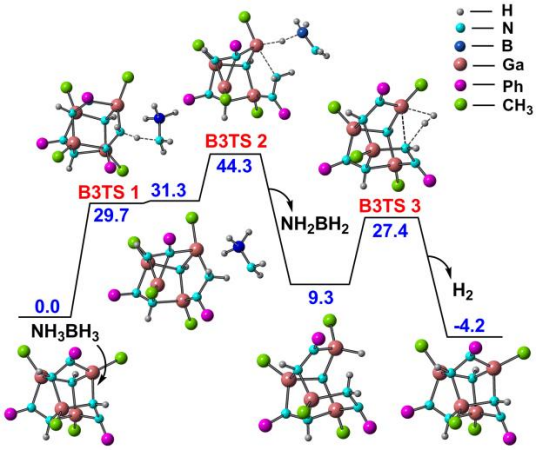

Scheme 4A.7. The free energy profile for the dehydrogenation of ammonia borane (AB) mediated by the Ga-N cage; a third, different Ga-N bond (**Bond_3**) for the model system $(CH_3Ga)_4(NH\text{-}NPh)_3NH$ has been considered in this case; all the structures shown are the fully optimized geometries from the DFT calculations; all the values are in kcal/mol.

For the case of **Bond_2**, the removal of the hydridic and protic hydrogens was found to occur in a concerted fashion – only one barrier of 22.8 kcal/mol was obtained. The Ga-N bond regeneration step was found to have a barrier of 25.0 kcal/mol. This result suggests that there are multiple sites (that is, different Ga-N bonds) in the Ga-N cage that can mediate the dehydrogenation of AB, thereby increasing the catalytic potential of the molecular cage. For the case of **Bond_3**, however, the barriers were found to be higher, with the second transition state being 44.3 kcal/mol higher than the separated reactants (see Scheme 4A.7). Calculations determining the energy required to displace the nitrogen from the gallium in each of the bonds: **Bond_1**, **Bond_2** and **Bond_3**, shows nearly the same energy profile (see Figure 4A.5). Also, a charge analysis done with NBO[32] shows nearly the same charges present in the case of the gallium and nitrogen atoms in **Bond_1** (Ga: +1.709 and N: -0.978) and **Bond_3** (Ga: +1.721 and N: -0.978). (The values for **Bond_2** are: Ga: +1.721 and N: -0.603). These results suggest that the reason for the higher barrier in the case of **Bond_3** lies in the nature of the transition state structure: it is seen that the cage rearrangement during the reaction in the **Bond_3** case involves the formation of a three membered ring, which is a strained structure. This result indicates that not all the Ga-N bonds in the cage are susceptible to attack by AB.

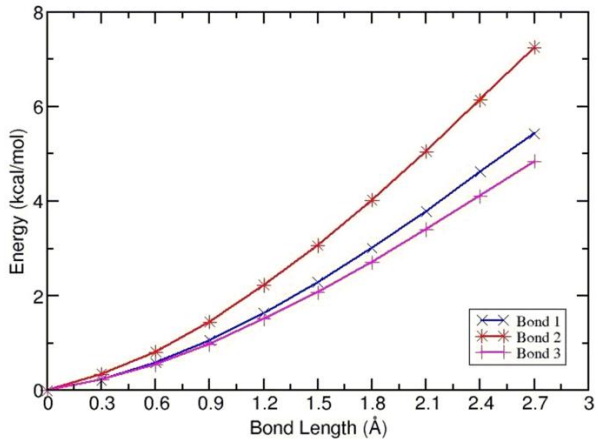

Figure 4A.5. Bond length vs Energy diagram for the various bonds (**Bond_1**, **Bond_2**, **Bond_3**) considered for the reaction of ammonia borane with the Ga-N cage.

Finally, in order to analyse the influence of the phenyl group in the considered Ga-N cage, we have done some calculations with a modified Ga-N cage having

tertiary butyl groups in place of the phenyl groups in the cage structure. Such a cage structure (referred to henceforth as "Ga-N_mod") have also been synthesized[9]. For these investigations, in order to avoid the computational expense of the TZVPP basis set, we have optimized the geometries with the TZVP[19] basis set and then calculated the single point energies with the TZVPP basis set. The zero point energy, internal energy and entropy calculations have also been done at the TZVP level and then added to the single point TZVPP energies in order to obtain the free energies for the reaction pathway. Solvent corrections have been included as before, with COSMO[22], using toluene ($\varepsilon = 2.38$) as the solvent. That this approach will yield reliable results has been verified by repeating the AB dehydrogenation cycle calculations shown in Scheme 4A.4 by following this same procedure. The results are shown in Scheme 4A.8 and show that the ΔG values match almost exactly with the values obtained with the full TZVPP calculations, thus validating this approach.

Shown in Scheme 4A.9 is the energy profile of AB dehydrogenation employing Ga-N_mod, with the corresponding **Bond_1** case considered here. What has been found is that the barriers are lower for this particular case in comparison to the corresponding **Bond_1** case in the Ga_N cage. This suggests that the phenyl ring does not play an important electronic role in stabilizing the transition state, and that the tertiary butyl group would be better at influencing the AB dehydrogenation kinetics. Thus, the calculations indicate that Ga_N_mod would be a better catalyst for dehydrogenating AB in comparison to Ga-N cage.

It is also to be noted that we have only considered the first step in the AB dehydrogenation process. This would lead to the formation of the amino borane species, NH_2BH_2, along with the released dihydrogen. As has been experimentally[33] and computationally[34] shown, amino borane can then subsequently react in solution with AB, independent of the catalyst, to yield a soluble polymeric species known as polyborazylene, producing another equivalent of dihydrogen in the process. Apart from this, computational investigations of Zimmerman[34] *et al*. and Yang *et al*.[35] have also shown that amino borane can dimerize in an exothermic reaction to yield $(NH_2BH_2)_2$, which can then take part in further reactions[33]. Since these subsequent reactions are considered to take place independent of the catalyst, they have not been further considered in the investigation. One last point is with regard to the possibility

of NH_2BH_2 interacting with the Ga-N bonds of the cage structures to yield new expanded cage structures. Such interesting possibilities, and their implications with regard to the possible formation of new catalytic species, will be considered in future investigations.

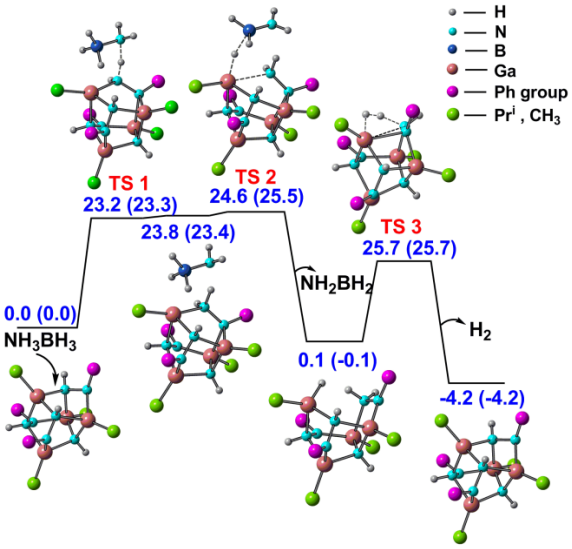

Scheme 4A.8. The comparison of the free energy profiles obtained for AB dehydrogenation using TZVPP and TZVP/TZVPP approaches; the Ga-N bond considered is the same as in Scheme 4A.4; all the structures shown are the fully optimized geometries from the DFT calculations; all values are in kcal/mol.

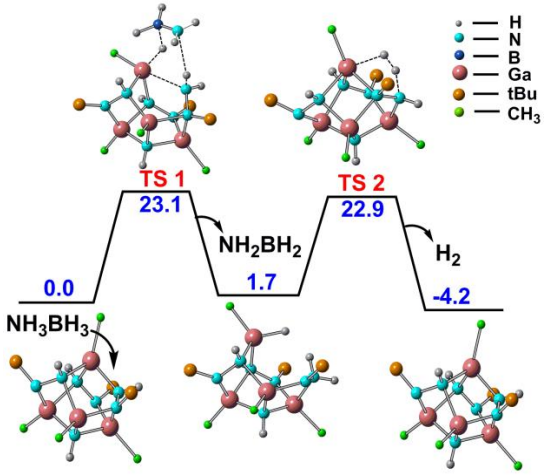

Scheme 4A.9. The free energy profile for the dehydrogenation of ammonia borane (AB) mediated by the Ga-N_mod model cage $(CH_3Ga)_4(NH\text{-}N^tBu)_3NH$; all the structures shown are the fully optimized geometries from the DFT calculations; all the values are in kcal/mol.

4A.4 Conclusions

Full quantum mechanical calculations have been done to investigate the potential of recently synthesized molecular Ga-N cage compounds to catalyze important reactions such as ammonia borane dehydrogenation. The computational investigations have shown that the Ga-N cages contain multiple favourable sites for the activation of small molecules. The calculations therefore open up interesting new possibilities in the field of small molecule activation and homogeneous catalysis by molecular cages containing main group elements, a potentially important area that has remained unexplored to date.

4A.5 References

(1) Welch, G. C.; Juan, R. R. S.; Masuda, J. D.; Stephan, D. W. *Science* **2006**, *314*, 1124-1126.

(2) Stephan, D. W.; Erker, G. *Angew. Chem. Int. Ed.* **2010**, *49*, 46-76.

(3) Kohl, S. W.; Weiner, L.; Schwartsburd, L.; Konstantinovski, L.; Shimon, L. J. W.; Ben-David, Y.; Iron, M. A.; Milstein, D. *Science* **2009**, *324*, 74-77.

(4) Blaquiere, N.; Diallo-Garcia, S.; Gorelsky, S. I.; Black, D. A.; Fagnou, K. *J. Am. Chem. Soc.* **2008**, *130*, 14034-14035.

(5) Friedrich, A.; Drees, M.; Schmedt auf der Günne, J.; Schneider, S. *J. Am. Chem. Soc.* **2009**, *131*, 17552-17553.

(6) Driess, M. *Nat. Chem.* **2012**, *4*, 525-526.

(7) Mandal, S. K.; Roesky, H. W. *Acc. Chem. Res.* **2011**, *45*, 298-307.

(8) Pal, A.; Vanka, K. *Chem. Commun.* **2011**, *47*, 11417-11419.

(9) Uhl, W.; Abel, T.; Hagemeier, E.; Hepp, A.; Layh, M.; Rezaeirad, B.; Luftmann, H. *Inorg. Chem.* **2011**, *50*, 325-335.

(10) Boudreau, J.; Courtemanche, M. A.; Fontaine, F.-G. *Chem. Commun.* **2011**, *47*, 11131-11133.

(11) Roters, S.; Appelt, C.; Westenberg, H.; Hepp, A.; Slootweg, J. C.; Lammertsma, K.; Uhl, W. *Dalton Trans.* **2012**, *41*, 9033-9045.

(12) Roters, S.; Hepp, A.; Slootweg, J. C.; Lammertsma, K.; Uhl, W. *Chem. Commun.* **2012**, *48*, 9616-9618.

(13) Uhl, W.; Rezaeirad, B.; Layh, M.; Hagemeier, E.; Würthwein, E.-U.; Ghavtadze, N.; Kuzu, I. *Chem. - Eur. J.* **2010**, *16*, 12195-12198.

(14) Uhl, W.; Voß, M.; Müller, J.; Seubert, K. *Chem. - Eur. J.* **2011**, *17*, 7852-7857.

(15) Uhl, W.; Layh, M.; Rezaeirad, B. *Inorg. Chem.* **2011**, *50*, 12275-12283.

(16) Uhl, W.; Hepp, A.; Layh, M.; Rezaeirad, B. *Chem. Commun.* **2012**, *48*, 1799-1801.

(17) Ahlrichs, R.; Bär, M.; Häser, M.; Horn, H.; Kölmel, C. *Chem. Phys. Lett.* **1989**, *162*, 165-169.

(18) Perdew, J. P.; Burke, K.; Ernzerhof, M. *Phys. Rev. Lett.* **1996**, *77*, 3865.

(19) Ansgar, S.; Christian, H.; Reinhart, A. *J. Chem. Phys.* **1994**, *100*, 5829-5835.

(20) Eichkorn, K.; Treutler, O.; Öhm, H.; Häser, M.; Ahlrichs, R. *Chem. Phys. Lett.* **1995**, *240*, 283-289.

(21) Sierka, M.; Hogekamp, A.; Ahlrichs, R. *J. Chem. Phys.* **2003**, *118*, 9136.

(22) Klamt, A.; Schuurmann, G. *J. Chem. Soc., Perkin Trans. 2* **1993**, 799-805.

(23) Mammen, M.; Shakhnovich, E. I.; Deutch, J. M.; Whitesides, G. M. *J. Org. Chem.* **1998**, *63*, 3821-3830.

(24) Hellweg, A.; Grun, S. A.; Hattig, C. *Phys. Chem. Chem. Phys.* **2008**, *10*, 4119-4127.

(25) Goumans, T. P. M.; Ehlers, A. W.; Lammertsma, K.; Würthwein, E.-U.; Grimme, S. *Chem. - Eur. J.* **2004**, *10*, 6468-6475.

(26) Staubitz, A.; Robertson, A. P. M.; Manners, I. *Chem. Rev.* **2010**, *110*, 4079-4124.

(27) Marder, T. B. *Angew. Chem. Int. Ed.* **2007**, *46*, 8116-8118.

(28) Stephens, F. H.; Baker, R. T.; Matus, M. H.; Grant, D. J.; Dixon, D. A. *Angew. Chem. Int. Ed.* **2007**, *46*, 746-749.

(29) Etzenbach-Effers, K.; Berkessel, A.; List, B.; Springer Berlin / Heidelberg: 2009; Vol. 291, p 38-69.

(30) Paul, A.; Musgrave, C. B. *Angew. Chem.* **2007**, *119*, 8301-8304.

(31) Ray, M.; Nakao, Y.; Sato, H.; Sakaba, H.; Sakaki, S. *J. Am. Chem. Soc.* **2006**, *128*, 11927-11939.

(32) Alan, E. R.; Robert, B. W.; Frank, W. *J. Chem. Phys.* **1985**, *83*, 735-746.

(33) Pons, V.; Baker, R. T.; Szymczak, N. K.; Heldebrant, D. J.; Linehan, J. C.; Matus, M. H.; Grant, D. J.; Dixon, D. A. *Chem. Commun.* **2008**, *0*, 6597-6599.

(34) Zimmerman, P. M.; Paul, A.; Zhang, Z.; Musgrave, C. B. *Inorg. Chem.* **2009**, *48*, 1069-1081.

(35) Yang, X.; Hall, M. B. *J. Organomet. Chem.* **2009**, *694*, 2831-2838.

Chapter 4B

Catalytic Dihydrogen Generation Reaction Using Ge (II) Hydride Compounds

Abstract

The protolytic cleavage of the O-H bond in water and alcohols is a very important reaction, and an important source for producing dihydrogen. Full quantum chemical studies with density functional theory (DFT) reveal that germanium based complexes, such as HC{CMeArB}$_2$GeH (Ar = 2,6-^{i}Pr$_2$C$_6$H$_3$), with the assistance of silicon based compounds such as SiF_3H, can perform significantly better than the existing state-of-the-art post-transition metal based system for catalyzing the dihydrogen generation from water and alcohols through the protolysis reaction.

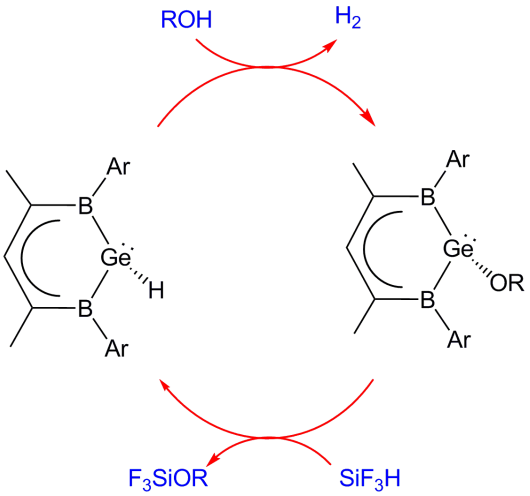

Ar = 2,6-^{i}Pr$_2$C$_6$H$_3$

4B.1 Introduction

The replacement of existing fossil fuels with an efficient alternative energy resource is essential to meet growing energy demands. A promising candidate for this purpose is dihydrogen, a fuel which is known to have the highest energy density per unit of mass compared to the other known fuels. Furthermore, dihydrogen is also non-toxic and green. Therefore, many attempts have been made through important chemical reactions such as the steam reforming processes,[1] the water gas shift reaction[2-4] (WGSR), as well as through the biomass conversion of hydrocarbons[5,6] and alcohols[7-11] to improve dihydrogen production. However, the handling of hydrogen fuel for practical applications is still difficult, since it requires better storage and transport facilities. Therefore, there is considerable interest in the possibility of the chemical storage of hydrogen. Significant efforts have been made in this area, including the dehydrogenation of ammonia borane,[12-16] alcohols[8,9,11] and formic acid,[17-19] the protolysis of organosilanes[20-26] with water or alcohols and the use of organic heterocycles[27, 28] as storage materials. This approach has traditionally involved the use of transition metal based catalyst systems for the necessary small molecule activation.

However, recent studies have focused on the replacement of transition metal based catalysts with compounds belonging to the main group, which are often observed to be less toxic and cheaper than transition metal complexes. In this regard, some of the important developments include frustrated lewis acid-base pairs,[29,30] molecular cages,[31, 32] carbenes[33] and their higher analogues.[34-41] An important class of compounds in this category are the Group 14 compounds. The alkyne and the alkene analogues of Group 14 compounds show reactivity towards small molecules,[40,42] *via* the activation of C-C, C=C, C=N and N=N bonds, and play an important role in various metathesis processes. The synthetic difficulty involved in making these compounds has been resolved either by the use of sterically encumbered ligands,[43,44] or by the formation of donor-acceptor complexes with BH_3 or metal carbonyl complexes.[45-49] Low-valent Group 14 hydrides, in particular, have been shown to be significant in small molecule activation.[44,50-54] The monomeric terminal hydrides LMH [M = Ge or Sn, L = $CH\{N(Ar)(CMe)\}_2$, Ar = 2, 6-$^{i}Pr_2C_6H_3$] (**GeH-1**) activate small molecules such as CO_2, ketones, alkenes, as well as azo and diazo compounds.[55-59] Here, the reaction gives the corresponding formate, alkoxide, vinyl

and hydrazone derivative of the Ge (II) hydride, denoted as **GeH-1** in Figure 4B.1 below.

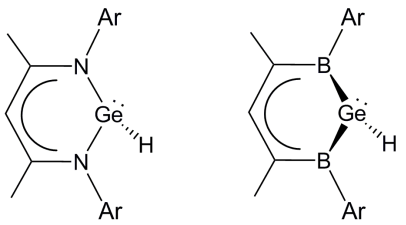

GeH-1 **GeH-2**

Ar = 2,6-$^{i}Pr_2C_6H_3$

Figure 4B.1. The Ge (II) hydrides, **GeH-1** and **GeH-2**.

It is important to note, though, that computational investigations by Sakaki and co-workers[53] have shown that, due to the presence of a strong Ge-O bond in alkoxide and formate intermediates, a complete catalytic cycle is not possible with **GeH-1** through the oxidative addition of the H_2 molecule, as is the case with transition metal complexes. A solution to this problem has been obtained through the use of the hydrosilylation process using silanes,[53] a process that regenerates the Ge-H species, thereby completing the catalytic cycle. In place of silanes, HBpin has also been employed[54] along with germanium (II) and tin (II) hydride compounds to convert carbonyl compounds to their hydroborated analogues, with efficiencies rivalling the most active catalysts presently available for such reactions.

However, a catalytic cycle has not yet been reported for dihydrogen generation by the protolytic cleavage of O-H bond in water or alcohols using Ge (II) hydride compounds. Most of the reported catalytic cycles for this reaction involve transition metal based systems, employing precious metals such as rhodium, rhenium, platinum and gold.[21-23,60-65] Recently, Parkin and co-workers have reported a catalytic cycle with the zinc hydride catalyst: [Tris(2-pyridylthio)methyl]zinc hydride ([κ^3-Tptm]ZnH) for the hydrolysis and alcoholysis of phenylsilanes.[26] A computational study by Sakaki and co-workers on [κ^3-Tptm]ZnH has shown that various hydrosilanes can be effective in this reaction, since the reaction requires a small activation energy.[66] Experimental and theoretical calculations by Shubina and co-workers have shown that the proton-transfer and H_2-elimination reactions in the

presence of alcohols can also be performed by main group Group 13 hydrides.[67,68] They have also provided a detailed mechanistic investigation on the reaction process.

The focus of the current work is to computationally explore the possibility of main group systems, specifically Ge (II) hydrides, catalyzing the protolytic cleavage of the O-H bond in water and alcohols, followed by the reaction with hydrosilanes, leading to the formation of dihydrogen and completing the catalytic cycle. Employing a full quantum chemical approach with density functional theory (DFT), we have proposed a new Ge (II) hydride compound (**GeH-2**) (shown in Figure 4B.1), which is a modification of **GeH-1**, that can cleave the O-H bond in water, methanol and ethanol efficiently to provide dihydrogen. We have proposed the regeneration of **GeH-2** with the assistance of the hydrosilane, SiF_3H. Our aim is to explore the potential of Ge (II) hydrides in important catalytic processes, by employing a theoretical, predictive approach – showing how modifications to existing Ge (II) hydrides can lead to significant improvement in activity. It is expected that such an approach will provide insight for both experimental and computational groups working in the area of developing new main group catalysts for dihydrogen generation and other reactions, like the work of Sakaki and coworkers.[53] As will be demonstrated in the Results and Discussion Section, the proposed Ge (II) hydride compound would not only be considerably more efficient than **GeH-1**, it would rival and, indeed, be an improvement on the state-of-the art zinc based system in catalyzing the important protolytic cleavage reaction, for all the three substrates that have been considered.

4B.2 Computational Details

All the calculations have been done with Turbomole 6.4,[69] using the TZVP basis set[70] and the PBE functional.[71,72] Dispersion corrections[73-75] using DFT-D3 has been included in all the geometry optimization calculations. Solvent effects have been incorporated through single point calculations with COSMO,[76] with THF (epsilon = 7.5) as the solvent. The resolution of identity (RI),[77] along with the multipole accelerated resolution of identity (marij)[78] approximations have been employed for an accurate and efficient treatment of the electronic Coulomb term in the DFT calculations. The values reported are ΔG values, with zero point energy, internal energy and entropic contributions included through frequency calculations on the

optimized minima and transition state structures, with the temperature taken to be 298.15 K. The same thermodynamic treatment has been done for the free energy values reported in the Schemes 4B.1-4B.4, 4B.6, 4B.7, 4B.10. All the obtained transition states were confirmed to have only a single negative frequency corresponding to the correct normal mode. In addition, Intrinsic Reaction Coordinate (IRC)[79] calculations were done with all the transition states in order to further confirm that they were the correct transition states, yielding the correct reactant and product structures. In order to obtain the frontier molecular orbitals of the Ge (II) hydride complexes the structures of the complexes were optimized with Gaussian 09.[80]

In order to estimate the level of accuracy of our calculations using PBE/TZVP, we have also performed single point calculations with the B3LYP functional and the QZVP basis set for the case of the Ge (II) hydride reaction with water. The results show that the trend in the potential energy surface obatined at the PBE/TZVP level of theory is also found when the potential energy surface is obtained at the B3LYP/QZVP level of theory (see Scheme 4B.4 in the results and discussion section). Please note that the reported gas phase free energy values at the B3LYP/QZVP level of theory includes zero point energy, internal energy and entropic contributions taken from frequency calculations on the optimized minima and transition state structures obtained at the PBE/TZVP level of theory.

Table 4B.1: Comparative study of the thermodynamic parameters obtained from full geometry optimization carried out at PBE/TZVP and B3LYP/QZVP.

System	PBE/TZVP		B3LYP/QZVP	
	Internal Energy	Entropy	Internal Energy	Entropy
H_2	7.631453	0.032622	7.774857	0.032569
H_2O	14.64627	0.046601	15.03824	0.046527
CH_3OH	33.01864	0.057048	33.85516	0.05718
C_2H_5OH	51.10421	0.06441	52.30641	0.064304
SiF_3H	13.28633	0.069536	13.84799	0.068709
SiF_3OH	17.63384	0.076671	18.19073	0.076205
$HC\{CMeHB\}_2GeH$	53.18595	0.081283	54.38576	0.080796
$HC\{CMePhB\}_2GeH$	159.0942	0.134634	163.3437	0.130696

Validation of this approach has been provided through full optimization of selected small molecules at the B3LYP/QZVP level and the subsequent comparison of the thermodynamic parameters with the PBE/TZVP level of calculations (See Table 4B.1 above). The values in Table 4B.1 above suggest that the entropy values vary less than only 0.004 kcal/mol for the considered systems between PBE/TZVP and B3LYP/QZVP//PBE/TZVP level of calculations. The same procedure has been employed for the singlet and triplet state calculations for **GeH-2**.

4B.3 Results and Discussions

4B.3.1 Dihydrogen production with a reported germanium (II) hydride: As discussed in the Introduction, the Ge (II) hydride compound $HC\{CMeArN\}_2GeH$ (Ar = 2,6-$^{i}Pr_2C_6H_3$) (**GeH-1**) (see Figure 4B.1) has been reported to react with many substrates such as CO_2, ketone, alkene, azo and diazo compounds.[55-59] However, the reaction of GeH-1 with H_2O and alcohols such as CH_3OH and C_2H_5OH has not yet been reported. Since water and alcohols are an important feedstock to provide dihydrogen through protolysis, it is necessary to consider the dihydrogen generation through the protolytic cleavage of O-H bond in these molecules using the Ge (II) hydride. Therefore, in the current work we have considered the hydrogen generation from water, methanol and ethanol using **GeH-1**. As also mentioned in the Introduction, we will investigate the same protolysis reaction using a modified version of **GeH-1**: **GeH-2** (see Figure 4B.1).

The optimized geometry of **GeH-1** is shown in Figure 4B.2. The calculated geometrical parameters at the PBE/TZVP level were found to be in very good agreement with the experimentally reported values.[55] The reaction energy profile of **GeH-1** with one molecule of water, methanol and ethanol leading to the corresponding alkoxide compound and H_2 molecule is shown in Scheme 4B.1 (A). The reaction of **GeH-1** with R-OH (R=H, CH_3, C_2H_5) was found to be thermodynamically favourable by 6.2 kcal/mol, 6.4 kcal/mol and 7.3 kcal/mol respectively. However, as seen in Scheme 4B.1 (A), each of the reactions requires a high barrier: the energy barriers corresponding to the three reactions are 38.4 kcal/mol, 34.2 kcal/mol and 35.0 kcal/mol respectively. It is to be noted that, as Scheme 4B.1 (A) illustrates, the reaction involves a four membered transition state,

GeH-1-4MTS. Since a four membered transition state is more strained, a six membered transition state (**GeH-1**-6MTS) can be considered for the same reaction by having two participating ROH (R=H, CH_3, C_2H_5) molecules. A similar six membered transition state has been reported for the Zn based catalyst with the water and methanol substrates by Sakaki and co-workers[66].

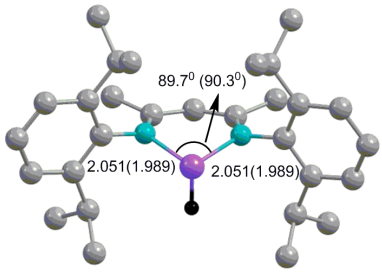

Figure 4B.2. The optimized geometry of the Ge (II) hydride HC{CMeArN}$_2$GeH (Ar = 2,6-^{i}Pr$_2$C$_6$H$_3$) (**GeH-1**); the experimental values are given inside the parenthesis.

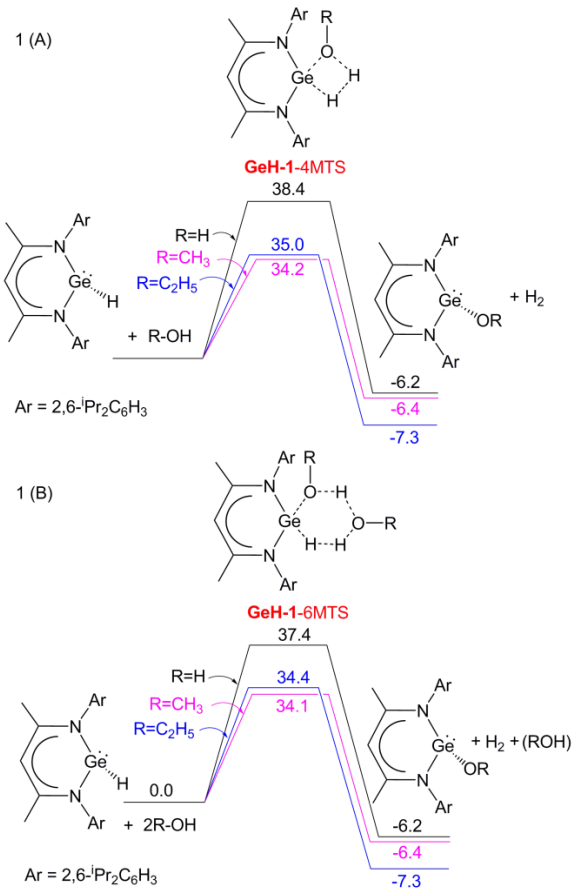

Scheme 4B.1. The free energy profile for the reaction of **GeH-1** with R-OH (R=H, CH_3, C_2H_5).

The free energy profile for the reaction of **GeH-1** with two R-OH (R=H, CH_3, C_2H_5) molecules is shown in Scheme 4B.1(B). The results indicate that the energy barrier decreases slightly for the reaction involving the six membered transition state in comparison to the four membered transition state pathway: the corresponding barriers for the reactions are 37.4 kcal/mol, 34.1 kcal/mol, and 34.4 kcal/mol respectively. The high barriers obtained suggest that the reaction is not feasible at room temperature. Furthermore, as will be shown later, the values are significantly higher than those for the zinc–based system.

However, since the reaction shows a thermodynamical favourability and since Ge (II) hydride systems are generally known to have very good reactivity towards a variety of small molecules, [44, 50-54,55-59] we have considered the modification of **GeH-1** to create a system that can cleave the O-H bond efficiently in water and alcohols. This will be discussed in the next section.

4B.3.2 On demand hydrogen generation by the new Ge (II) hydride, GeH-2, from water, methanol and ethanol: Recent studies have shown that the boron based ligands are very good in stabilizing main group compounds. Aldridge and co-workers have synthesized acyclic silylene complexes stabilized by boryl ligands.[82] Also, recently they have shown that boryl ligands can even stabilize Group 13 radical compounds.[83] The unusual stability of these compounds has been achieved by the strong σ donating ability of the boryl ligands.[84] Moreover, such ligands were found to help reduce the HOMO-LUMO gap in some of these compounds, which were observed to activate small molecules even under ambient conditions.[37,82,85] Therefore, in our current study, we have considered the modification of **GeH-1** by replacing the two nitrogen atoms coordinated to the germanium atom in the ring with two boron atoms. The optimized geometry of the predicted Ge (II) hydride compound $HC\{CMeArB\}_2GeH$ (Ar = 2,6-$^{i}Pr_2C_6H_3$) (**GeH-2**) is shown in Figure 4B.3 below. Compared to **GeH-1**, the germanium atom in **GeH-2** is seen to project out of the ring plane to a greater extent. The frontier molecular orbitals of **GeH-1** and **GeH-2** are shown in Figure 4B.4 and the natural charges obtained from the NBO analysis are given in Table 4B.2. The calculations show that, for GeH-2, the singlet is more stable, with the singlet-triplet energy gap being 1.3 kcal/mol, which is considerably smaller than that of GeH-1, where the value obtained was 39.2 kcal/mol. However,

subsequent single point calculations with B3LYP/QZVP shows the triplet ground state for the **GeH-2** system: the gas phase free energy value obtained at B3LYP/QZVP//PBE/TZVP as shown in Figure 4B.5(a) indicates that the triplet state is stable by 3.8 kcal/mol over the singlet. However, as will be discussed below when the free energy profiles of the reaction of **GeH-2** system with water are described, it is likely that the reactions with the **GeH-2** system will occur through the singlet pathway.

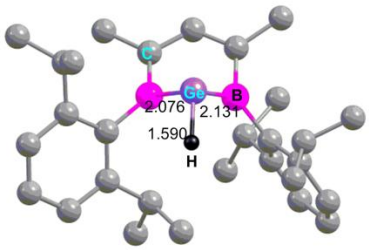

Figure 4B.3. The optimized geometry of the Ge (II) hydride, HC{CMeArB}$_2$GeH (Ar = 2,6-^{i}Pr$_2$C$_6$H$_3$) (**GeH-2**).

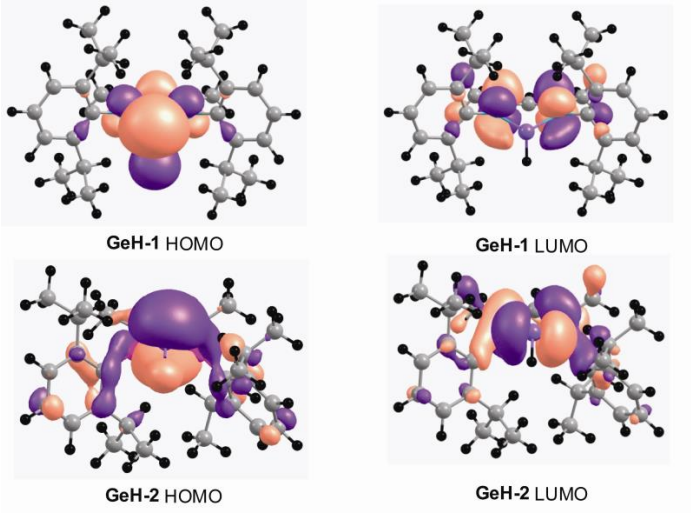

Figure 4B.4. Frontier molecular orbitals of **GeH-1** and **GeH-2**.

Table 4B.2. NBO charges for **GeH-1** and **GeH-2**.

GeH-1		**GeH-2**	
Ge	0.686	Ge	0.519
H	-0.247	H	-0.163
N_1	-0.603	B_1	0.428
N_2	-0.604	B_2	0.287

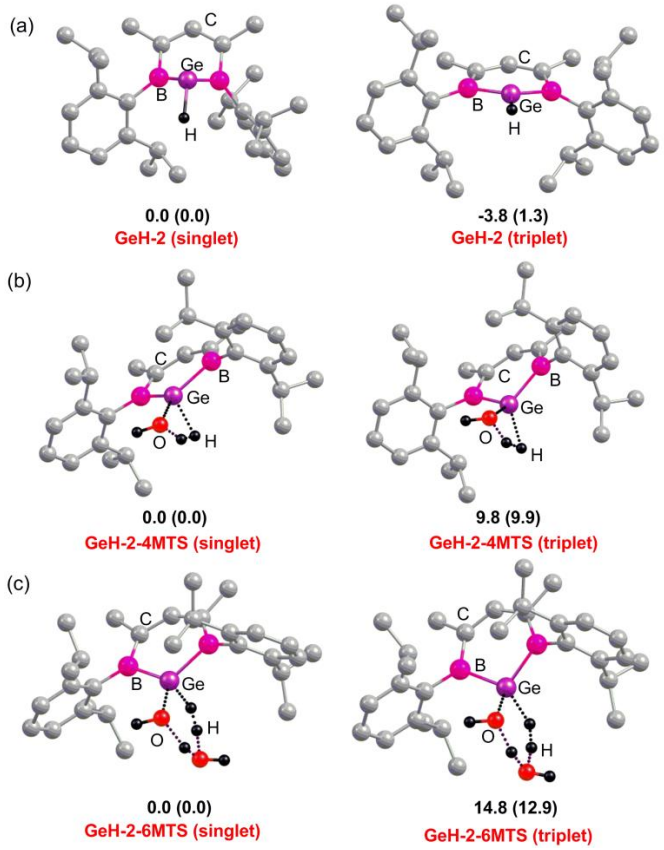

Figure 4B.5 Comparative study for the singlet and triplet states of **GeH-2**; the values outside the parentheses correspond to the gas phase free energies at the B3LYP/QZVP//PBE/TZVP level and the values inside the parentheses correspond to the gas phase free energies at the PBE/TZVP level of theory.

We have investigated the generation of the dihydrogen molecule from water, methanol and ethanol through the protolysis reaction by singlet **GeH-2**. The free energy profile for the reaction pathway involving a six membered transition state (**GeH-2-**6MTS) is shown below in Scheme 4B.2. The formation of the corresponding alkoxide and the H_2 molecule was found to be thermodynamically favourable by 5.1 kcal/mol, 5.7 kcal/mol and 3.8 kcal/mol respectively. The corresponding barriers were calculated to be 15.3 kcal/mol, 14.5 kcal/mol and 12.5 kcal/mol respectively for water, CH_3OH and C_2H_5OH. The activation barrier was found to be decreased considerably with respect to the pathway involving a four membered transition state (**GeH-2-**4MTS), where the corresponding barriers are 25.3 kcal/mol, 22.5 kcal/mol and 22.1 kcal/mol respectively (see Scheme 4B.3). This suggests the feasibility of

employing **GeH-2** over **GeH-1** in the cleavage of the O-H bond and subsequent dihydrogen generation from substrates of the type R-OH.

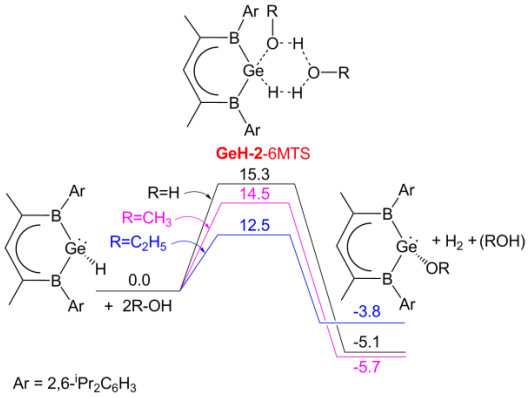

Scheme 4B.2. The free energy profile for the reaction of **GeH-2** with R-OH (R=H, CH_3, C_2H_5).

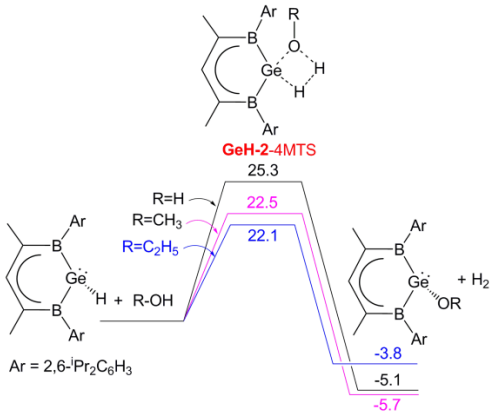

Scheme 4B.3. Free energy profile for the reaction of **GeH-2** with ROH (R=H, CH_3, C_2H_5) through a four membered transition state.

It is to be noted that all the results reported in the previous paragraph consider the singlet pathway, even though, as mentioned earlier, the ground state of the **GeH-2** system at the B3LYP/QZVP//PBE/TZVP level is a triplet. The reason for this is that the barriers for the process are significantly higher if it goes through a triplet pathway. We have considered the triplet state calculations of the barrier for both the four and six membered transition states, **GeH-2**-4MTS and **GeH-2**-6MTS, for the case of the reaction with water. As shown is Figure 4B.5(b) and 4B.5(c) above, the calculations at PBE/TZVP, as well as B3LYP/QZVP//PBE/TZVP show a higher barrier for the triplet transition state. The gas phase free energy profile for the whole cycle with water for the comparative study is shown in Scheme 4B.4. The difference in the gas

phase singlet and triplet free energy barriers for the 4M and 6M transition states in the case of water is 9.9 kcal/mol and 12.9 kcal/mol respectively at the PBE/TZVP level; and 10.2 kcal/mol and 14.8 kcal/mol at the B3LYP/QZVP//PBE/TZVP level, thereby eliminating the possibility of a triplet pathway. Similar observations have been reported by Apeloig and co-workers for the intramolecular C−H bond insertion reaction involving the triplet silylene.[86] Based on these observations, we have considered the reaction of singlet **GeH-2** in further calculations.

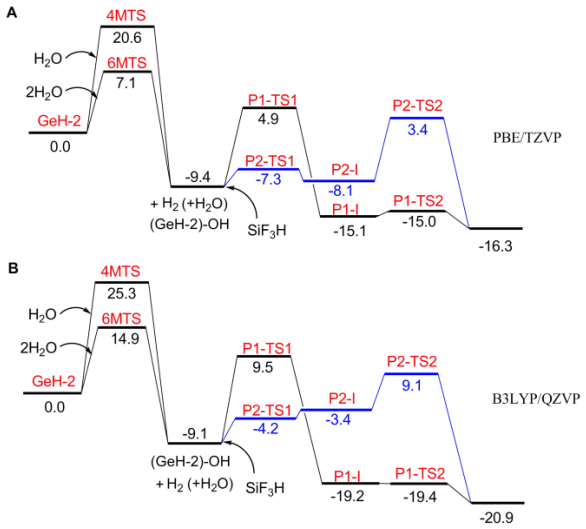

Scheme **4B.4.** Gas phase free energy profiles for the reaction of **GeH-2** with water: comparative study of the calculations at PBE/TZVP and the B3LYP/QZVP//PBE/TZVP level of theory.

In order to understand the difference in reactivity of **GeH-2** in comparison with **GeH-1**, we have analyzed the HOMO-LUMO gap of these two systems. The HOMO-LUMO gap corresponding to **GeH-1** and **GeH-2** are 54.5 kcal/mol and 34.5 kcal/mol respectively for the singlet state and 27.5 kcal/mol and 15.5 kcal/mol respectively for the triplet case. As pointed out by Sakaki and co-workers, donation and back-donation between the frontier orbitals of a germanium hydride and the incoming substrate both play a role in bond cleavage reactions.[53] Hence, having a small HOMO-LUMO gap (analogous to transition metal systems) would be particularly advantageous in such systems, and explains the significant improvement in the barrier heights when going from **GeH-1** to **GeH-2**. It is also reported that lower HOMO-LUMO gap is essential for many small molecule activation processes, such as the activation of dihydrogen by silylenes.[37,82,85]

It is notable that while the HOMO-LUMO gap is 34.5 kcal/mol in singlet **GeH-2**, the singlet is more stable than the triplet by only 1.3 kcal/mol. This is because the nature of the orbitals is altered considerably for **GeH-2** upon going singlet to triplet. As shown in Figure 4B.6, the HOMO and the LUMO in singlet **GeH-2** is considerably different in shape in comparison to the HOMO and the LUMO in triplet **GeH-2** (see Figure 4B.6).

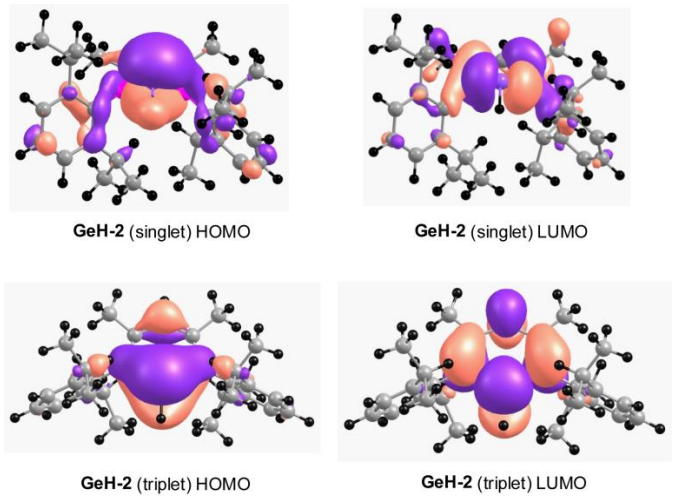

Figure 4B.6. Frontier molecular orbitals of **GeH-2** (singlet) and **GeH-2** (triplet).

4B.3.3 Protolysis in ROH (R=H, CH_3, C_2H_5) molecules: a comparative study of GeH-2 with an experimentally reported system: Parkin and coworkers have experimentally shown that the zinc based catalyst, [Tris(2-pyridylthio)methyl]zinc hydride ([κ^3-Tptm]ZnH), is an efficient, multifunctional post-transition metal catalyst capable of catalyzing the rapid release of dihydrogen from water and methanol with the aid of the protolytic cleavage of phenyl silane under ambient conditions (see Scheme 4B.5 below).[26] In order to understand the efficiency of the newly proposed compound, **GeH-2**, we have determined the free energy profile for the first step of the reaction: the protolytic cleavage of O-H bond in ROH molecules to yield H_2, by employing this existing, state-of-the-art post-transition metal based catalyst system. The reason we have focused on the first step is because Sakaki and coworkers have shown that the first step leading to the generation of H_2 is the rate-determining step and the subsequent reaction with various silanes to complete the catalytic cycle required a smaller barrier.[66] Shown in Scheme 4B.6 is the free energy profile for the protolysis of ROH (R=H, CH_3, C_2H_5) with the zinc catalyst [κ^3-Tptm]ZnH. Here, the

first step involves a metathesis reaction between the O-H bond of the ROH (R=H, CH_3, C_2H_5) molecule and the ZnH bond of the catalyst to generate the dihydrogen and the zinc alkoxide. This reaction is thermodynamically favourable by 3.8 kcal/mol, 4.0 kcal/mol and 5.5 kcal/mol for water, methanol and ethanol respectively.

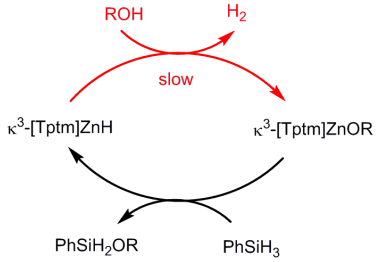

Scheme 4B.5. The reported catalytic cycle for the reaction of [κ^3-Tptm]ZnH with R-OH (R=H, CH_3) and phenyl silane.

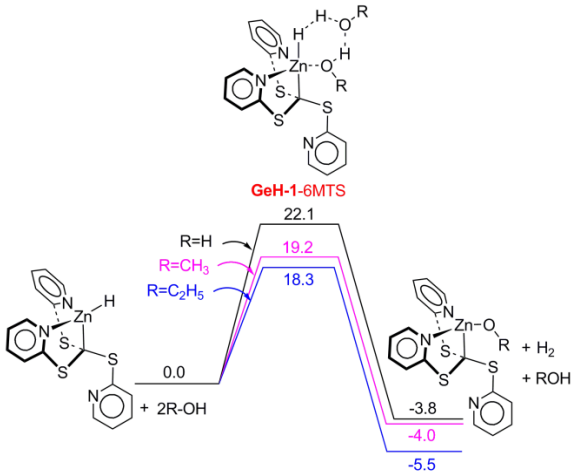

Scheme 4B.6. The free energy profile for the reaction of [κ^3-Tptm]ZnH with R-OH (R=H, CH_3, C_2H_5).

The barriers corresponding to this metathesis step, involving a six membered transition state, are 22.1 kcal/mol, 19.2 kcal/mol and 18.3 kcal/mol (See Scheme 4B.6). The corresponding barriers for a four membered transition state are 22.5 kcal/mol, 20.4 kcal/mol and 20.4 kcal/mol respectively (see Scheme 4B.7). For the same reaction, the barrier heights with the proposed **GeH-2** catalyst were found to be lower by 5.8 kcal/mol, 4.7 kcal/mol and 5.8 kcal/mol respectively for the water, methanol and ethanol cases (the more feasible six-membered transition states are compared here). This indicates that **GeH-2** would be significantly better than the zinc-

based complex for the on-demand dihydrogen generation through the O-H bond cleavage in water and alcohols. This also highlights the potential of main group compounds to compete with, and even be superior to, post-transition metal complexes in the protolytic cleavage of the O-H bond in water and alcoholic substrates.

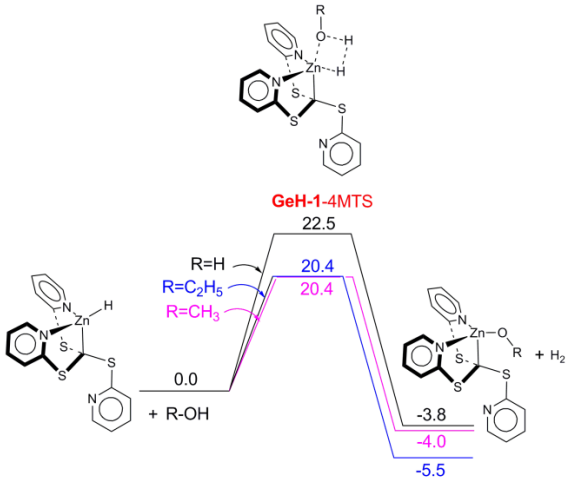

Scheme 4B.7. Free energy profile for the reaction of [κ^3-Tptm]ZnH with ROH (R=H, CH_3, C_2H_5) through a four membered transition state.

For the same reaction, the barrier heights with the proposed **GeH-2** catalyst were found to be lower by 5.8 kcal/mol, 4.7 kcal/mol and 5.8 kcal/mol respectively for the water, methanol and ethanol cases (the more feasible six-membered transition states are compared here). This indicates that **GeH-2** would be significantly better than the zinc-based complex for the on-demand dihydrogen generation through the O-H bond cleavage in water and alcohols. This also highlights the potential of main group compounds to compete with, and even be superior to, post-transition metal complexes in the protolytic cleavage of the O-H bond in water and alcoholic substrates.

4B.3.4 The full catalytic cycle for the formation of H_2 from ROH (R=H, CH_3, C_2H_5) by the GeH-2 catalyst: For the zinc catalyst [κ^3-Tptm]ZnH, the complete catalytic cycle has been reported, with the catalytic cycle being completed with the aid of hydrosilanes.[66] Sakaki and coworkers have shown that the reaction of the [κ^3-Tptm]ZnOR complex, formed as the intermediate during the catalytic cycle, with hydrosilanes requires only a small barrier and various silanes can be utilized for this purpose.[66] This would lead to the completion of the catalytic cycle and regenerate the

[κ^3-Tptm]ZnH species. In case of main group compounds, the reaction of the Ge (II) hydride, GeH-1 with CO_2, ketone or azo compounds has been reported to form the corresponding formate alkoxide or hydrazine compounds.[55-59] Previously, in order to regenerate the Ge (II) hydride from the Ge (II) formate complex formed by the activation of CO_2, the reaction was carried out under conditions separate from the reaction conditions required for CO_2 activation.[56, 58, 59] However, subsequent studies have stated that a complete reaction cycle can be generated for the Ge (II) hydride under the same reaction conditions, with the help of hydrosilanes.[53] Not just for CO_2 activation, this has also been shown to be true for ketones and imines.[53] The complete catalytic cycle for the case of a ketonic substrate is shown in Scheme 4B.8 The reason a complete catalytic cycle is feasible is because, in order to regenerate the Ge (II) hydride from the germanium alkoxide complex, the reaction has to be thermodynamically favorable, and employing hydrosilanes makes it so. This is due to the fact that the Ge-O bond is weaker than the Si-O bond, and hence the formation of the Ge-H and the Si-O bonds upon the reaction of germanium intermediate with the hydrosilane present in the system is a thermodynamically favorable process. Sakaki and coworkers have shown through computational studies that, in the presence of a silane, the Ge (II) hydride can be regenerated, along with the alcoholic product in the form of a silylether, with the reactions being energetically favorable.[53] This reaction step involves a four membered transition state, where the Ge-H bond formation and the Si-H bond dissociation takes place simultaneously (see Scheme 4B.8). It is known that the dissociation of the Si-H bond is a facile reaction in silanes, especially when the reaction is done in conjunction with the formation of the Si-O bond.[56, 58, 59] The silylether formed can be further hydrolyzed easily to the required alcoholic product.

In the current study, in order to complete the catalytic cycle, we have considered the silane, SiF_3H. This silane has also been employed by Sakaki and coworkers in their computational studies mentioned above.[53] We have analysed two pathways leading to the formation of the silyl alkoxy ether product and the catalyst **GeH-2** (see Scheme 4B.9 below). As shown in Scheme 4B.9, a planar tetra coordinated germanium intermediate **P1-I** is formed in Pathway 1. The subsequent dissociation of the Ge-O bond in **P1-I** leads to the corresponding silyl alkoxy ether products of R-OH (R=H, CH_3, C_2H_5OH) and the regenerated catalyst **GeH-2**. Pathway 1 involves two transition states, **P1-TS1**, which leads to the intermediate **P1-**

I, and **P1-TS2**, which gives the products through the Ge-O bond dissociation of **P1-I**. Pathway 2 has a non-planar germanium alkoxide-silane adduct: **P2-I**, as the intermediate with the corresponding transition state **P2-TS1**. The subsequent step involves a metathesis reaction between the Si-H bond and the Ge-O bond in the adduct **P2-1** through the transition state **P2-TS2**, regenerating the catalyst **GeH-2** (see Scheme 4B.9).

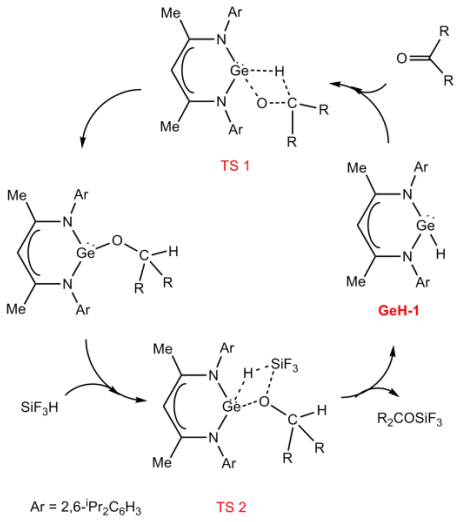

Scheme 4B.8. Free energy profile for the reaction of **GeH-1** with C=O bond in ketone, with SiF_3H employed to complete the cycle.

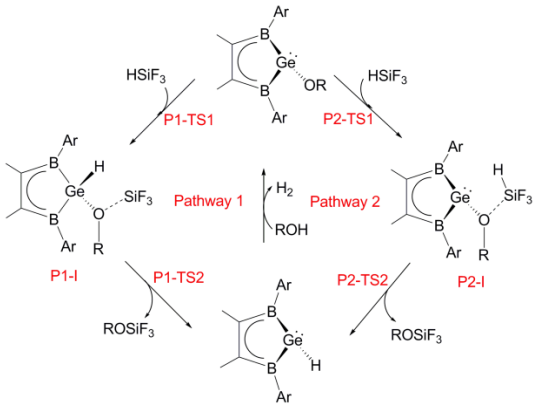

Scheme 4B.9. The reaction pathways for the catalytic activation of ROH molecules with **GeH-2** in presence of the silane, SiF_3H.

The free energy profile for the complete catalytic cycle for **GeH-2**, employing SiF_3H to complete the cycle and ROH (R = H, CH_3 and C_2H_5) as the substrate, is shown in Scheme 4B.10. For the first step, as also observed and noted in the previous sections, the six membered transition state (6MTS) is lower in energy in comparison

to the four membered transition state (4MTS). Furthermore, the energy profile shows that, similar to the zinc catalyst, [κ^3-Tptm]ZnH, case,[66] the rate determining step is the formation of alkoxide intermediate through the protolytic cleavage in ROH molecules, for R = H and R = CH_3.

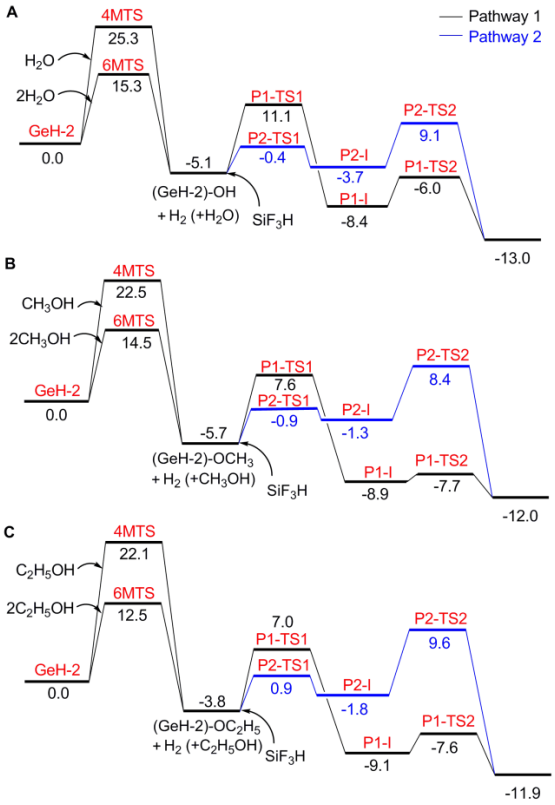

Scheme 4B.10. The free energy profile for the catalytic reaction of **GeH-2** with R-OH (R=H, CH_3, C_2H_5), with SiF_3H employed to complete the cycle.

The further reaction of the alkoxide intermediate with the silane, SiF_3H, requires a small barrier. In all ROH substrates, the formation of the tetra coordinated germanium intermediate in Pathway 1 (**P1-I**) is found to be lower in energy in comparison to the germanium alkoxide-silane adduct obtained in Pathway 2 (**P2-I**). **P1-I** is more stable by 8.4 kcal/mol, 8.9 kcal/mol and 9.1 kcal/mol (ΔG values) in comparison to the reactant species and **P2-I** is more stable by 3.7 kcal/mol, 1.3 kcal/mol and 1.8 kcal/mol (ΔG values), respectively for water, methanol and ethanol. However, in all systems, the energy barrier for the formation of **P1-I** is higher than the barrier for **P2-I** formation. The barrier corresponding to the transition state **P1-TS1** is 16.2 kcal/mol, 13.3 kcal/mol and 10.8 kcal/mol respectively, and 4.7 kcal/mol, 4.8 kcal/mol and 4.7 kcal/mol, respectively for **P2-TS1**. As mentioned earlier, in

Pathway 1, the third step is the dissociation of the Ge-O bond in **P1-I**, which requires a very small barrier and the corresponding values for the transition state **P1-TS2** from the intermediate **P1-I** are 2.4 kcal/mol, 1.2 kcal/mol and 1.5 kcal/mol respectively. In Pathway 2, the third step is a metathesis process involving the transition state **P2-TS2**, having a higher energy barrier compared to **P1-TS2**, and the obtained values are 12.8 kcal/mol, 9.7 kcal/mol and 11.4 kcal/mol.

Essentially, the free energy profiles suggest that Pathway 1 is the thermodynamically favoured pathway, and would be operational if the reaction was to take place over a long period of time. On the other hand, Pathway 2 is the kinetically controlled route, with the barriers corresponding to **P2-TS1** being lower for all the three cases studied, in comparison to the competing barrier for Pathway 1, corresponding to **P1-TS1**. Hence, Pathway 2 would be likely to be operational if the reaction were to occur over a shorter length of time. Since catalysis processes generally occur over a short period of time, the results indicate that Pathway 2 would be predominant during the catalysis process. All the optimized transition state geometries are shown in Figure 4B.7 below.

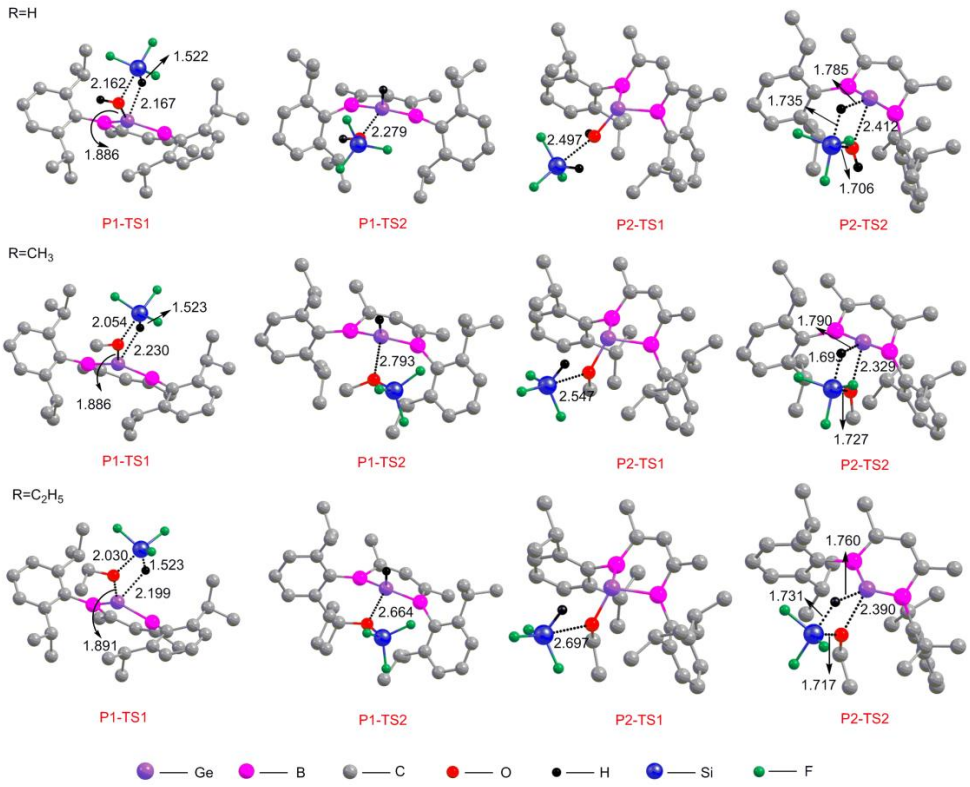

Figure 4B.7. Optimized geometries of all the transition states.

What is heartening to note is that the barrier for the slowest step over the entire cycle, employing **GeH-2**, is lower than the barrier for the slowest step for the state-of-the-art zinc based catalyst system, discussed earlier. This shows the potential of main group complexes to rival or be better than existing transition metal based systems in doing important chemical transformations such as the catalytic generation of dihydrogen molecule from water and alcohols.

4B.4 Conclusions

There is a need to investigate new catalytic systems that can do important chemical transformations, such as the catalytic generation of the dihydrogen molecule from water and alcohols. While the post-transition metal based system, [κ^3-Tptm]ZnH, has been shown to be an effective catalyst for this process under ambient conditions,[66] what the current study demonstrates, with full quantum chemical calculations with density functional theory (DFT), is that main group systems can be designed that would be significantly more effective at catalyzing the same reaction. Specifically, a new germanium complex has been proposed in the current work, with a coordinating bidentate diboryl ring system: HC{CMeArB}$_2$GeH (Ar = 2,6-^{i}Pr$_2$C$_6$H$_3$), denoted as **GeH-2**. For three different substrate cases: water, methanol and ethanol, it has been shown that the complete catalytic cycle employing **GeH-2** leads to barriers that are significantly lower than the barrier for the slowest step in the catalytic cycle involving the zinc based catalyst system. This has added significance, considering the need to substitute transition metal based systems with main group based alternatives.

As such, the current chapter reveals the potential of main group systems to catalyze important chemical transformations, and should, therefore, serve as a guide to researchers in this important area of research.

4B.5 References

(1) Collodi, G.; Wheeler, F. *Chem. Eng. Trans.* **2010**, *19*.

(2) Ford, P. C. *Acc. Chem. Res.* **1981**, *14*, 31-37.

(3) Laine, R. M.; Rinker, R. G.; Ford, P. C. *J. Am. Chem. Soc.* **1977**, *99*, 252-253.

(4) Kuriakose, N.; Kadam, S.; Vanka, K. *Inorg. Chem.* **2012**, *51*, 377-385.

(5) Kunkes, E. L.; Simonetti, D. A.; West, R. M.; Serrano-Ruiz, J. C.; Gärtner, C. A.; Dumesic, J. A. *Science* **2008**, *322*, 417-421.

(6) Huber, G. W.; Shabaker, J. W.; Dumesic, J. A. *Science* **2003**, *300*, 2075-2077.

(7) Navarro, R. M.; Peña, M. A.; Fierro, J. L. G. *Chem. Rev.* **2007**, *107*, 3952-3991.

(8) Palo, D. R.; Dagle, R. A.; Holladay, J. D. *Chem. Rev.* **2007**, *107*, 3992-4021.

(9) Mattos, L. V.; Jacobs, G.; Davis, B. H.; Noronha, F. B. *Chem. Rev.* **2012**, *112*, 4094-4123.

(10) Piscina, P. R. d. l.; Homs, N. *Chem. Soc. Rev.* **2008**, *37*, 2459-2467.

(11) Sun, J.; Wang, Y. *ACS Catal.* **2014**, *4*, 1078-1090.

(12) Buss, J. A.; Edouard, G. A.; Cheng, C.; Shi, J.; Agapie, T. *J. Am. Chem. Soc.* **2014**, *136*, 11272-11275.

(13) Rossin, A.; Rossi, A.; Peruzzini, M.; Zanobini, F. *ChemPlusChem* **2014**, *79*, 1316-1325.

(14) Baker, R. T.; Gordon, J. C.; Hamilton, C. W.; Henson, N. J.; Lin, P.-H.; Maguire, S.; Murugesu, M.; Scott, B. L.; Smythe, N. C. *J. Am. Chem. Soc.* **2012**, *134*, 5598-5609.

(15) Paul, A.; Musgrave, C. B. *Angew. Chem.* **2007**, *119*, 8301-8304.

(16) Denney, M. C.; Pons, V.; Hebden, T. J.; Heinekey, D. M.; Goldberg, K. I. *J. Am. Chem. Soc.* **2006**, *128*, 12048-12049.

(17) Johnson, T. C.; Morris, D. J.; Wills, M. *Chem. Soc. Rev.* **2010**, *39*, 81-88.

(18) Enthaler, S.; von Langermann, J.; Schmidt, T. *Energy Environ. Sci.* **2010**, *3*, 1207-1217.

(19) Grasemann, M.; Laurenczy, G. *Energy Environ. Sci.* **2012**, *5*, 8171-8181.

(20) Luo, X. L.; Crabtree, R. H. *J. Am. Chem. Soc.* **1989**, *111*, 2527-2535.

(21) Matarasso-Tchiroukhine, E. *J. Chem. Soc., Chem. Commun.* **1990**, 681-682.

(22) Schubert, U.; Lorenz, C. *Inorg. Chem.* **1997**, *36*, 1258-1259.

(23) Chang, S.; Scharrer, E.; Brookhart, M. *J. Mol. Catal. A: Chem.* **1998**, *130*, 107-119.

(24) Blackwell, J. M.; Foster, K. L.; Beck, V. H.; Piers, W. E. *J. Org. Chem.* **1999**, *64*, 4887-4892.

(25) Brunel, J. M. *Int. J. Hydrogen Energy* **2010**, *35*, 3401-3405.

(26) Sattler, W.; Parkin, G. *J. Am. Chem. Soc.* **2012**, *134*, 17462-17465.

(27) Crabtree, R. H. *Energy Environ. Sci.* **2008**, *1*, 134-138.

(28) Teichmann, D.; Arlt, W.; Wasserscheid, P.; Freymann, R. *Energy Environ. Sci.* **2011**, *4*, 2767-2773.

(29) Stephan, D. W.; Erker, G. *Angew. Chem. Int. Ed.* **2010**, *49*, 46-76.

(30) Chapman, A. M.; Haddow, M. F.; Wass, D. F. *J. Am. Chem. Soc.* **2011**, *133*, 18463-18478.

(31) Pal, A.; Vanka, K. *Chem. Commun.* **2011**, *47*, 11417-11419.

(32) Kuriakose, N.; Vanka, K. *Inorg. Chem.* **2013**, *52*, 4238-4243.

(33) Siemeling, U. *Aust. J. Chem.* **2011**, *64*, 1109-1112.

(34) Tokitoh, N.; Okazaki, R. *Coord. Chem. Rev.* **2000**, *210*, 251-277.

(35) Becerra, R.; Cannady, J. P.; Walsh, R. *J. Phys. Chem. A* **2002**, *106*, 4922.

(36) Wang, Y.; Ma, J. *J. Organomet. Chem.* **2009**, *694*, 2567-2575.

(37) Driess, M. *Nat. Chem.* **2012**, *4*, 525–526.

(38) Kuriakose, N.; Vanka, K. *Dalton Trans.* **2014**, *43*, 2194-2201.

(39) Yao, S.; Xiong, Y.; Driess, M. *Organometallics* **2011**, *30*, 1748-1767.

(40) Brown, Z. D.; Power, P. P. *Inorg. Chem.* **2013**, *52*, 6248-6259.

(41) Alberto, M. E.; Russo, N.; Sicilia, E. *Chem. -Eur. J.* **2013**, *19*, 7835-7846.

(42) Power, P. P. *Chem. Rec.* **2012**, *12*, 238-255.

(43) Eichler, B. E.; Power, P. P. *J. Am. Chem. Soc.* **2000**, *122*, 8785-8786.

(44) Rivard, E.; Power, P. P. *Dalton Trans.* **2008**, 4336-4343.

(45) Al-Rafia, S. M. I.; Malcolm, A. C.; Liew, S. K.; Ferguson, M. J.; Rivard, E. *J. Am. Chem. Soc.* **2011**, *133*, 777-779.

(46) Thimer, K. C.; Al-Rafia, S. M. I.; Ferguson, M. J.; McDonald, R.; Rivard, E. *Chem. Commun.* **2009**, 7119-7121.

(47) Inoue, S.; Driess, M. *Angew. Chem. Int. Ed.* **2011**, *50*, 5614-5615.

(48) Abraham, M. Y.; Wang, Y.; Xie, Y.; Wei, P.; Schaefer, H. F.; Schleyer, P. v. R.; Robinson, G. H. *J. Am. Chem. Soc.* **2011**, *133*, 8874-8876.

(49) Swarnakar, A. K.; McDonald, S. M.; Deutsch, K. C.; Choi, P.; Ferguson, M. J.; McDonald, R.; Rivard, E. *Inorg. Chem.* **2014**, *53*, 8662-8671.

(50) Rodriguez, R.; Gau, D.; Contie, Y.; Kato, T.; Saffon-Merceron, N.; Baceiredo, A. *Angew. Chem. Int. Ed.* **2011**, *50*, 11492-11495.

(51) Fang, H.; Ling, Z.; Brothers, P. J.; Fu, X. *Chem. Commun.* **2011**, *47*, 11677-11679.

(52) Choong, S. L.; Woodul, W. D.; Schenk, C.; Stasch, A.; Richards, A. F.; Jones, C. *Organometallics* **2011**, *30*, 5543-5550.

(53) Takagi, N.; Sakaki, S. *J. Am. Chem. Soc.* **2013**, *135*, 8955-8965.

(54) Hadlington, T. J.; Hermann, M.; Frenking, G.; Jones, C. *J. Am. Chem. Soc.* **2014**, *136*, 3028-3031.

(55) Pineda, L. W.; Jancik, V.; Starke, K.; Oswald, R. B.; Roesky, H. W. *Angew. Chem. Int. Ed.* **2006**, *45*, 2602-2605.

(56) Jana, A.; Ghoshal, D.; Roesky, H. W.; Objartel, I.; Schwab, G.; Stalke, D. *J. Am. Chem. Soc.* **2009**, *131*, 1288-1293.

(57) Jana, A.; Roesky, H. W.; Schulzke, C. *Dalton Trans.* **2010**, *39*, 132-138.

(58) Jana, A.; Tavcar, G.; Roesky, H. W.; John, M. *Dalton Trans.* **2010**, *39*, 9487-9489.

(59) Mandal, S. K.; Roesky, H. W. *Acc. Chem. Res.* **2012**, *45*, 298-307.

(60) Tan, S. T.; Kee, J. W.; Fan, W. Y. *Organometallics* **2011**, *30*, 4008-4013.

(61) Ison, E. A.; Corbin, R. A.; Abu-Omar, M. M. *J. Am. Chem. Soc.* **2005**, *127*, 11938-11939.

(62) Corbin, R. A.; Ison, E. A.; Abu-Omar, M. M. *Dalton Trans.* **2009**, 2850-2855.

(63) Choi, E.; Lee, C.; Na, Y.; Chang, S. *Organic Letters* **2002**, *4*, 2369-2371.

(64) Chauhan, B. P. S.; Sarkar, A.; Chauhan, M.; Roka, A. *Appl. Organomet. Chem.* **2009**, *23*, 385-390.

(65) John, J.; Gravel, E.; Hagège, A.; Li, H.; Gacoin, T.; Doris, E. *Angew. Chem. Int. Ed.* **2011**, *50*, 7533-7536.

(66) Deshmukh, M. M.; Sakaki, S. *Inorg. Chem.* **2014**, *53*, 8485-8493.

(67) Ahlrichs, R.; Bär, M.; Häser, M.; Horn, H.; Kölmel, C. *Chem. Phys. Lett.* **1989**, *162*, 165-169.

(68) Ansgar, S.; Christian, H.; Reinhart, A. *J. Chem. Phys.* **1994**, *100*, 5829-5835.

(69) Perdew, J. P.; Wang, Y. *Phys. Rev. B* **1992**, *45*, 13244-13249.

(70) Perdew, J. P.; Burke, K.; Ernzerhof, M. *Phys. Rev. Lett.* **1996**, *77*, 3865-3868.

(71) Grimme, S.; Antony, J.; Ehrlich, S.; Krieg, H. *J. Chem. Phys.* **2010**, *132*, 154104-19.

(72) Grimme, S. *J. Comput. Chem.* **2004**, *25*, 1463-1473.

(73) Grimme, S. *J. Comput. Chem.* **2006**, *27*, 1787-1799.

(74) Klamt, A.; Schuurmann, G. *J. Chem. Soc., Perkin Trans. 2* **1993**, 799-805.

(75) Eichkorn, K.; Treutler, O.; Öhm, H.; Häser, M.; Ahlrichs, R. *Chem. Phys. Lett.* **1995**, *240*, 283-290.

(76) Marek, S.; Annika, H.; Reinhart, A. *J. Chem. Phys.* **2003**, *118*, 9136-9148.

(77) Fukui, K. *Acc. Chem. Res.* **1981**, *14*, 363-368.

(78) Frisch, M. J. T., G. W.; Schlegel, H. B.; Scuseria, G. E.;; Robb, M. A. C., J. R.; Scalmani, G.; Barone, V.; Mennucci, B.;; Petersson, G. A. N., H.; Caricato, M.; Li, X.; Hratchian, H. P.;; Izmaylov, A. F. B., J.; Zheng, G.; Sonnenberg, J. L.; Hada, M.;; Ehara, M. T., K.; Fukuda, R.; Hasegawa, J.; Ishida, M.; Nakajima,; T.; Honda, Y. K., O.; Nakai, H.; Vreven, T.; Montgomery, J. A., Jr.;; Peralta, J. E. O., F.; Bearpark, M.; Heyd, J. J.; Brothers, E.; Kudin,; K. N.; Staroverov, V. N. K., R.; Normand, J.; Raghavachari, K.;; Rendell, A. B., J. C.; Iyengar, S. S.; Tomasi, J.; Cossi, M.; Rega,; N.; Millam, J. M. K., M.; Knox, J. E.; Cross, J. B.; Bakken, V.;; Adamo, C. J., J.; Gomperts, R.; Stratmann, R. E.; Yazyev, O.;; Austin, A. J. C., R.; Pomelli, C.; Ochterski, J. W.; Martin, R. L.;; Morokuma, K. Z., V. G.; Voth, G. A.; Salvador, P.;; Dannenberg, J. J. D., S.; Daniels, A. D.; Farkas, Ö.;; Foresman, J. B. O., J. V.; Cioslowski, J.; Fox, D. J., Gaussian 09, revision. B.01; *Gaussian, Inc., Wallingford, CT, 2009*.

(79) Protchenko, A. V.; Birjkumar, K. H.; Dange, D.; Schwarz, A. D.; Vidovic, D.; Jones, C.; Kaltsoyannis, N.; Mountford, P.; Aldridge, S. *J. Am. Chem. Soc.* **2012**, *134*, 6500-6503.

(80) Protchenko, A. V.; Dange, D.; Harmer, J. R.; Tang, C. Y.; Schwarz, A. D.; Kelly, M. J.; Phillips, N.; Tirfoin, R.; Birjkumar, K. H.; Jones, C.; Kaltsoyannis, N.; Mountford, P.; Aldridge, S. *Nat. Chem.* **2014**, *6*, 315-319.

(81) Segawa, Y.; Yamashita, M.; Nozaki, K. *Science* **2006**, *314*, 113-115.

(82) Protchenko, A. V.; Schwarz, A. D.; Blake, M. P.; Jones, C.; Kaltsoyannis, N.; Mountford, P.; Aldridge, S. *Angew. Chem. Int. Ed.* **2013**, *52*, 568-571.

Chapter 5

Small Molecule Activation by Acyclic Silylene Complexes

Abstract

Recently synthesized acyclic silylene complexes have the potential to rival transition metal complexes in doing single site small molecule activation, which is significant because of the need to find cheap and green alternatives to transition metal complexes for this important class of reactions. However, a full quantum chemical investigation with density functional theory, demonstrates that undesired side reactions would be competitive in these systems during small molecule activation. The current chapter, in addition to shedding light on this problem, also provides solutions for how the undesired side reactions during small molecule activation can be avoided.

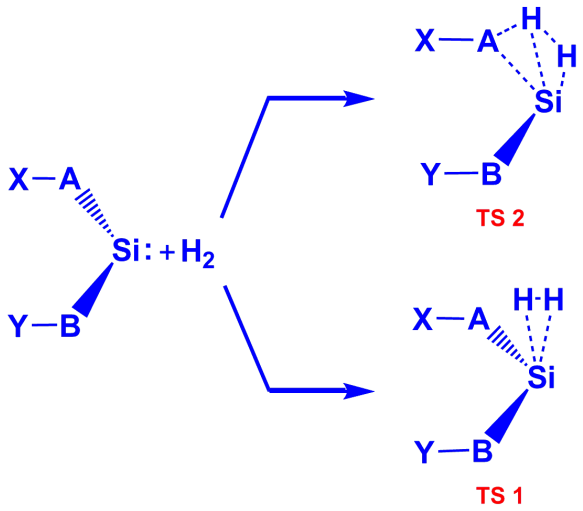

5.1 Introduction

The activation or cleavage of bonds in small molecules: small molecule activation, is an important problem, with relevance in biological processes,[1-3] as well as to important new areas of research such as hydrogen storage.[4-6] Transition metal complex systems have, by and large, held a monopoly in this field.[1,7,8] Various new strategies involving transition metal complexes have recently been developed in order to activate the C-H, N-H and O-H bonds in small molecules.[9-11]

While transition metal complexes have been highly successful at small molecule activation, methods that employ systems that move away from transition metals hold special interest, because main-group systems have the advantage of being cheaper and, often, greener than transition metal systems. In this regard, recent developments in carbene chemistry[12-15] are noteworthy, because carbenes, like transition metal systems, have the dual advantage of a lone pair that can donate electron density, as well as a vacant orbital than can accept electron density. These properties of carbenes have led to them being successfully employed for the activation of H-H and C-H bonds in small molecules.[12,13,16]

Like carbenes, higher analogues such as silylenes can also play a prominent role in activation processes. As discussed in the in the introduction, synthesis of many stable silylene and metallylenes have been reported in the literature.[17-23] The chemical properties of metallylene are important because of their similarities, as well as their differences when compared to carbenes. The reported systems include isolable cyclic silylenes,[17,18,21,24-26] and functionalized silylenes with increased coordination number at the silicon atom.[27-32] Some of these systems are reported to have implications in small molecules activation processes.[33-39]

However, reports on acyclic dicoordinate silylenes have been rare, as the isolation of such compounds as stable monomeric species is difficult. Of the acyclic silylenes synthesized and investigated experimentally,[20,40-46] two silylenes are of particular interest. They are (i) a stable mixed (amido) boryl silylene (**I**), $Si\{B(NDippCH)_2\}\{N(SiMe_3)Dipp\}$, (Dipp = 2,6-$^{i}Pr_2C_6H_3$), synthesized by Protchenko *et al*.[47] and (ii) the silyl coordinated silylene[48] (**II**), $Si\{Si(SiMe_3)_3\}\{N(SiMe_3)Dipp\}$, also reported by the same group. These two acyclic

silylenes are interesting in that both have been reported to split H_2 in a facile manner at room temperature to yield the silane, $SiR_1R_2H_2$, thus providing two of the few known examples of single site small molecule activation done without employing transition metal complexes. The structures of the two silylenes are shown in Figure 5.1 below.

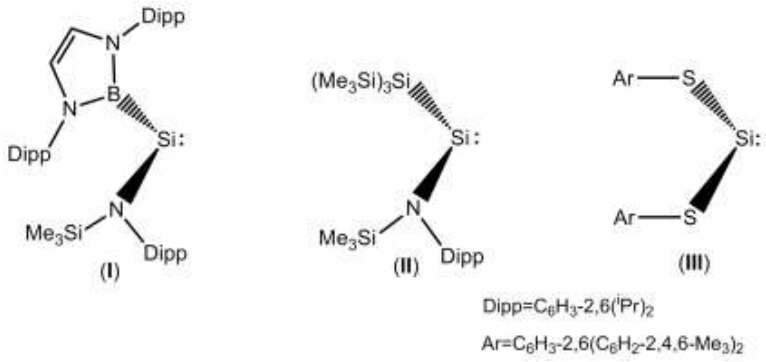

Figure 5.1. The structures of the three recently synthesized stable acyclic silylenes.

This result gives rise to the important question of why the other acyclic silylenes, such as the two thiolate sulphur groups coordinated silylene, such as $Si\{S(C_6H_3\text{-}2,6(C_6H_2\text{-}2,4,6\text{-}Me_3)_2)\}_2$ (**III**, the structure also shown in Figure 5.1), have not been reported to activate dihydrogen, or show evidence of other types of small molecule activation. The reason for this could be the possibility of competitive side reactions occurring during small molecule activation by the silylene. In the case of the thiolate coordinated silylene, **III**, for instance, the presence of the thiolate group is necessary in order to provide a strong σ donor coordination to the silicon center and also helps to decrease the HOMO-LUMO gap.[20,49] However, our computational studies reveal that the HOMO and the LUMO of the molecule are smeared over the silicon and the two adjoining sulphur atoms (see Figure 5.2 below). This suggests that small molecule activation, such as H_2 splitting, could occur as a cooperative process between the silicon and an adjoining sulphur atom, since it is well known[50,51] that small molecule activation can occur as a heterolytic process of splitting, with the LUMO accepting electron density and the HOMO providing electron density to the small molecule being activated. Since the LUMO for the cases of the silylene **I** and **II** are shown to be localized on the silicon atom, the possibility of a cooperative process involving silicon and an adjoining atom are less in these two cases, which would provide the explanation as to why only these two acyclic silylenes have been reported

to show single site splitting of H_2.The HOMO and the LUMO for **I**, **II** and **III** are shown in Figure 5.2 below. However, since the HOMO in these two cases is also smeared out over three atoms (see Figure 5.2), the possibility of cooperativity cannot be entirely ruled out even here. Hence, it is quite possible that one could have a cooperative pathway for small molecule activation that would compete with the desired small molecule activation only at the silicon center. Such a competing pathway would decompose the silylene, and if competitive, would significantly reduce the effectiveness of the silylene. Hence, the propensity of silylenes to undergo such undesired side reactions needs to be thoroughly studied and understood.

This is the focus of the computational investigation discussed in the chapter. A careful study of the competing possibilities: desired and undesired reactions of silylenes with small molecules, has been done. To this end, full quantum mechanical (QM) calculations using density functional theory (DFT) have been employed, for investigating the mixed (amido) boryl silylene, **I**, for the silyl silylene (**II** in Figure 5.1) and for the silylene with the thiolate coordinated sulphur groups (**III** in Figure 5.1). The results, discussed below, provide important insights into the different competitive possibilities that exist for dihydrogen activation by the different silylene systems. Possible means by which the undesired side reactions can be avoided has also been discussed.

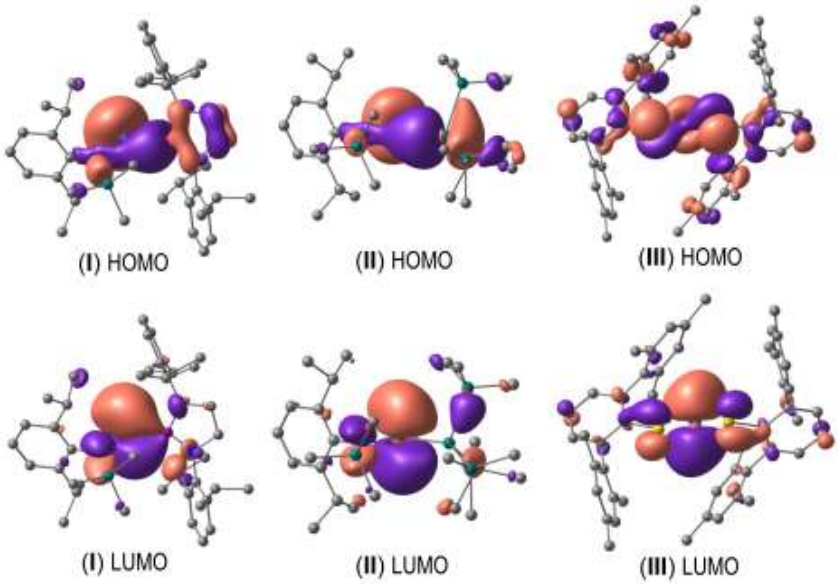

Figure 5.2. The HOMO and the LUMO for the silylenes **I**, **II** and **III**.

5.2 Computational Details

All the calculations have been done with Turbomole 6.4,[52] using the TZVP basis set[53] and the PBE functional.[54,55] Dispersion corrections[56-58] have been included in all the geometry optimization calculations. For the dispersion correction calculation, a modified empirical dispersion correction, DFT-D3 proposed by Grimme[56-58] has been employed. Solvent effects have been incorporated through single point calculations with COSMO,[59] with benzene (epsilon = 2.30) as the solvent, for the case of all the reactions with the silylene **I**, with hexane (epsilon = 1.88) as the solvent for the reactions involving silylene **II,** and with toluene (epsilon = 2.38) as the solvent, for the case of all the reactions with silylene **III**. The resolution of identity (RI),[60] along with the multipole accelerated resolution of identity (marij)[61] approximations have been employed for an accurate and efficient treatment of the electronic Coulomb term in the DFT calculations. The values reported are ΔG values, with zero point energy, internal energy and entropic contributions included through frequency calculations on the optimized minima and transition state structures, with the temperature taken to be 298.15 K. All the obtained transition states were confirmed to have only a single negative frequency corresponding to the correct normal mode. In addition, intrinsic reaction coordinate (IRC)[62] calculations were done with all the transition states in order to further confirm that they were the correct transition states, yielding the correct reactant and product structures.

In order to obtain the HOMO and the LUMO for the silylenes **I**, **II** and **III**, the geometries of the silylenes were optimized with Gaussian 09.[63] The TZVP basis set and the PBE functional have been employed in these calculations.

5.3 Results and Discussion

5.3.1 Competitive pathways for dihydrogen activation: Out of the three silylene **I**, **II** and **III**, the one which is most likely to have a competitive cooperative pathway during small molecule activation is **III**, having thiolate groups coordinated to the silicon center. Shown in Scheme 5.1 are the energy profiles for the reaction of **III** with H_2. The desired reaction is the formation of the tetravalent $Si(R)_2H_2$ product (**III**-H_2), i.e., the single site activation of the dihydrogen molecule at the silicon center. As

Scheme 5.1 indicates, the path leading to the splitting of H_2 and the formation of **III**-H_2 has a free energy barrier of 38.4 kcal/mol corresponding to the transition state TS A (see Scheme 5.1). The undesired, competing pathway to this would lead to the decomposition of the silylene, forming the products HSi{S(C_6H_3-2,6(C_6H_2-2,4,6-Me_3)$_2$)} and HS(C_6H_3-2,6(C_6H_2-2,4,6-Me_3)$_2$). The four-membered transition state for this route is denoted as TS B in Scheme 5.1. The calculations show that this path is significantly more favored, having a barrier of 32.0 kcal/mol. This difference of 6.4 kcal/mol between the two pathways suggests that the addition of H_2 to the system would result in the decomposition of the silylene **III**, instead of into the preferred formation of the silylene dihydrogen product. It should be noted that the product of the decomposition reaction for **III** is endergonic by 7.6 kcal/mol (see Scheme 5.1). However, this does not imply that the products can reversibly recombine to give the original silylene **III**. This is because the product of the decomposition of **III** is again a silylene: an "Si-H" silylene species, which would be expected to be quite reactive in solution. This new species can form other stable products with high exergonicity, by reacting with other moieties present in the reaction mixture. Hence, the calculations indicate that the decomposition of the silylene **III** in the presence of dihydrogen is a very likely possibility. This provides the explanation as to why Rekken *et al*. did not observe the formation of the $Si(R)_2H_2$ species when they reacted H_2 with **III**[20]: even if the reaction vessel were to be heated to higher temperatures, the much higher probability of obtaining the decomposed products over $Si(R)_2H_2$ would make $Si(R)_2H_2$ the significantly minor product during the reaction.

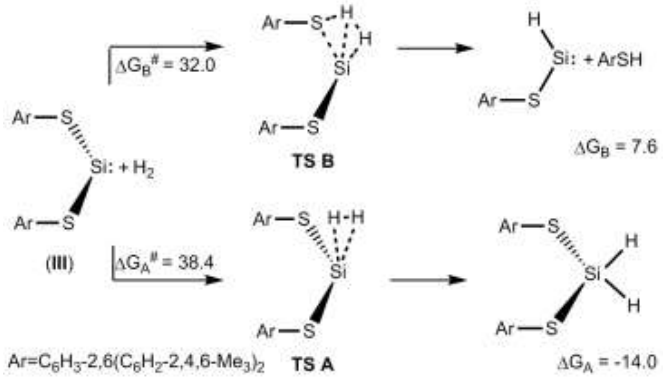

Scheme 5.1. The free energy profiles for the reaction with the silylene, **III**, with H_2; all values are in kcal/mol.

On the other hand, as Schemes 5.2 and 5.3 indicate, the competition between

the desired single site activation pathway over the cooperative, decomposition pathway is in favor of the desired route for both **I** and **II**. As had been explained in the Introduction, this is because of the localization of the LUMO over the silicon center in **I** and **II**. Hence the successful single site splitting of H_2 that has been experimentally observed for both these silylene cases. However, it is to be noted that the decomposition pathway is very competitive for both case **I** (the gap between the favored and disfavored routes is only 1.0 kcal/mol), and for case **II** (gap: 1.5 kcal/mol). This suggests that for all the stable acyclic silylenes that have been successfully synthesized to date, it is important to consider the possibility of unwanted side reactions that can occur.

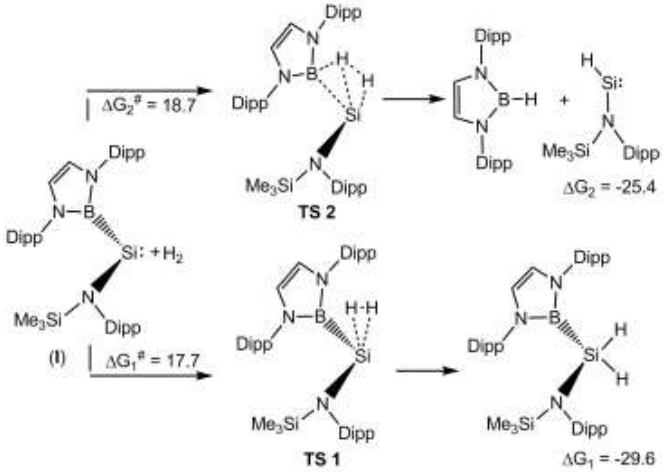

Scheme 5.2. The free energy profiles for the reaction of the mixed (amido) boryl silylene, **I** with H_2; all values are in kcal/mol.

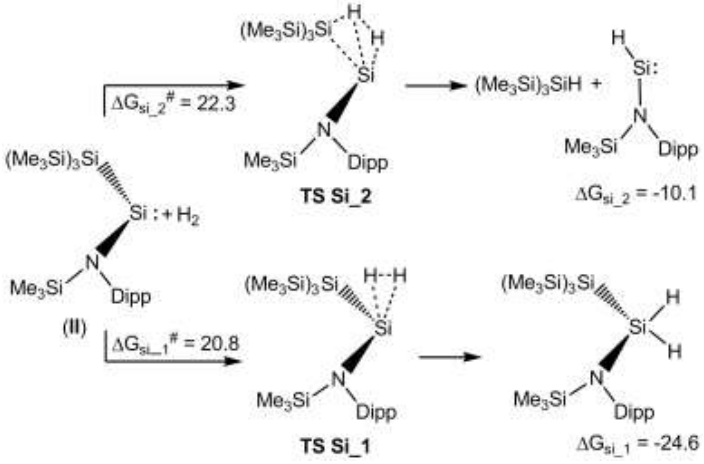

Scheme 5.3. The free energy profiles for the reaction with the silylene, **II**, with H_2; all values are in kcal/mol.

In a computational study, Wang *et al*.[64] predicted that the acyclic silylenes that have a large obtuse angle at the central silicon atom can imitate transition metals in the activation of small molecules (the angle in question is the one made with the binding atoms of the coordinating ligands: for the case **III**, for instance, the angle is the S-Si-S angle). This emphasises the importance of geometry, especially the angle at the silicon atom, on the reaction behaviour of silylenes. The analysis of the effect of this parameter on both the single site and dissociation pathways provides further insight into this. The angle obtained for the silylenes **II**, **I**, and **III** are 114.6°,109.6° and 90.4° respectively. As shown in Table 5.1, the barrier gap between the decomposition and the single site pathways for case **II**, having a large Si-Si-N obtuse angle, is 1.5 kcal/mol, and it decreases for the case of silylene **I** to 1.0 kcal/mol, where the B-Si-N angle is 109.6^0. In other words, the reduction in the angle at the silicon center leads to the dissociative pathway becoming more competitive with the single site pathway. Indeed, when the angle becomes even smaller, as in the case of silylene **III** having an S-Si-S obtuse angle of 90.4^0, it is seen that the preference of the pathways is reversed: the dissociation pathway is now favoured over the single site pathway significantly, by 6.4 kcal/mol. Therefore, the results indicate that the preference of the silylene for the single site or the decomposition pathway depends on the angle at the central silicon.

Table 5.1. Correlation between the angle at the central silicon and the barrier gap: the difference in the barriers between the decomposition and the single site pathways.

	Angle at Si	Barrier Gap (kcal/mol)
Silylene **II**	Si-Si-N = 114.6°	1.5
Silylene **I**	B-Si-N = 109.6°	1.0
Silylene **III**	S-Si-S = 90.4°	-6.4

The angle at the central silicon is also correlated to the absolute values of the activation barriers. For the silylenes **II** and **I**, where the angles are 114.6°and 109.6° respectively, the barriers, which are in the range of 17.0-23.0 kcal/mol for the single site and the dissociation pathways (see Schemes 5.2 and 5.3), are lower in comparison to silylene **III**, where the angle is smaller: 90.4°, and the barriers are higher: 30.2 kcal/mol for the dissociation pathway and 38.4 kcal/mol for the single site activation route. We have also calculated the energy barriers for both the single site and the

dissociation pathways without adding dispersion effects during the geometry optimization, for all the three silylene cases. The comparison of these calculated values with the dispersion corrected values are shown in Table 5.2. As the results show, in the absence of dispersion correction, the dissociation pathway for silylene **II** becomes favourable over the single site pathway, by 0.2 kcal/mol. For the other two silylenes, **I** and **III**, the favourable pathways are consistent with the previous dispersion corrected calculations, but the barrier gap in the case of silylene **I** is 2.3 kcal/mol, as opposed to 1.0 kcal/mol after including dispersion effects. In other words, there is a significant change in the trend as well as in the barrier height differences when dispersion effects are considered. This indicates the importance of including dispersion corrections in the calculations when studying such complexes. This has also been noted in a recent study by Rekken *et al*. on the acyclic, monomeric tetrylene dichalcogenolates of formula $M(ChAr)_2$ (M = Si, Ge, Sn, Pb; Ch = O, S, or Se; Ar = bulky m-terphenyl ligand), where dispersion forces were found to play an important role in stabilizing the acute inter-ligand angles.[46]

Table 5.2. A comparison of the energy barriers for the silylene cases **I**, **II**, and **III** in the presence and absence of the dispersion correction; all values are in kcal/mol.

	Transition state	Barrier without dispersion	Barrier with dispersion
Silylene **I**	TS 1	18.5	17.7
	TS 2	20.8	18.7
Silylene **II**	TS_si_1	20.6	20.8
	TS_si_2	20.4	22.3
Silylene **III**	TS A	39.8	38.4
	TS B	33.5	32.0

5.3.2 Further reactions of the "Si-H" silylene: The discussion of the calculations in the previous section indicates that the formation of a silylene species with a hydride: an "Si-H" silylene, is quite a feasible possibility, especially when the silylene **III** is reacted with H_2. Now, since this, too, is a silylene, it may also be expected to be quite reactive in solution. The most likely possibility is that such an Si-H silylene species would dimerize, since the steric bulk protection provided by the thiolate ligand

$S(C_6H_3\text{-}2,6(C_6H_2\text{-}2,4,6\text{-}Me_3)_2)$ has been removed in this species. As shown in Scheme 5.4 below, such a process is seen to be favorable, being exergonic by 10.7 kcal/mol. This is seen to be a barrierless process. A linear transit calculation that was conducted by varying the Si-Si bond length between the two Si-H silylenes showed that the dimerization took place without any saddle point along the reaction coordinate. The graph for this is shown in Figure 5.3.

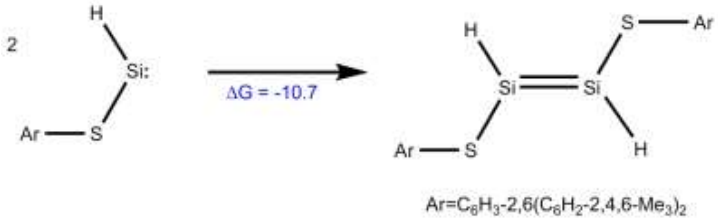

Scheme 5.4. The formation of the silylene dimer; the value reported is in kcal/mol.

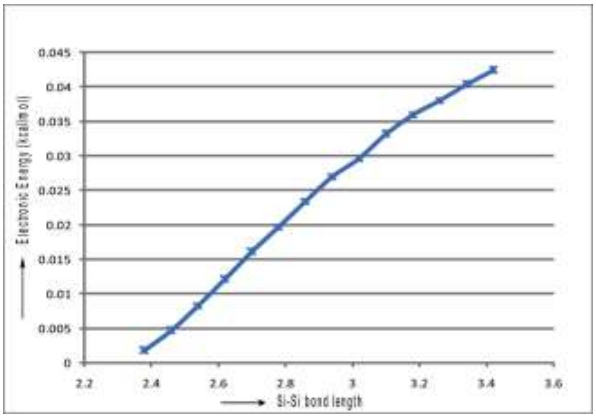

Figure 5.3. A linear transit calculation, showing the drop in energy as two Si-H silylenes approach each other; the reaction coordinate chosen is the Si-Si bond length, the energy values, in kcal/mol, are the ΔE values.

However, since the Si-H silylene is not the original species during the reaction, it may be that its concentration may build up slowly during the reaction of **III** with H_2. In such a scenario, the dimerization may not be the most likely possibility. A competitive reaction in this case would be the reaction of H_2, with the Si-H silylene being converted to the silane, "SiH_3" (see Scheme 5.5 below). Such a reaction has been found to be exergonic by 23.3 kcal/mol (with a barrier of 24.5 kcal/mol), indicating its high favorability: it is 12.6 kcal/mol more exergonic than the dimerization process. Further calculations, shown in Scheme 5.6, indicate that such a

species is likely to be stable and unlikely to take further part in reactions, such as the transfer of hydrogens to **III**, the barrier for which was found to be high (51.1 kcal/mol, see Scheme 5.6).

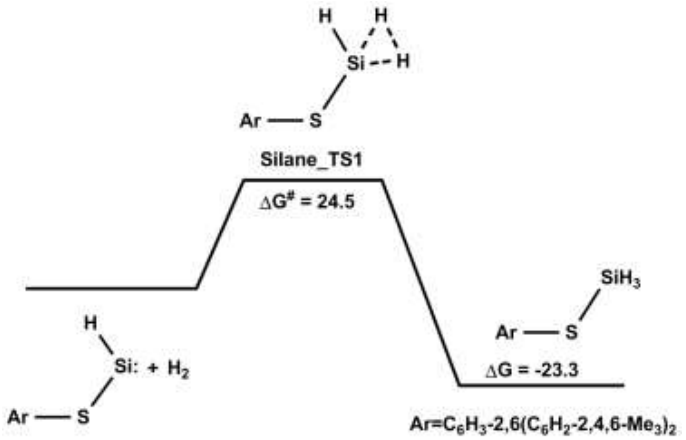

Scheme 5.5 The reaction for the formation of the silane; the value reported is in kcal/mol.

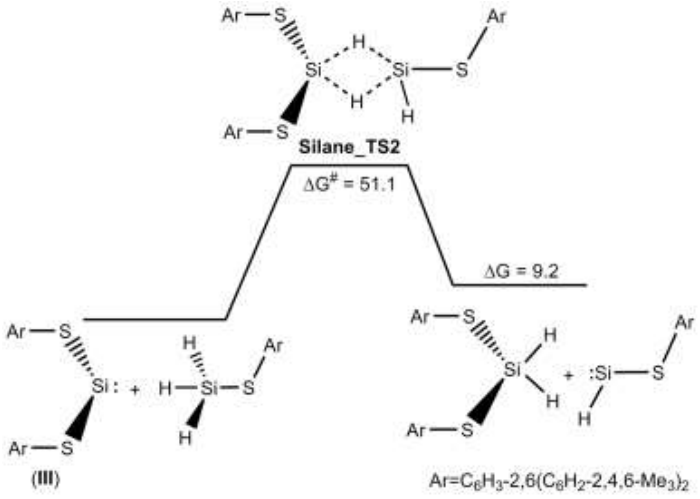

Scheme 5.6 The free energy profile obtained for the reaction of **III** with silane; all values are in kcal/mol.

5.3.3 Intramolecular ring formation for the silylenes: It may be possible for the silylenes to decompose even in the absence of dihydrogen, through intramolecular interactions between the silicon center and the coordinating functional groups. Scheme 5.7 shows a possibility that exists for the formation of a Si-C bond for case **III** by the reaction of a methyl group on the thiolate ligand with the silicon center, leading to the stable product **III**_ring_pdt (see Scheme 5.7). This reaction has a

barrier of 38.0 kcal/mol, which suggests that it is less likely by 6.0 kcal/mol than the decomposition reaction in the presence of H_2, discussed above. However, the unimolecular decomposition pathway involving the thiolate ligand processes would become feasible at higher temperatures, as has been observed experimentally for the cases **I**[47] and **II**.[48] In the case of silylenes I and II, the isopropyl C-H bond activation at the silicon leads to the corresponding ring product, as shown in the Schemes 5.8-5.10.

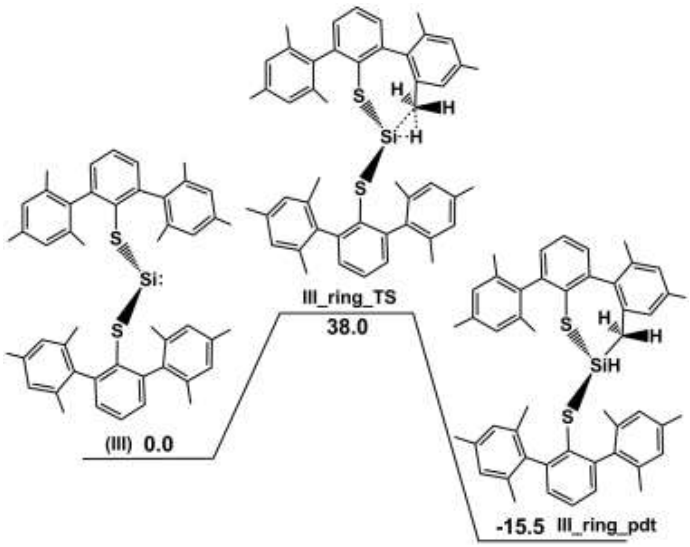

Scheme 5.7 The free energy profile obtained for the ring formation reaction of **III** with $–CH_3$ group on the ligand; all values are in kcal/mol.

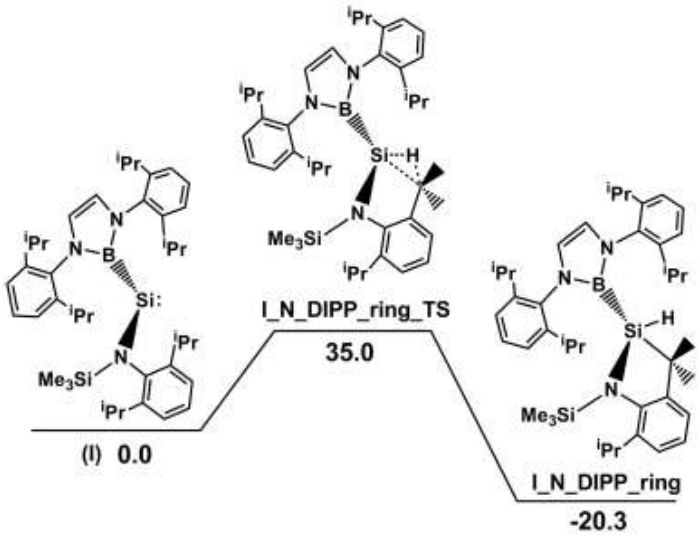

Scheme 5.8 The free energy profile obtained for the ring formation reaction of **I** by the amido Dipp isopropyl C-H bond activation; all values are in kcal/mol.

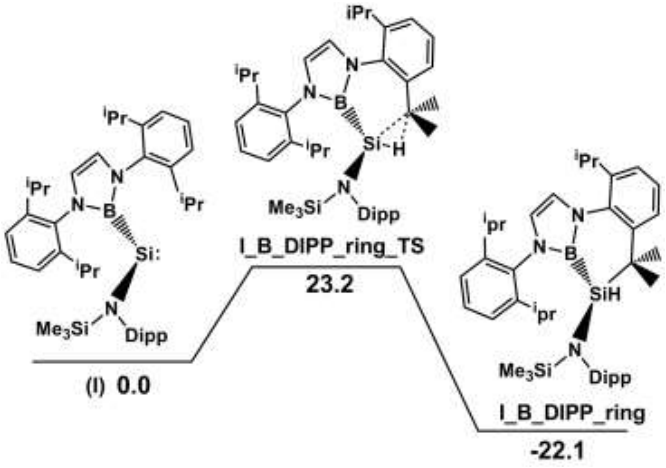

Scheme 5.9 The free energy profile obtained for the ring formation reaction of **I** by the boryl Dipp isopropyl C-H bond activation; all values are in kcal/mol.

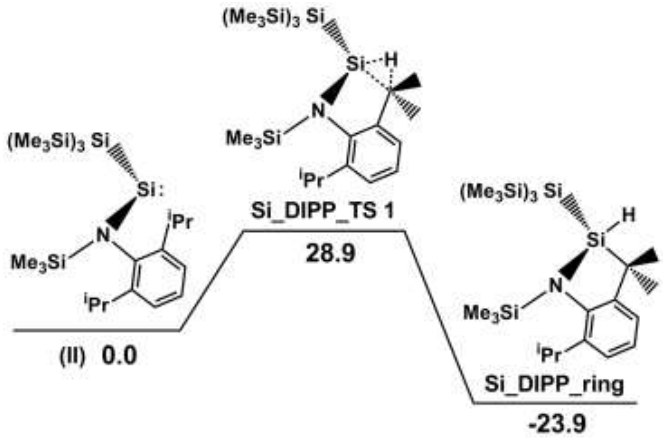

Scheme 5.10 The free energy profile obtained for the ring formation reaction of **II** by the amido Dipp isopropyl C-H bond activation; all values are in kcal/mol.

The transition state structures and the barriers for the silylenes **I**, **II** and **III** leading to the corresponding ring product have been shown in Figure 5.4. In the case of silylene **I**, there are two possibilities of such activation, one at the Dipp isopropyl C-H bond in the boryl ligand and another at the Dipp isopropyl C-H bond in the amido ligand. The barrier for the intramolecular Dipp isopropyl C-H bond activation at the amido ligand involves a higher barrier of 35.0 kcal/mol when compared to the corresponding Dipp isopropyl C-H activation at the boryl ligand, which is 23.2 kcal/mol. This significant preference for the Dipp isopropyl C-H activation at the boryl ligand explains why, in the absence of H_2 molecule, only the ring formation by the boryl Dipp isopropyl C-H bond activation has been observed experimentally.[47]

Similarly, for silylene **II**, the Dipp isopropyl C-H bond activation at the amido ligand leads to a ring system which was found to involve a barrier of 28.9 kcal/mol, which explains the requirement of a higher temperature than the silylene **I** boryl C-H activation for the isolation of the ring product, as shown by Aldridge and co-workers.[48]

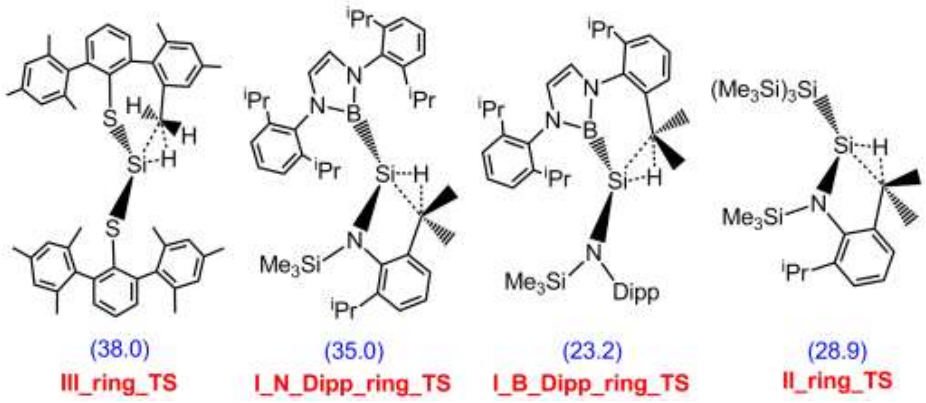

Figure 5.4 The transition state structures and the barriers for the silylenes **I**, **II** and **III** for the intramolecular reaction leading to the ring product.

5.3.4 Solution to the problem of side reactions: As mentioned earlier, the single site activation of small molecules at the silicon center is a highly desirable reaction, because of the potential of replacing transition metal complexes with inexpensive and green silylenes. It is therefore necessary to explore possibilities of eliminating the decomposition pathway in favor of the single site pathway. One possible solution may lie in the use of hydrogenating agents in place of H_2. The reason for this is that the barrier to the single site pathway can be reduced if the ring size of the transition state can be increased from the constraining three-membered ring in the case of the transition state TS 1. A perusal of the optimized TS 1 structure (see Figure 5.5 below), shows that the H-Si-H angle in the transition state is only 39.2 degrees, while the H-Si-H angle in the stable product from the reaction, $SiR_1R_2H_2$, is 105.3 degrees: 66.1 degrees more than in TS 1. Therefore, any reaction where the H-Si-H angle can be increased in the transition state would be likely to reduce the barrier, and thus make it the dominant pathway over the alternate decomposition route. Since employing ammonia borane (AB) as the hydrogenating agent in place of H_2 would increase the ring size of the transition state from three to five, this could serve to make the single

site pathway the dominant one. AB, it is to be noted, has been effectively employed as a hydrogenating agent in several reactions.[4,65]

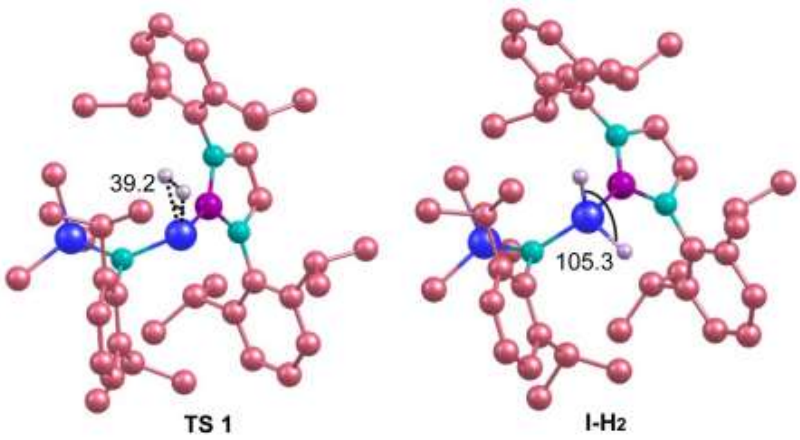

Figure 5.5 The comparison of the H-Si-H angles in **TS 1** and **I-H_2**; H atoms have been omitted for the purpose of clarity.

As shown in Scheme 5.11, the reaction between AB and **III** leads to a significant change in the nature of the hydrogenation process: now the addition of the hydrogens to the single site – to the silicon center – is more favored over the decomposition pathway: while the barrier involving Si-S cooperativity is now 26.4 kcal/mol, the barrier for the desired single site reaction of silicon with AB has a barrier of 25.7 kcal/mol. This indicates that if AB were to be employed in place of H_2, one would tilt the competition between single site H_2 activation and decomposition in favor of the desired single site process. What is also interesting is that for the **I** and **II** cases, this would lead to a significant difference between the single site and the decomposition processes: the desired single site process would become much more favored (difference of 20.5 kcal/mol in case of **I**, 19.7 kcal/mol in case of **II**) in both the cases, essentially eliminating the possibility of the decomposition pathway for these systems (see scheme 5.12 and scheme 5.13). The calculations therefore suggest that, for silylenes that cannot do single site activation of small molecules such as H_2, one can obtain the same final product by employing alternative reagents, such as hydrogenating agents instead of H_2, as discussed above.

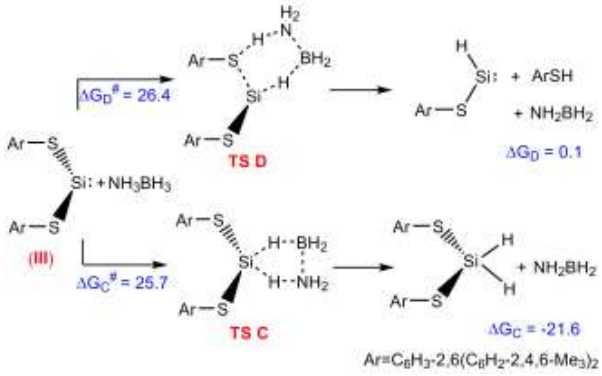

Scheme 5.11 The free energy profile for the hydrogenation of the silylene, **III**, by NH_3BH_3; all values are in kcal/mol.

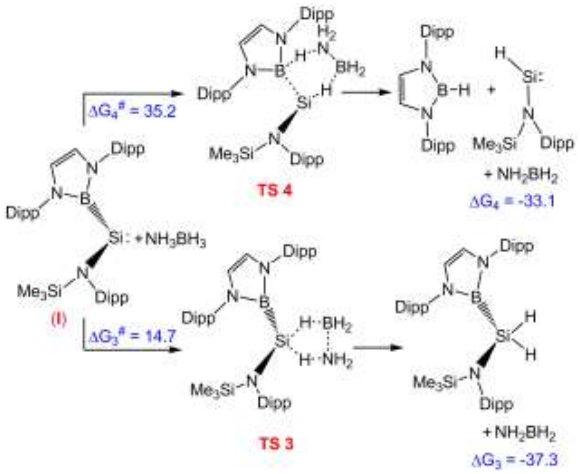

Scheme 5.12 The free energy profile for the hydrogenation of the silylene, **I**, by NH_3BH_3; all values are in kcal/mol.

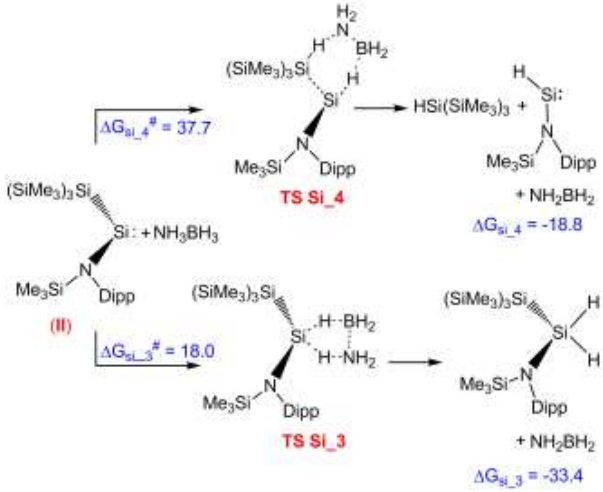

Scheme 5.13 The free energy profile for the hydrogenation of the silylene, **II**, by NH_3BH_3; all values are in kcal/mol.

5.4 Conclusions

Full quantum mechanical calculations indicate that some recently synthesized stable acyclic silylenes[47,48] can do single site small molecule activation. However, other compounds of this family fail to display single site activation[20] because of undesired, competing side reactions, leading to the decomposition of the silylenes. The competitive nature of the decomposition pathways has been shown for three acyclic silylenes that have been recently synthesized: the "B-Si-N" silylene (**I**),[47] the "Si-Si-N" silylene (**II**)[48] and the "S-Si-S" silylene (**III**).[20] The subsequent reaction possibilities for the decomposed silylenes have also been studied. Moreover, the possibility of other decomposition pathways such as the experimentally observed[47,48] intramolecular C-H activation by the central silylene has also been investigated for the three acyclic silylenes. It has been shown that for silylenes that cannot display single site small molecule activation due to the preference for competing side reactions, the desired final product can still be obtained by employing other reagents, such as hydrogenating agents in place of dihydrogen.

The current work should therefore serve as a guide to experimentalists for the design of effective main-group systems such as silylenes for single site small molecule activation.

5.5 References

(1) Shaver, M. P.; Fryzuk, M. D. *Adv*. *Synth*. *Catal*. **2003**, *345*, 1061-1076.

(2) Fryzuk, M. D.; Johnson, S. A. *Coord*. *Chem*. *Rev*. **2000**, *200*, 379-409.

(3) MacKay, B. A.; Fryzuk, M. D. *Chem*. *Rev*. **2004**, *104*, 385-402.

(4) Staubitz, A.; Robertson, A. P. M.; Manners, I. *Chem*. *Rev*. **2010**, *110*, 4079-4124.

(5) Staubitz, A.; Robertson, A. P. M.; Sloan, M. E.; Manners, I. *Chem*. *Rev*. **2010**, *110*, 4023-4078.

(6) Power, P. P. *Chem*. *Rec*. **2012**, *12*, 238-255.

(7) Blaquiere, N.; Diallo-Garcia, S.; Gorelsky, S. I.; Black, D. A.; Fagnou, K. *J*. *Am*. *Chem*. *Soc*. **2008**, *130*, 14034-14035.

(8) Paul, A.; Musgrave, C. B. *Angew*. *Chem*. **2007**, *119*, 8301-8304.

(9) Park, Y. J.; Park, J.-W.; Jun, C.-H. *Acc*. *Chem*. *Res*. **2008**, *41*, 222-234.

(10) Khaskin, E.; Iron, M. A.; Shimon, L. J. W.; Zhang, J.; Milstein, D. *J*. *Am*. *Chem*. *Soc*. **2010**, *132*, 8542-8543.

(11) Kohl, S. W.; Weiner, L.; Schwartsburd, L.; Konstantinovski, L.; Shimon, L. J. W.; Ben-David, Y.; Iron, M. A.; Milstein, D. *Science* **2009**, *324*, 74-77.

(12) Frey, G. D.; Lavallo, V.; Donnadieu, B.; Schoeller, W. W.; Bertrand, G. *Science* **2007**, *316*, 439-441.

(13) Martin, D.; Soleilhavoup, M.; Bertrand, G. *Chem*. *Sci*. **2011**, *2*, 389-399.

(14) Liddle, S. T.; Edworthy, I. S.; Arnold, P. L. *Chem*. *Soc*. *Rev*. **2007**, *36*, 1732-1744.

(15) Liu, W.; Gust, R. *Chem*. *Soc*. *Rev*. **2013**, *42*, 755-773.

(16) Power, P. P. *Acc*. *Chem*. *Res*. **2011**, *44*, 627-637.

(17) Denk, M.; Lennon, R.; Hayashi, R.; West, R.; Belyakov, A. V.; Verne, H. P.; Haaland, A.; Wagner, M.; Metzler, N. *J*. *Am*. *Chem*. *Soc*. **1994**, *116*, 2691-2692.

(18) Arduengo, A. J.; Harlow, R. L.; Kline, M. *J*. *Am*. *Chem*. *Soc*. **1991**, *113*, 361.

(19) Gynane, M. J. S.; Harris, D. H.; Lappert, M. F.; Power, P. P.; Riviere, P.; Riviere-Baudet, M. *J*. *Chem*. *Soc*., *Dalton Trans*. **1977**, 2004-2009.

(20) Rekken, B. D.; Brown, T. M.; Fettinger, J. C.; Tuononen, H. M.; Power, P. P. *J*. *Am*. *Chem*. *Soc*. **2012**, *134*, 6504-6507.

(21) Driess, M.; Yao, S.; Brym, M.; van Wüllen, C.; Lentz, D. *J*. *Am*. *Chem*. *Soc*. **2006**, *128*, 9628-9629.

(22) Yao, S.; Xiong, Y.; Driess, M. *Organometallics* **2011**, *30*, 1748-1767.

(23) Driess, M.; Yao, S.; Brym, M.; van Wüllen, C. *Angew*. *Chem*. *Int*. *Ed*. **2006**, *45*, 4349-4352.

(24) Kira, M.; Ishida, S.; Iwamoto, T.; Kabuto, C. *J*. *Am*. *Chem*. *Soc*. **1999**, *121*, 9722-9723.

(25) Kira, M. *J*. *Organomet*. *Chem*. **2004**, *689*, 4475-4488.

(26) Asay, M.; Inoue, S.; Driess, M. *Angew*. *Chem*. *Int*. *Ed*. **2011**, *50*, 9589-9592.

(27) Nagendran, S.; Roesky, H. W. *Organometallics* **2008**, *27*, 457-492.

(28) So, C.-W.; Roesky, H. W.; Magull, J.; Oswald, R. B. *Angew*. *Chem*. *Int*. *Ed*. **2006**, *45*, 3948-3950.

(29) Sen, S. S.; Roesky, H. W.; Stern, D.; Henn, J.; Stalke, D. *J*. *Am*. *Chem*. *Soc*. **2010**, *132*, 1123-1126.

(30) Sen, S. S.; Hey, J.; Herbst-Irmer, R.; Roesky, H. W.; Stalke, D. *J*. *Am*. *Chem*. *Soc*. **2011**, *133*, 12311-12316.

(31) Ghadwal, R. S.; Roesky, H. W.; Merkel, S.; Henn, J.; Stalke, D. *Angew*. *Chem*. *Int*. *Ed*. **2009**, *48*, 5683-5686.

(32) Filippou, A. C.; Chernov, O.; Schnakenburg, G. *Angew*. *Chem*. *Int*. *Ed*. **2009**, *48*, 5687-5690.

(33) Chu, J. O.; Beach, D. B.; Estes, R. D.; Jasinski, J. M. *Chem*. *Phys*. *Lett*. **1988**, *143*, 135-139.

(34) Becerra, R.; Bowes, S.-J.; Steven Ogden, J.; Pat Cannady, J.; Adamovic, I.; Gordon, M. S.; Almond, M. J.; Walsh, R. *Phys*. *Chem*. *Chem*. *Phys*. **2005**, *7*, 2900-2908.

(35) Becerra, R.; Walsh, R. *J*. *Am*. *Chem*. *Soc*. **2000**, *122*, 3246-3247.

(36) Becerra, R.; Goldberg, N.; Cannady, J. P.; Almond, M. J.; Ogden, J. S.; Walsh, R. *J*. *Am*. *Chem*. *Soc*. **2004**, *126*, 6816-6824.

(37) Becerra, R.; Cannady, J. P.; Walsh, R. *J*. *Phys*. *Chem*. *A* **2003**, *107*, 11049-11056.

(38) Nowek, A.; Leszczynski, J. *J*. *Phys*. *Chem*. *A* **1997**, *101*, 3784-3788.

(39) So, S. P. *J*. *Phys*. *Chem*. *A* **2001**, *105*, 4988-4991.

(40) Alder, R. W.; Allen, P. R.; Murray, M.; Orpen, A. G. *Angew*. *Chem*. *Int*. *Ed*. *Eng*. **1996**, *35*, 1121-1123.

(41) Lee, G.-H.; West, R.; Muller, T. *J*. *Am*. *Chem*. *Soc*. **2003**, *125*, 8114-8115.

(42) Jutzi, P.; Mix, A.; Rummel, B.; Schoeller, W. W.; Neumann, B.; Stammler, H.-G. *Science* **2004**, *305*, 849-851.

(43) Jutzi, P.; Leszczyńska, K.; Neumann, B.; Schoeller, W. W.; Stammler, H.-G. *Angew*. *Chem*. *Int*. *Ed*. **2009**, *48*, 2596-2599.

(44) Jutzi, P.; Leszczyńska, K.; Mix, A.; Neumann, B.; Rummel, B.; Schoeller, W.; Stammler, H.-G. *Organometallics* **2010**, *29*, 4759-4761.

(45) Inoue, S.; Leszczyńska, K. *Angew*. *Chem*. *Int*. *Ed*. **2012**, *51*, 8589-8593.

(46) Rekken, B. D.; Brown, T. M.; Fettinger, J. C.; Lips, F.; Tuononen, H. M.; Herber, R. H.; Power, P. P. *J*. *Am*. *Chem*. *Soc*. **2013**, *135*, 10134-10148.

(47) Protchenko, A. V.; Birjkumar, K. H.; Dange, D.; Schwarz, A. D.; Vidovic, D.; Jones, C.; Kaltsoyannis, N.; Mountford, P.; Aldridge, S. *J*. *Am*. *Chem*. *Soc*. **2012**, *134*, 6500-6503.

(48) Protchenko, A. V.; Schwarz, A. D.; Blake, M. P.; Jones, C.; Kaltsoyannis, N.; Mountford, P.; Aldridge, S. *Angew*. *Chem*. *Int*. *Ed*. **2013**, *52*, 568-571.

(49) Driess, M. *Nat*. *Chem*. **2012**, *4*.

(50) Paul, A.; Musgrave, C. B. *Angew*. *Chem*. *Int*. *Ed*. **2007**, *46*, 8153-8156.

(51) Roy, L.; Zimmerman, P. M.; Paul, A. *Chem*. *–Eur*. *J*. **2011**, *17*, 435-439.

(52) Ahlrichs, R.; Bär, M.; Häser, M.; Horn, H.; Kölmel, C. *Chem*. *Phys*. *Lett*. **1989**, *162*, 165-169.

(53) Ansgar, S.; Christian, H.; Reinhart, A. *J*. *Chem*. *Phys*. **1994**, *100*, 5829-5835.

(54) Perdew, J. P.; Wang, Y. *Phys*. *Rev*. *B* **1992**, *45*, 13244-13249.

(55) Perdew, J. P.; Burke, K.; Ernzerhof, M. *Phys*. *Rev*. *Lett*. **1996**, *77*, 3865-3868.

(56) Grimme, S.; Antony, J.; Ehrlich, S.; Krieg, H. *J*. *Chem*. *Phys*. **2010**, *132*, 154104-19.

(57) Grimme, S. *J*. *Comput*. *Chem*. **2004**, *25*, 1463-1473.

(58) Grimme, S. *J*. *Comput*. *Chem*. **2006**, *27*, 1787-1799.

(59) Klamt, A.; Schuurmann, G. *J*. *Chem*. *Soc*., *Perkin Trans*. *2* **1993**, 799-805.

(60) Eichkorn, K.; Treutler, O.; Ohm, H.; Haser, M.; Ahlrichs, R. *Chem*. *Phys*. *Lett*. **1995**, *240*, 283-290.

(61) Marek, S.; Annika, H.; Reinhart, A. *J*. *Chem*. *Phys*. **2003**, *118*, 9136-9148.

(62) Fukui, K. *Acc*. *Chem*. *Res*. **1981**, *14*, 363-368.

(63) Frisch, M. J. T., G. W.; Schlegel, H. B.; Scuseria, G. E.;; Robb, M. A. C., J. R.; Scalmani, G.; Barone, V.; Mennucci, B.;; Petersson, G. A. N., H.; Caricato, M.; Li, X.; Hratchian, H. P.;; Izmaylov, A. F. B., J.; Zheng, G.; Sonnenberg, J. L.; Hada, M.;; Ehara, M. T., K.; Fukuda, R.; Hasegawa, J.; Ishida, M.; Nakajima,; T.; Honda, Y. K., O.; Nakai, H.; Vreven, T.; Montgomery, J. A., Jr.;; Peralta, J. E. O., F.; Bearpark, M.; Heyd, J. J.; Brothers, E.; Kudin,; K. N.; Staroverov, V. N. K., R.; Normand, J.; Raghavachari, K.;; Rendell, A. B., J. C.; Iyengar, S. S.; Tomasi, J.; Cossi, M.; Rega,; N.; Millam, J. M. K., M.; Knox, J. E.; Cross, J. B.; Bakken, V.;; Adamo, C. J., J.; Gomperts, R.; Stratmann, R. E.; Yazyev, O.;; Austin, A. J. C., R.; Pomelli, C.; Ochterski, J. W.; Martin, R. L.;; Morokuma, K. Z., V. G.; Voth, G. A.; Salvador, P.;; Dannenberg, J. J. D., S.; Daniels, A. D.; Farkas, O.; Foresman, J. B. O., J. V.; Cioslowski, J.; Fox, D. J., Gaussian 09, revision. B.01; *Gaussian, Inc*., *Wallingford, CT, 2009*.

(64) Wang, Y.; Ma, J. *J*. *Organomet*. *Chem*. **2009**, *694*, 2567-2575.

(65) Coyle, E. E.; O'Brien, C. J. *Nat*. *Chem*. **2012**, *4*, 779–780.

Chapter 6

Summary

6.1 Introduction

Many of the chemical reactions involve activation or cleavage of a chemical bond. These are especially relevant in biological processes,[1] industrially important chemical reactions, as well as in the conversion of toxic molecules to less toxic or useful feedstocks.[2] Some of the small molecules contain strong chemical bonds. Therefore, in order to make the activation processes more efficient, we need the help of transition metal or main group based compounds. These compounds assist the chemical reactions through stoichiometric or catalytic activation of the specific bonds. What is also important is that the advances in the field of homogeneous catalysis allow the reactions to be completed in mild conditions with high efficiency. Therefore, the development of such compounds in homogeneous reaction conditions is an important area of research. Computational Investigations using density functional theory (DFT) allow the modification or prediction of such compounds for small molecule activation. This also provides better understanding in problems associated with some of the activation processes.

6.2 Focus of the thesis

The development of efficient transition metal or main group based compounds that activate the chemical bonds either stoichiometrically or catalytically to enhance the yield of a chemical reaction is of prime importance in our study. Our objective has been to investigate the potential of new or modified compounds in important chemical reactions such as the homogeneous water gas shift reaction (WGSR), olefin metathesis, the dehydrogenation of ammonia borane, dihydrogen generation and activation with main group compounds by employing DFT. These reactions have relevance in the field of small molecule activation processes as well as in the generation of industrially important products such as dihydrogen and functionalized polymers.[3-5] The focus has been to explore the thermodynamic and kinetic understanding that can be achieved from the computational analysis of the chief intermediates and transition states in the reaction cycle. This information has then been used to understand the problems associated with some of the activation processes and to design new catalyst systems that can improve the activity and selectivity of the reactions.

6.2 Methodology used

Geometry optimizations and vibrational frequency calculations were performed with Turbomole 6.4[6] using the TZVP[7] or TZVPP[7] basis sets and the PBE[8,9] functional and in Gaussian 09[10] using the 6-31++g(d,p)[11] basis set and the B3LYP[12,13] functional. The resolution of identity (RI),[14] along with the multipole accelerated resolution of identity (marij)[15] approximations have been employed for an accurate and efficient treatment of the electronic Coulomb term in the DFT calculations performed with the Turbomole 6.4 software. Solvent effects were incorporated by using the COSMO[16] model in Turbomole 6.4 and PCM-SMD[17] model in Gaussian 09. For dispersion correction calculations, an empirical dispersion correction proposed by Grimme has been employed.[18,19] The values reported are ΔG values, with zero point energy, internal energy and entropic contributions included through frequency calculations on the optimized minima and transition state structures, with the temperature taken to be 298.15 K. All the obtained transition states were confirmed to have only a single negative frequency corresponding to the correct normal mode. In addition, intrinsic reaction coordinate (IRC)[20] calculations were done with all the transition states in order to further confirm that they were the correct transition states, yielding the correct reactant and product structures.

6.4 Summary of the results

1) In order to improve the experimentally known catalysts for homogeneous WGSR and homogeneous olefin metathesis reactions, different strategies such as metal-metal cooperativity in the WGSR catalyst $Fe(CO)_5$ and ligand modification using allene ligands in the second generation Grubbs' olefin metathesis catalyst have been studied. Full quantum mechanical calculations show that metal−metal cooperativity plays an important role in improving the yield of WGSR.[21] The calculations also indicate that bimetallic catalysts would be likely to be more highly active than mononuclear metal-based catalysts for the WGSR. The modification of the second generation Grubbs' catalysts with allenes and their derivatives as leaving groups show that they would all perform significantly (up to several orders in magnitude) better than the existing ligand PCy_3, when employed as a leaving group in the metathesis reaction. The calculations also suggest that the presense of electron

withdrawing groups as well as the supramolecular interactions on the allene ligand assist them to act as the most effective leaving groups.[22]

2) Hydrogen is considered as the fuel of the future. Main group compounds that can assist the catalytic dihydrogen production can provide a greener or cheaper solution towards the problems associated with the current non-renewable fossil based fuel economy. In this regard, new compounds that can mediate important reactions such as the catalytic dehydrogenation of ammonia borane as well as dihydrogen generation from water and alcohols have been predicted through DFT studies. Computational investigation on recently synthesized Ga−N molecular cage compounds shows that it can catalyze the ammonia borane dehydrogenation reaction through the opening and closing of labile bonds present in it.[23] Also, our studies show through a predictive approach that a modified germanium (II) hydride with boron atoms, such as $HC\{CMeArB\}_2GeH$ (Ar = 2,6-$iPr_2C_6H_3$), with the assistance of silicon based compounds such as SiF_3H, can perform significantly better than the existing state-of-the-art post-transition metal based systems for catalyzing the dihydrogen generation from water and alcohols through the protolysis reaction.

3) Previous studies present in the literature on higher acyclic analogues of carbenes such as the acyclic silylene compounds show that main group compounds can imitate the transition metal compounds in small molecule activation processes. A full quantum chemical investigation with density functional theory demonstrates that undesired side reactions would be competitive in these systems during small molecule activation. Our studies show that for silylenes that cannot display single site small molecule activation due to the preference for competing side reactions, the desired final product can still be obtained by employing other reagents, such as hydrogenating agents in the place of dihydrogen.[24]

1.4 References

(1) Fryzuk, M. D.; Johnson, S. A. *Coord*. *Chem*. *Rev*. **2000**, *200*, 379-409.

(2) Staubitz, A.; Robertson, A. P. M.; Manners, I. *Chem*. *Rev*. **2010**, *110*, 4079-4124.

(3) Kunkes, E. L.; Simonetti, D. A.; West, R. M.; Serrano-Ruiz, J. C.; Gartner, C. A.; Dumesic, J. A. *Science* **2008**, *322*, 417-421.

(4) Kim, W. B.; Voitl, T.; Rodriguez-Rivera, G. J.; Dumesic, J. A. *Science* **2004**, *305*, 1280-1283.

(5) Huber, G. W.; Shabaker, J. W.; Dumesic, J. A. *Science* **2003**, *300*, 2075-2077.

(6) Ahlrichs, R.; Bär, Michael; Häser, M.; Horn, H.; Kölmel, C. *Chem*. *Phys*. *Lett*. **1989**, *162*, 165-169.

(7) Ansgar, S.; Christian, H.; Reinhart, A. *J*. *Chem*. *Phys*. **1994**, *100*, 5829-5835.

(8) Perdew, J. P.; Wang, Y. *Phys*. *Rev*. *B* **1992**, *45*, 13244-13249.

(9) Perdew, J. P.; Burke, K.; Ernzerhof, M. *Phys*. *Rev*. *Lett*. **1996**, *77*, 3865-3868.

(10) Frisch, M. J. T., G. W.; Schlegel, H. B.; Scuseria, G. E.;; Robb, M. A. C., J. R.; Scalmani, G.; Barone, V.; Mennucci, B.;; Petersson, G. A. N., H.; Caricato, M.; Li, X.; Hratchian, H. P.;; Izmaylov, A. F. B., J.; Zheng, G.; Sonnenberg, J. L.; Hada, M.;; Ehara, M. T., K.; Fukuda, R.; Hasegawa, J.; Ishida, M.; Nakajima,; T.; Honda, Y. K., O.; Nakai, H.; Vreven, T.; Montgomery, J. A., Jr.;; Peralta, J. E. O., F.; Bearpark, M.; Heyd, J. J.; Brothers, E.; Kudin,; K. N.; Staroverov, V. N. K., R.; Normand, J.; Raghavachari, K.;; Rendell, A. B., J. C.; Iyengar, S. S.; Tomasi, J.; Cossi, M.; Rega,; N.; Millam, J. M. K., M.; Knox, J. E.; Cross, J. B.; Bakken, V.;; Adamo, C. J., J.; Gomperts, R.; Stratmann, R. E.; Yazyev, O.;; Austin, A. J. C., R.; Pomelli, C.; Ochterski, J. W.; Martin, R. L.;; Morokuma, K. Z., V. G.; Voth, G. A.; Salvador, P.;; Dannenberg, J. J. D., S.; Daniels, A. D.; Farkas, O.; Foresman, J. B. O., J. V.; Cioslowski, J.; Fox, D. J., Gaussian 09, revision. B.01; *Gaussian, Inc., Wallingford, CT, 2009*.

(12) Axel, D. B. *J*. *Chem*. *Phys*. **1993**, *98*, 5648-5652.

(13) Lee, C.; Yang, W.; Parr, R. G. *Phys*. *Rev*. *B* **1988**, *37*, 785.

(14) Eichkorn, K.; Treutler, O.; Öhm, H.; Häser, M.; Ahlrichs, R. *Chem*. *Phys*. *Lett*. **1995**, *240*, 283-290.

(15) Sierka, M.; Hogekamp, A.; Ahlrichs, R. *J*. *Chem*. *Phys*. **2003**, *118*, 9136-9148.

(16) Klamt, A.; Schuurmann, G. *J*. *Chem*. *Soc*., *Perkin Trans*. *2* **1993**, 799-805.

(17) Marenich, A. V.; Cramer, C. J.; Truhlar, D. G. *J*. *Phys*. *Chem*. *B* **2009**, *113*, 6378-6396.

(18) Stefan, G.; Jens, A.; Stephan, E.; Helge, K. *J*. *Chem*. *Phys*. **2010**, *132*, 154104.

(19) Grimme, S.; Ehrlich, S.; Goerigk, L. *J*. *Comput*. *Chem*., *32*, 1456-1465.

(20) Fukui, K. *Acc*. *Chem*. *Res*. **1981**, *14*, 363-368.

(21) Kuriakose, N.; Kadam, S.; Vanka, K. *Inorg*. *Chem*. **2012**, *51*, 377-385.

(22) Kuriakose, N.; Vanka, K. *J*. *Comput*. *Chem*. **2015**, *36*, 795-804.

(23) Kuriakose, N.; Vanka, K. *Inorg*. *Chem*. **2013**, *52*, 4238-4243.

(24) Kuriakose, N.; Vanka, K. *Dalton Trans*. **2014**, *43*, 2194-2201.